Chair of Designing Plastics and Composite Materials

Doctoral Thesis

Modeling fatigue damage in composite laminates

Dipl.-Ing. Matthias Anton Drvoderic, BSc

April 2023

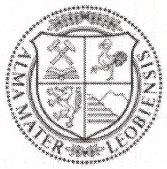

MONTANUNIVERSITÄT LEOBEN
www.unileoben.ac.at

AFFIDAVIT

I declare on oath that I wrote this thesis independently, did not use other than the specified sources and aids, and did not otherwise use any unauthorized aids.

I declare that I have read, understood, and complied with the guidelines of the senate of the Montanuniversität Leoben for "Good Scientific Practice".

Furthermore, I declare that the electronic and printed version of the submitted thesis are identical, both, formally and with regard to content.

Date 21.04.2023

Signature Author
Matthias Anton Drvoderic

Acknowledgements

This work was carried out at the Chair of Designing Plastics and Composite Materials at Montanuniveristaet Leoben withing the COMET project *Experimental and numerical analysis of the damage tolerance behavior of manufactured induced defects and bonded repairs in structural aerospace composite parts*. I would like to express my gratitude to all persons supporting over the course of this thesis.

First of all, i want to thank Univ.-Prof. Clara Schuecker, for the opportunity to be part of this project. I am grateful for the support and the guidance throughout the whole project as my academic supervisor. Thanks for sharing the experience and skills to perform this research. The inspiring discussions helped to progress the work past setbacks and helped to transition experimental insights to computational models.

Specials thanks go to Dr. Martin Pletz for all the vivid discussions that helped to stay focused. They provided interesting insights into micromechanics and modelling, which influenced many parts of this work. Also, for all the help with scientific writing and graphical illustrations which are now part in all papers and presentations from this project.

I want to thank my mentor Univ.-Prof. Clemens Brand for his interest in the work and the discussions about numerical methods for image processing.

I would also like to thank my colleagues from the Chair of Designing Plastics and Composite materials who were always willing to help when it came to issues with code, algorithms or methods and the colleagues from the Chair of Materials Science and Testing of Polymers who performed the necessary tests for my research. For helping with all organisational measures i thank Heike who always aided all formal processes and registrations.

On this occasion, I do not want to miss the opportunity to thank my family and friends, especially my parents Ilse and Stjepan who always supported me during my studies, Christoph for his helpful attitude and my partner Veronika for the all the encouragement over the last years.

Abstract

The ability to design lightweight yet strong and durable components with composite materials has driven their continuous development. Nowadays, components from high-performance composite materials are used in a wide range of applications mostly aircraft, wind turbines, automotive and sports equipment. To ensure their safety, understanding the fatigue behaviour of composites is essential. Up to now, no universal fatigue-damage model exists for composite laminates despite continuous developments in this field over the past decades. This reflects the difficulty of developing such a model for composite laminates where effects on different length scales influence the development of fatigue damage. The anisotropic material behaviour, multiple damage modes and complex interactions have shown to be significant obstacles in the development of a universal fatigue-damage model. Many proposed models have critical limitations when it comes to their applicability to real-world components, which hinders them to become widespread engineering tools. Given the fact that fatigue modelling generally requires more experimental data than static analysis due to multiple added effects from fluctuating loads, the amount of tests needed for the calibration of models is particularly important. This thesis takes a rather engineering approach with regard to physical damage phenomena for the development of a ply-based fatigue damage model for matrix cracks. As of now, parts of the model are still under development, as this work marks the beginning of the development of a fatigue-damage model with the aim to provide an efficient and easy-to-use framework. A special focus is the applicability of the model and the ability to calibrate the model with standard experimental campaigns. The model builds upon the static ply-based damage model from Schuecker et al., which uses a multi-scale approach to compute the effects of matrix cracks on the stiffness of a laminate. The classical laminate theory is used for stress analysis of a given laminate. The effects of matrix damage are computed with a Mori-Tanaka model, which is an analytical micromechanical method. In order to develop such a model, information on the damage state during tests is essential. For this, a crack detection framework is presented which enables efficient quantification of the damage state for fatigue experiments. Also, the correlation with other measures and the effects of different stress states on the formation and evolution of matrix cracks is studied in detail.

Kurzfassung

Die kontinuierliche Entwicklung von Verbundwerkstoffen wurde von deren Möglichkeit leichte aber dennoch starke und haltbare Bauteile zu konstruieren vorangetrieben. Heutzutage werden Bauteile aus Hochleistungsverbundwerkstoffen in einer Vielzahl von Anwendungen, vor allem in Flugzeugen, Windkraftanlagen, Kraftfahrzeugen und Sportgeräten, eingesetzt. Um deren Sicherheit zu gewährleisten ist ein grundlegendes Verständnis des Ermüdungsverhaltens von Verbundwerkstoffen unerlässlich. Dennoch gibt es bisher kein universelles progressives Schädigungsmodell für die Ermüdung von Schichtverbunden, obwohl in den letzten Jahrzehnten kontinuierliche Entwicklungen in diesem Bereich stattgefunden haben. Dies spiegelt die Schwierigkeit wider, ein solches Modell für Laminate aus Verbundwerkstoffen zu entwickeln, da Effekte auf unterschiedlichen Längenskalen die Entwicklung von verschiedenen Schädigungsmechanismen beeinflussen. Anisotropes Materialverhalten, mehrere Schädigungsarten und komplexe Wechselwirkungen haben sich als erhebliche Hindernisse bei der Entwicklung eines universellen Ermüdungsmodells erwiesen. Viele der vorgeschlagenen Modelle weisen kritische Einschränkungen auf, wenn es um ihre Anwendbarkeit auf reale Komponenten geht und verhindert somit deren Verbreitung und Einsetzbarkeit als technische Werkzeuge. Da im Vergleich zu statischen Belastungen zahlreiche zusätzliche Effekte durch wechselnde Belastungen auftreten erfordern Ermüdungsmodelle im Allgemeinen mehr experimentelle Daten zur Kalibrierung. In dieser Arbeit wird daher ein eher ingenieurmäßiger Ansatz im Hinblick auf physikalische Schädigungsphänomene für die Entwicklung eines lagenbasierten Modells für die Effekte von Schädigung durch Ermüdungsbelastung aufgrund von Matrixrissen gewählt. Diese Arbeit markiert den Beginn der Entwicklung des Ermüdungsmodells mit dem Ziel, ein Werkzeug zu schaffen das effizient und einfach zu verwendenden ist. Ein besonderer Schwerpunkt liegt auf der Anwendbarkeit des Modells und der Möglichkeit, das Modell mit Standardversuchen zu kalibrieren. Das Modell baut auf dem statischen lagenbasierten Schädigungsmodell von Schuecker et al. auf. Es wird ein Multiskalenansatz zur Berechnung der Auswirkungen von Matrixrissen auf die Steifigkeit eines Laminats verwendet. Für die Spannungsanalyse eines gegebenen Laminats wird die klassische Laminattheorie genutzt. Die Auswirkungen von Matrixschäden werden mit einer analytischen mikromechanischen Methode, dem Mori-Tanaka-Modell, berechnet. Für die Entwicklung eines solchen Modells sind Informationen über den Schädigungszustand während Materialtests unerlässlich. Zu diesem Zweck wird zusätzlich ein Framework für die Risserkennung vorgestellt. Dies ermöglicht eine effiziente Quantifizierung des Schädigungszustands bei Ermüdungsversuchen. Weiters werden Korrelation mit anderen Messgrößen und die Auswirkungen verschiedener Spannungszustände auf die Entstehung und Entwicklung von Matrixrissen eingehend untersucht.

Contents

List of Abbreviations and Symbols

Abbreviations

CLD	Constant Life Diagram
CLT	Classical Laminate Theory
FEM	Finite Element Method
FRP	Fibre-Reinforced Polymer
TWLI	Transilluminated White Light Imaging

Symbols

a	Crack length
A	Area
D	Damage
E	Young's modulus
G	Strain energy release rate
n_i	i$^{\text{th}}$ cycle number
N_f	Cycles until failure
K_I	Stress concentration factor
L	Length
R	R-ratio
U	Strain energy
U_v	Dilatational energy density
λ	stress ratio
ν	Poisson's ratio
ρ_c	Crack density
σ	Stress
σ_{22}	Stress transverse to fibre direction
σ_{12}	In-plane shear stress
σ_h	Local hydrostatic stress
σ_I	Local maximum principal stress
σ_y	Yield stress
$\sigma(t)$	Stress as a function of time
ω	Size of the fracture process zone

List of Figures

1 Introduction

The question of: "How long does it take to break?" is probably one of the most asked questions in engineering. From August Wöhler, who performed fatigue test campaigns from specimens to full-scale wagon axles [1] more than 150 years ago up to now, this question still drives innovations in engineering and material science. In this work, this question is extended to "What happens until failure?" for fibre-reinforced polymer materials (FRPs). In a laminate made from FRPs, multiple damage modes can be active simultaneously. This leads to complex interactions between the failure modes and makes it hard to predict the degradation of the material accurately. Matrix cracks, often called off-axis cracks, are usually the first characteristic damage mode in components made from FRPs. These cracks trigger the onset and growth of other damage modes like delamination and fibre failure [2]. Therefore, the effect of matrix cracks is essential for the development of a universal fatigue model for FRPs, which is still an ongoing process [3–5]. Figure 1.1 shows a schematic representation of the effect of off-axis cracks on the stiffness of a composite laminate.

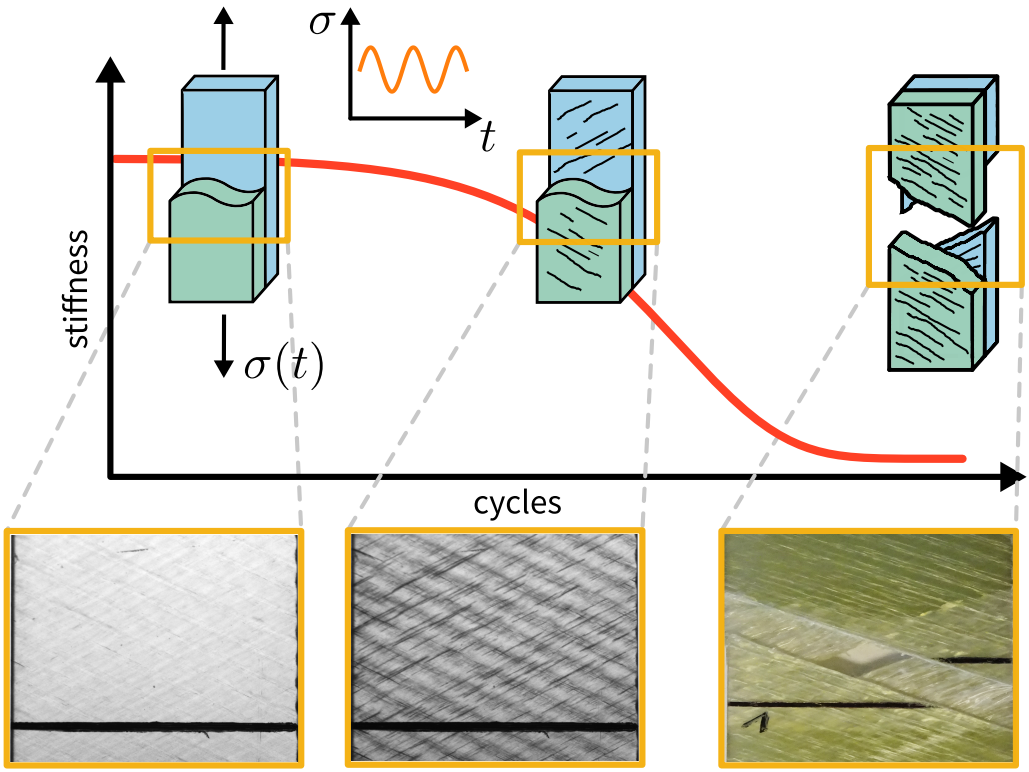

Figure 1.1: Schematic representation of the effect of off-axis cracks on the stiffness of a composite laminate. With the growing number of cracks, the stiffness decreases continuously. The images show a specimen at the beginning, during and after a fatigue test. The off-axis cracks are clearly visible in the image in the centre.

1.1 Composite laminates

Composites combine two or more materials to gain beneficial properties from all their constituents. This makes it possible to combine the positive properties of several materials and with a careful selection of the constituents, to balance unwanted properties. The constituents remain separate within the composite, which distinguishes composites from mixtures or solutions. One important sub-section of composite materials is fibre-reinforced composites, where usually long and thin fibres are combined with a matrix material. This combination makes it possible to use the high stiffness and strength of fibres for solid components where fibres bear the load and the matrix enables load transfer into the fibres.

A laminate is a thin structure of several bonded plies. Various ply types or materials can be combined in a laminate to tailor its properties for a specific load case. A laminate with plies in only one fibre direction would be the optimal structure if all loads were aligned in the same direction. Since this is nearly never the case in actual structures where several load cases must be accounted for, laminates with multiple fibre directions are the norm. Over the past decades, laminates from FRPs have seen continuous development because of their potential for weight reduction and are widely used in commercial and private applications. Especially in the aviation industry, where each saved kilogram of weight directly lowers the operating cost of an aircraft due to being more fuel efficient, the use of FRPs rose continuously. In wind turbine blades, composite materials enable the switch to more renewable energy and in sports equipment like tennis rackets, bike frames and hockey sticks, FRPs have found their way into daily life. Despite all the advantages, FPRs come with their own set of challenges. From a mechanical engineer's perspective, the transversal isotropy and effects on multiple length scales that must be accounted for make designing components a complex task [6].

Composite laminates are in themselves a complex structure comprised of fibres and a polymer matrix at the micro-scale. Single fibres (filaments) are usually processed into rovings or yarns for use in continuously reinforced composites. With classical laminate theory, multiple plies can be combined to compute the mechanical response of the whole laminate, which represents the mesoscale. This is done to reduce the complexity of numerical models of large components, which represent the macro-scale. The characteristic length scales are shown in Figure 1.2. The complexity across three length scales makes it obvious why simulating the mechanical response of composite materials is a demanding task. Models that predict damage and its effect on the micro-scale are usually way too complex to be used at the meso- or even macro-scale. Therefore, simplified models at the mesoscale are needed to reduce computational costs to a feasible level. This inevitable reduction of resolution leads to a loss of information at the meso-scale, which is needed to accurately predict the onset and growth of micro-damage, which in turn is needed to predict macro-damage.

Due to this complex geometry, multiple damage modes occur during the fatigue life. Damage initiates from weak points such as voids or other forms of stress concentrations at the micro-scale. Depending on the stress state of a ply, micro-damage grows into ply-level matrix cracks, delamination or triggers fibre failure [2]. The multiple distinct damage modes and their interactions make it obvious, that the development of a universal fatigue failure theory is equally complex and complicated. Therefore, as already mentioned, no general fatigue model for FRPs is available up to now.

1.2 Fatigue damage in FRPs

Matrix cracks, delamination and fibre failure are the three main damage modes at the meso-scale. At the micro-scale, damage initiates from imperfections in the material like voids, matrix-rich regions, inclusions of impurities, manufacturing errors etc. Up to now, the onset and interactions of all the damage modes are still not fully studied [4]. Especially micro-damage and its effects on the meso- and macro-scale is still an ongoing field of research. Figure 1.3 shows a schematic representation of the evolution of damage in composite laminates during fatigue loading.

It has to be noted that this is a schematic representation of the damage patterns that are observed in multi-directional laminates with in-plane stresses. For laminates with only one fibre direction, out-of-plane loading or other special layup configurations, these patterns may differ. At the early stages of the fatigue life, ply-level matrix cracks form in plies with transverse stresses. These matrix cracks originate from micro-damage in the form of micro-cracks or fibre-matrix interface failure [7–9] and grow along the fibre direction in number and size during the fatigue life. Diffuse delamination, also called interfacial debonding, often starts at

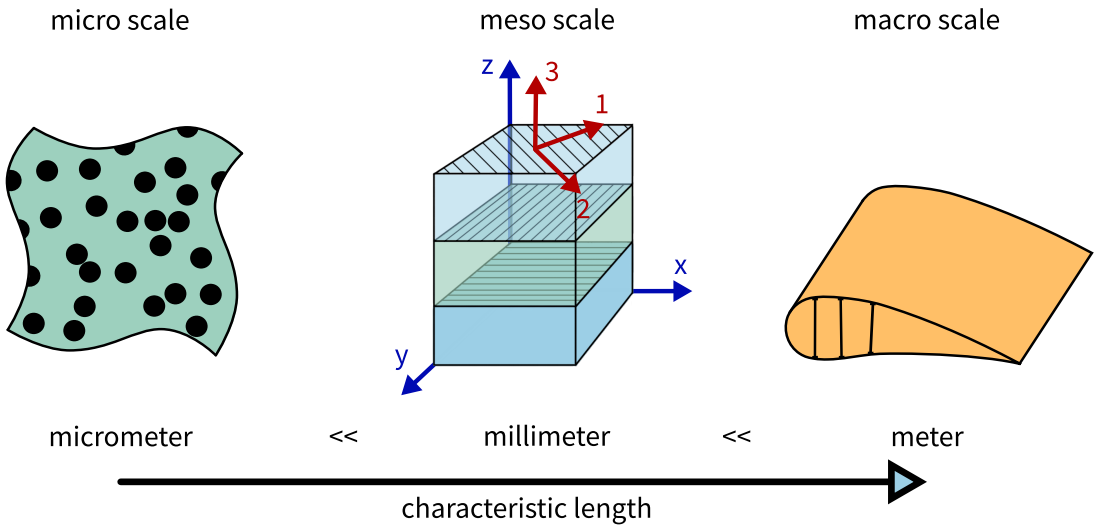

Figure 1.2: Characteristic length-scales of composite laminates with laminate- (x,y,z) and ply- (1,2,3) coordinate systems.

the tip of matrix cracks between two plies and also grows in number and size. This diffuse delamination grows into the delamination of bigger areas. These delaminated regions are already structural damage at the component level. From stress concentrations caused by the matrix cracks, fibre failure starts in neighbouring plies. This can already happen in relatively early stages of the fatigue life [10–12]. Since broken fibres cannot bear a load anymore, the load is redistributed to neighbouring fibres. Therefore, the fibres in the vicinity of a broken fibre are more likely to fail due to higher loads. This leads to the progressive growth of the region with broken fibres during the fatigue life. If the damage grows to a level where the load on the remaining intact laminate exceeds its strength, the rupture of the remaining intact fibres marks the end of the life of a component. Although matrix-crack-induced fibre failure often occurs already in the first and second stages, it is not the governing damage mechanism in this stage [2]. Matrix cracks are usually considered the first characteristic damage mode at the meso-level. They influence the onset and growth of delamination and fibre failure and therefore, great effort was dedicated to studying this damage mode in the past two decades [12–18]. Since this work also presents a model to predict the effect of off-axis cracks on the stiffness of the material, this damage mode is explained in detail.

1.3 Off-axis cracks

Off-axis matrix cracks are cracks that grow parallel to the fibres in the matrix or in the fibre-matrix interface. These cracks typically span the thickness of a ply and grow in number and

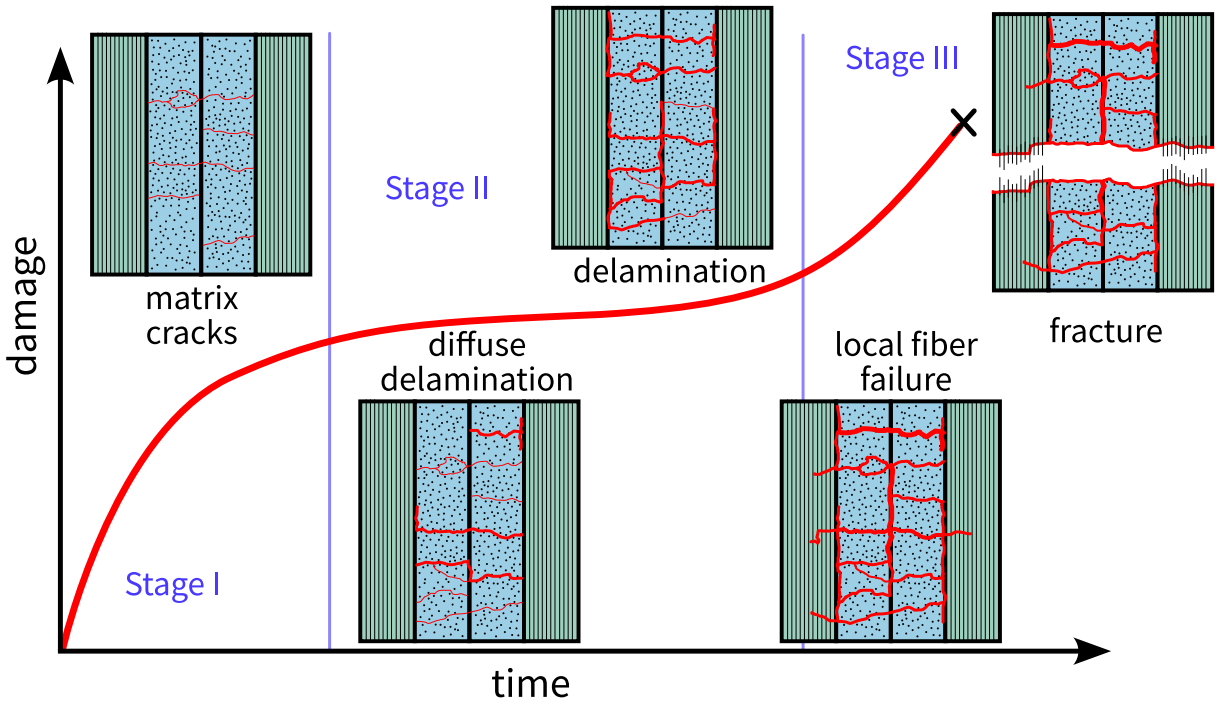

Figure 1.3: Characteristic damage states for a composite laminate during fatigue loading.

size during fatigue loading. Figure 1.4 shows typical matrix cracks in a glass-fibre reinforced laminate with a stacking sequence of $[+45°, -45°]_s$.

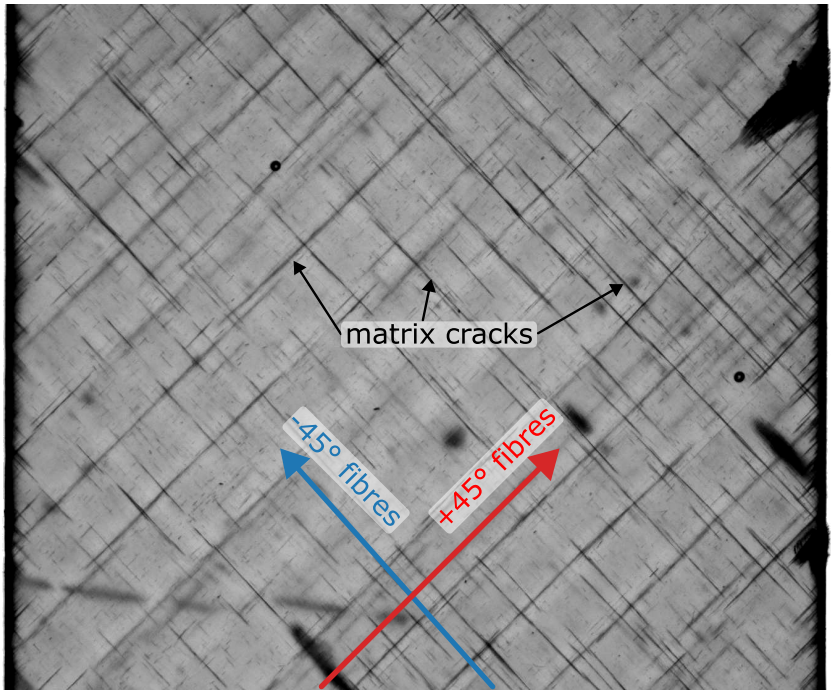

Figure 1.4: Matrix cracks in a $\pm 45°$ glass fibre laminate. By shining light through the specimen, matrix cracks appear as dark lines. The cracks grow along the fibre direction of each ply.

Describing the nucleation and propagation of off-axis cracks is a vital part of modelling fatigue of composites since other damage modes are triggered by these off-axis cracks. It is well known that these matrix cracks cause a significant loss of stiffness [9, 15–17, 19–21]. This can be shown by plotting stiffness over the number of cycles and normalising the cycles to the crack initiation, i.e. the point where ply-level cracks form, as shown by Wharmby et al. [21] (see Figure 1.5). Same as the ply stiffness, the degradation of stiffness is also anisotropic. The stiffness in the fibre direction is affected less than the transverse stiffness since the cracks grow parallel to the fibres [22, 23]. The fibres are not cracked and therefore, their load-bearing capacity mostly stays intact while a significant part of the matrix is damaged. Since the transverse stiffness of a unidirectional composite is mostly dependent on the properties of the matrix, it is clear that damaging the matrix will result in a loss of transverse stiffness.

Cracks on the ply-level are the result of accumulated microscopic damage in the form of micro-cracks that grow into one crack at the meso-level. Depending on the damage state at the micro-level, several distinct micro-damage modes form, which is confirmed by fractographic images [8, 14, 24]. For stress states with positive transverse stresses, σ_{22}, two micro damage modes can be identified. Fractographic images in this stress region show relatively smooth fracture surfaces for stress states dominated by transverse stress at the ply-level (σ_{22}) and rough fracture surfaces for stress states with a high proportion of in-plane shear σ_{12}. Quaresimin et al. showed this behaviour for tubular specimens where they progressively increased the ratio of in-plane shear to transverse stress $\lambda = \sigma_{22}/\sigma_{12}$ as shown in Figure 1.6.

For σ_{22} dominated failure, Asp et al. observed that matrix cracks form due to fibre-matrix interface failure or matrix failure parallel to the fibres and showed that the dilatational energy density can be used as a suitable failure criterion at the micro-scale [8]. The dilatational energy density as a function of the local (on the micro-scale) stresses is shown by

$$U_v = \frac{1-2\nu}{6E}(\sigma_{11}+\sigma_{22}+\sigma_{33})^2 = U_v^{crit} \ , \tag{1.1}$$

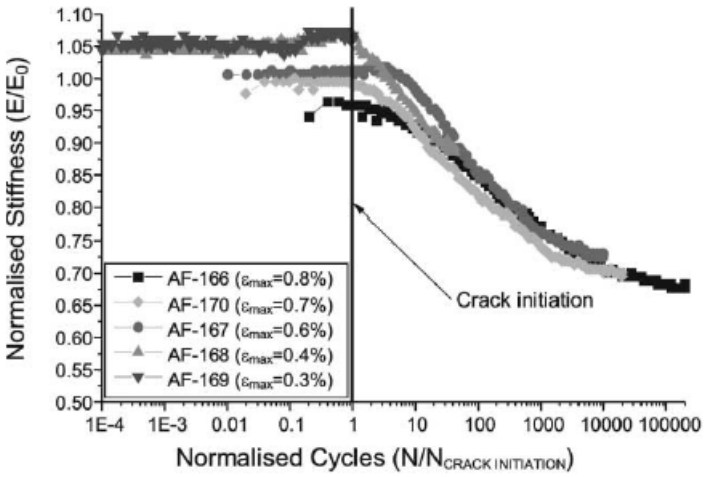

Figure 1.5: Wharmby showed that the loss of stiffness starts when matrix cracks at the ply-level form [21].

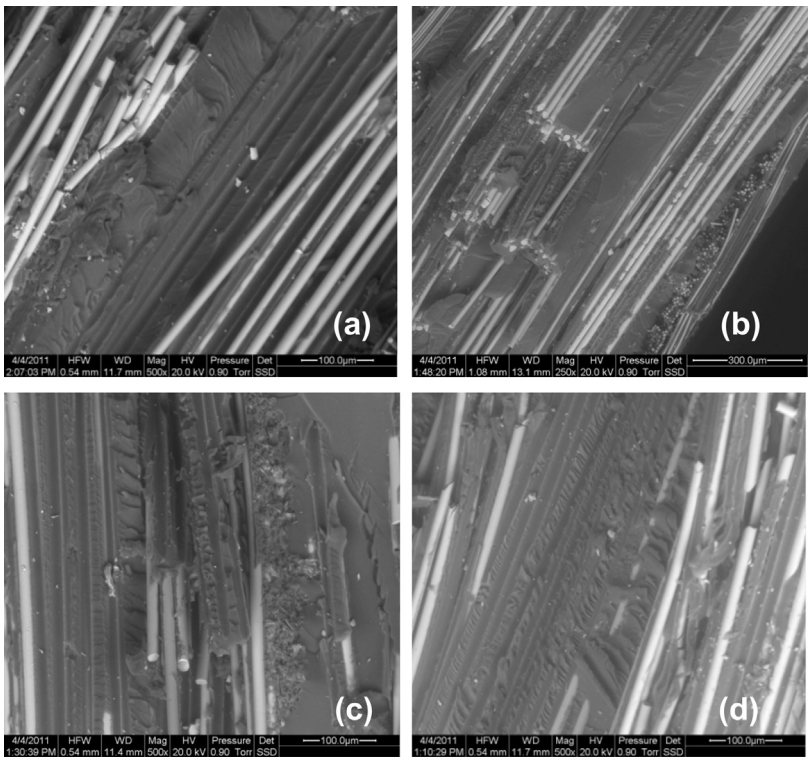

Figure 1.6: Quaresimin showed that the micro-damage modes change with the ratio of in-plane shear stress to transverse stress [17]. The transition from smooth to rough fracture surface is clearly visible in the images for λ = 0 (a), 0.5 (b), 1 (c) and 2 (d).

where the stresses σ_{11}, σ_{22} and σ_{33} as well as the Young´s modulus E and the Poisson's ratio ν must be known. This criterion can be expressed in terms of the first invariant of the stress tensor, which represents the hydrostatic part. The hydrostatic stress is the only changing part of dilatational energy for a given ply, considering the material of a ply is considered constant for all practical purposes. Therefore, a critical maximum hydrostatic stress can be found which describes the strength of the material for this damage mode.

For shear-dominated stress states, micro-cracks between the fibres have been observed. These micro-cracks develop in a specific fracture plane about 40°- 50° with respect to the fibre direction. This was shown by the work of Plumtree et al. [14]. An example of these micro-cracks is shown in Figure 1.7. The local maximum principal stress has been identified as the driving force for this damage mode [25].

Figure 1.7: Micro-cracks at a distinct crack angle between the fibres in a resin-rich region shown by Plumtree et al. [14].

The fact that fibres are embedded in the matrix inherently forces the matrix cracks onto a predefined path. Since fibres are usually orders of magnitude stronger than the matrix, the matrix will break first. The local nucleation plane can be different from the fibre direction, but the crack is forced to grow in the fibre direction, as long as the neighbouring fibre does not break. Even if the crack re-initiates on the opposite side of the neighbouring fibre, no substantial crack opening will occur as long as the fibre is intact. Even though the two micro-damage modes explain the phenomenon of the differing fracture surfaces depending on the stress state of the ply, the onset and growth of off-axis cracks are far from fully understood.

A separation of these two micro-damage modes is necessary for failure criteria that predict the onset of off-axis cracks in fatigue. Therefore, the stresses at the micro-scale i.e. local stresses must be computed in order to further compute the local maximum principal and local hydrostatic stress. Unfortunately, it is not feasible to compute local stresses directly in finite element models of whole components, since computation times and memory requirements would be too high for industrial use. From an engineer's perspective, failure models should be computationally inexpensive with low requirements for testing the needed material parameters. Static failure criteria like Puck and LaRC05, two state-of-the-art and widely accepted failure criteria, provide good predictions of static failure without needing to compute micro-stresses or micro-damage modes [26, 27]. Note that in these criteria, no differentiation of micro-damage modes is made, which is necessary for fatigue. This necessity

to differentiate between micro-damage modes in fatigue is also shown in Paper C of this thesis, where the stiffness degradation due to off-axis cracks is computed.

An efficient model to compute the critical damage driving force at the micro-level has been developed by Carraro et al. [28]. They showed that the computation of stresses at the micro-scale can be omitted by using a unit cell and computing a set of concentration factors with the finite element method. With the concentration factors, which can be computed in advance for a given material, the stresses on the micro-scale can be directly computed from the ply stresses. Furthermore, the model generation of a square unit cell is easy to automate. This is essential for the applicability of such models to whole components. They also showed that SN curves in the region of positive transverse stress and in-plane shear for various ply-stress states collapse into two master curves. This is shown by Carraro et al. by plotting the local hydrostatic stress σ_h and local maximum principal stress σ_I over the life to crack onset, as shown in Figure 1.8. This further demonstrates that the local maximum principal stress σ_I and the local hydrostatic stress σ_h are reliable measures for the driving forces of the micro-damage and can therefore be used as material properties for the fatigue strength. This is especially useful when considering that only two SN-curves are needed to characterise the material which vastly reduces the need of testing multiple SN-curves for various ply-stress states to just two master SN-curves. The applicability of Carraro's model is shown in Paper D, which also shows that the predictions of the model correlate well with fractographic images.

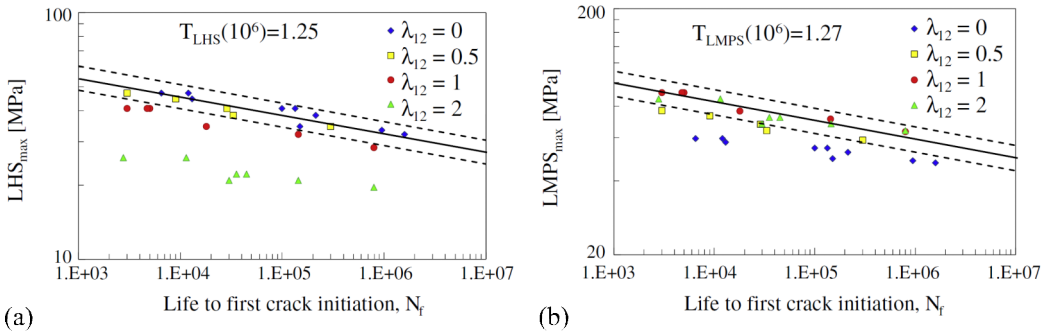

Figure 1.8: Tests with several stress ratios λ collapse into two master curves for local hydrostatic stress (a) and local maximum principal stress (b) as shown by Carraro [28].

1.3.1 Crack detection

In order to develop progressive damage models, information about the damage state during the fatigue tests is essential. This means, that the cracks or some other measure that directly correlates with the number of cracks in the material must be monitored during tests. In the past decades, the crack density has been used extensively as a damage parameter for matrix damage [12, 18–20, 22, 29–36]. Various methods have been used for detecting matrix cracks and quantifying the extent of damage in the matrix. One such method is direct crack detection

from images of specimens. This is only possible for at least semi-transparent specimens. Fortunately one of the most used composites, glass fibre-reinforced polymers, fulfils this criterion if a transparent matrix is used, which is often the case. In fatigue tests, Transilluminated White Light Imaging (TWLI) is usually used as an imaging technique. For this, a white light source is placed behind the specimen and images are taken from the other side. Since the crack surfaces in the specimen scatter the light passing through, these cracks appear as dark lines in the image. An example of this is shown in Figure 1.4. Before image processing was as advanced and easily accessible as today, these cracks were often counted manually to compute the crack density [20, 22, 23, 29, 31]. With the advancements in image processing and machine learning, automated methods to compute crack density have emerged. Especially for the inspection of large concrete structures and pavement, several automated methods to detect cracks have been developed [37, 38]. These image-based crack detection methods can be classified into two categories:

- *Image Processing* based crack detection. A variety of filters and signal-processing techniques are applied to one or more images to detect cracks. Gabor filter and Canny edge detection, two classical edge detection algorithms are often used in combination with several threshold and noise-reduction or background detection techniques [39].

- *Machine learning* based crack detection. Usually, a neuronal network is trained to detect cracks or patterns in images. A number of techniques like transfer learning, decision trees, encoder-decoder networks etc. are used in a variety of models [40].

Crack detection of off-axis cracks in composite materials is a niche application with the benefit of a pre-defined crack direction. This makes it easier to develop image processing-based algorithms, which have the advantage that no training data is needed. Over the past decade, a few crack detection algorithms for off-axis matrix cracks have been developed. Sket et al. used X-ray computed tomography to get around the fact that carbon fibres are not transparent for visible light and an algorithm based on the Hough transform [41]. Miskdjian et al. detected cracks only at the edge of the specimen [42]. This also allows to detect cracks in non-transparent composites. However, this approach gives no information about the length of the cracks. Another algorithm for transparent composites was developed by Glud et al. where a Gabor filter is used as line detection combined with an Otsu threshold to separate cracks and background [43–45]. Crack counting is performed by using a skeletonizing algorithm to reduce the area which is detected as a crack to a width of one pixel. From this, the beginning and end of each crack are used to compute its length. This algorithm showed good results in images like those shown in Figure 1.4, but due to the use of a floating threshold, which means the threshold to differentiate between cracks and background is computed based on the grey-values of the images, it has problems when hardly any cracks are present. This is due to the fact that the Otsu threshold will differentiate between crack or generally speaking foreground and background in any image, even if no cracks are present. This can yield wrong

results for low crack densities. Using floating thresholds brings the benefit that images with varying levels of illumination can be compared but the results may diverge for relatively similar inputs. Based on this algorithm, Bender et al. developed a more stable version that uses a fixed threshold and an altered sequence of filters, but with the same crack-counting technique [35]. With this algorithm, the beginning and end of each crack are evaluated and the crack density is computed as the total length of all cracks divided by the area of interest as given by

$$\rho_c = \frac{\sum_{i=1}^{n} L_i}{A} \text{ r} \tag{1.2}$$

where ρ_c is the crack density, L_i the length of the i-th crack and A the total area of interest. Similar to Glud's algorithm, Just et al. also developed a crack detection algorithm that uses a fixed threshold instead of Otsu's threshold for the same reasons as mentioned above [46]. They also used the Gabor filter to detect cracks in a given direction but the crack counting is done with an eigenvalue decomposition of the inertia tensor of each area detected as a crack. The length of the major axis of each crack area is used as the crack length. To compute the crack density the same definition as also used by Glud and Bender is used (see equation 1.2).

Prior to automated crack detection, manual crack counting where simply the number of cracks in an area or along a given path are counted was often used. This does not take the length of the individual cracks into account. It has been shown that including the crack lengths in the computation of the crack density results in a better description of the damage state [29, 47]. Some efforts have been made to account for the length of the cracks by Quaresimin et al., grouping the cracks into eight categories based on their length and computing a weighted crack density based on manual crack counting [31]. The categories are based on the width of the specimen which could lead to changing distributions of crack lengths for various specimen widths. Also, for fatigue test campaigns, manual crack counting is extremely time-consuming because multiple images for each test have to be evaluated. This quickly becomes unfeasible for bigger campaigns. Therefore, it is apparent that automated crack detection, once the tools are accessible and easy to use, will replace manual crack counting.

Crack detection algorithms are described in the literature but to the knowledge of the author, no open source package or commercial programme was available before, *CrackDect*, an open source crack detection package was developed in this thesis (see Paper A). The package is based on a modular design and includes Glud's and Bender's crack detection algorithms (see Paper A and Paper A2) [35, 45]. Generally, this lack of open and available algorithms or methods as an easy-to-use package seems to be a common occurrence in engineering as many methods are presented in the literature but the code is not made accessible or only developed for in-house use. Since *CrackDect* was only developed because of the unavailability of crack detection algorithms, the author hopes that the practice of also providing the code for the presented algorithms will become the standard in the future.

1.4 Effects of loading parameters on off-axis cracks

Fatigue can be described as the degradation of material properties due to fluctuating loads. Real-world load spectra are usually irregular with a changing stress amplitude and frequency. An example of such a load spectrum is shown in Figure 1.9a. Fatigue experiments on the coupon scale are usually performed with sinusoidal load cycles as schematically shown in Figure 1.9b. It is evident that there is a difference between the loads in the tests and for real applications. It is well known that the evolution of fatigue damage is affected by changing frequencies and stress amplitudes as well as changing from tension to compression. Here, the most important effects on the evolution of fatigue damage are discussed in order to give a basic understanding of what must be covered by a universal fatigue damage model.

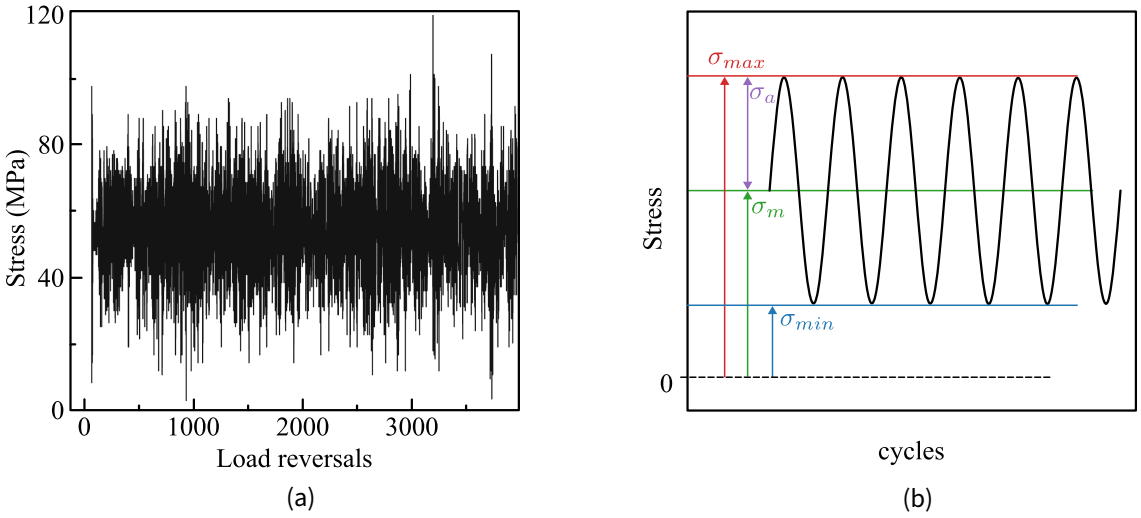

Figure 1.9: Example of a load history for wind turbine blades (a) from [3] and a schematic representation of the sinusoidal stress cycles for a fatigue experiment (b)

1.4.1 Block loading

A block load is referred to as a block with a certain amount of cycles of the same amplitude, maximal and minimal stresses and frequency. It is well known that when applying blocks with changing amplitudes, the fatigue life is affected by the order in which they are applied. Therefore, the fatigue life is not the same if a block with a low amplitude is applied before or after a block with a higher amplitude or vice versa. This sequence effect was shown by multiple researchers [13, 48–50]. Up to now, studies came to different conclusions about whether the fatigue life is longer for a high-low sequence or a low-high sequence [51]. Although various material systems, layups and material combinations might change the block loading effect, it is agreed that the Palgren-Miner's damage accumulation is not sufficient for composites. This damage accumulation method simply sums the damage of each block as given by

$$D = \sum_{i=1}^{k} \frac{n_i}{N_{fi}} \,, \tag{1.3}$$

where D is the measure for damage, n_i the number of applied cycles in the i$^{\text{th}}$ block and N_{fi} as the number of cycles to failure for the i$^{\text{th}}$ block [52]. This method was developed for metals and is widely used up to this day, even for composite materials, because it is easy to implement and does not require extensive test campaigns with block loading. The use of simply relating the applied cycles to the number of cycles to failure also has the drawback that the progression of damage is not considered. In this method, the damage is considered to grow linearly until failure, which is not the case for off-axis cracks. Also, differing damage mechanisms are not considered as well as the interactions between them. For matrix cracks, Bender et al. showed that the crack growth rate is highly dependent on the amplitude of the loading blocks and that there is a transition phase in the crack density growth rate when switching from a high amplitude block to a lower amplitude [35]. This is shown in Figure 1.10.

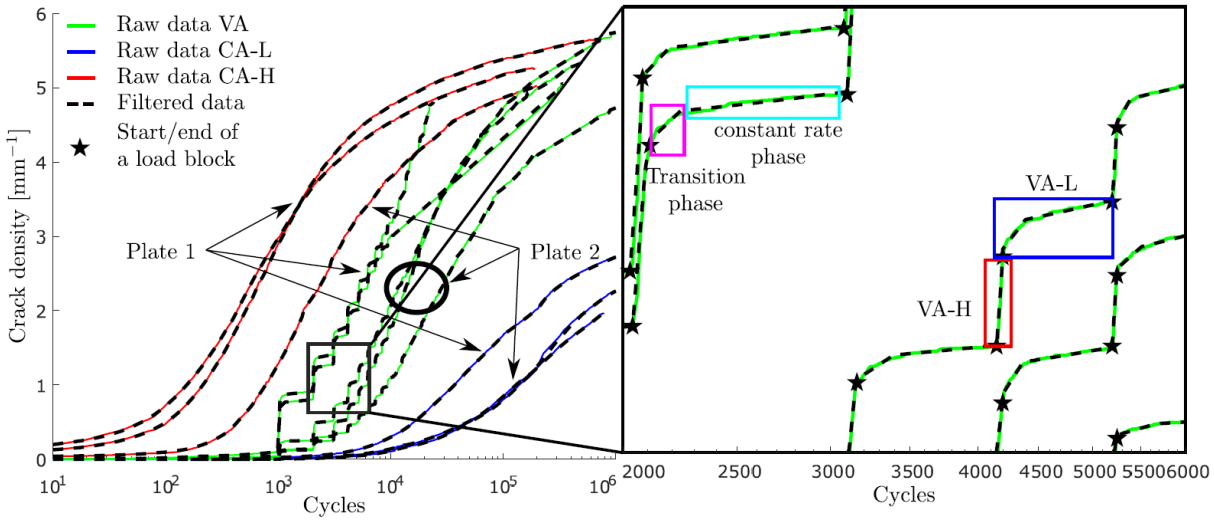

Figure 1.10: Evolution of the crack density for variable amplitude block loads. When switching between high and low amplitude blocks, the crack density follows a step-like pattern with a transition phase when switching from high to low amplitude [35].

The crack density for the alternating low-high amplitude blocks shows a step-like pattern. The low and high amplitude blocks show a relatively constant rate of crack growth. The transition phase only appeared when switching from high to low amplitude blocks as the crack growth rate slows down after the end of the high amplitude block. Note that a significant amount of crack density growth happens during this transition phase. When switching from a low to a high amplitude, no transition phase is spotted as the crack density growth increases nearly instantly and stays relatively constant for the duration of the high amplitude block. Overall, the diagram shows an S-like shape when plotted over the cycles on a logarithmic scale. Also, there is less absolute gain in crack density per high amplitude block at already high crack densities compared to the stage with low crack densities. Bender et al. also found

that the low-amplitude blocks are dominated by crack growth and the high-amplitude blocks are dominated by the initiation of new cracks. One explanation may be that during the high amplitude blocks the fracture process zone grows, since it scales with stress, as given by

$$\omega = \frac{1}{\pi}\left(\frac{K_I}{\sigma_y}\right)^2 \qquad with \qquad K_I = \sigma\sqrt{\pi a}\, f\left(a/W\right) \ , \tag{1.4}$$

where σ_y is the yield stress, a the length of the crack and $f(a/W)$ is a function of the geometry and the crack length. Although this equation for the process zone is strictly only valid for brittle materials, it shows that the process zone grows with the applied stress. In this zone, micro-damage grows in front of the crack tip [53]. For modelling fatigue on a macro scale, the specific micro damage might be not as important as the fact that the material in front of the crack tip is damaged. So, when the load is reduced and a block with a lower amplitude begins, the material in front of the existing cracks is already weakened. Therefore, the crack will grow for a certain distance until it grows out of the pre-damaged area and as it slowly grows out of this area, the crack density growth rate slowly comes down to the level of the low amplitude block. This could explain why there is a transition phase in the growth rate of the crack density. Also, the fact that the process zone is quickly enlarged when a high amplitude is applied but the crack needs to grow out of the enlarged process zone when changed to a low amplitude would explain why there is no transition phase for a change from a high to low amplitude. For a fatigue model that describes off-axis cracks on a macro level, not each matrix crack can be modelled and therefore, the crack density can be used as average damage of the material. These block-loading effects however must be implemented into a universal fatigue damage model.

1.4.2 Stress parameters

As already shown for static loading, the strength of composites is highly dependent on the stress state of the material. Even though static failure criteria compute a factor of effort to measure the current stress in relation to allowable stress, more information is usually needed to assess the type of failure. Puck's failure criterion provides additional information if fibre failure or matrix failure is the dominant failure mode. As shown in Figure 1.11 which shows an example of the well-known Puck diagram, matrix failure is further split into three distinct modes as three types of matrix cracks can be observed on the meso-scale. For positive transverse stress σ_{22}, the cracks are opened whereas, for negative transverse stress, the crack faces are pressed together. In the region of negative transverse stress, two types of cracks develop depending on the ratio σ_{12}/σ_{22}, as shown in Figure 1.11 by the straight line that separates mode B and mode C. In mode B, the crack grows in the z-direction whereas, in mode C, slanted cracks develop [26]. Compared to Puck'c criterion for fibre and matrix damage, LaRC05 differentiates even more failure modes for fibre failure and delamination [27]. The

three modes for off-axis cracks are also present in fatigue loading. Therefore, the effect of matrix damage on the laminate is highly dependent on the stress state.

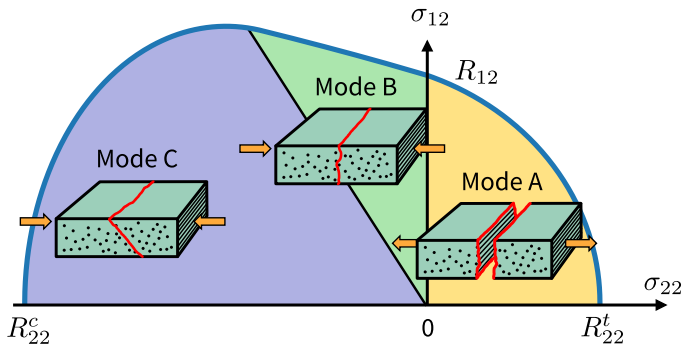

Figure 1.11: Puck criterion for matrix damage and plane stress. The three modes differentiate between opening matrix cracks, closed matrix cracks and closed but slanted cracks.

As already shown in Figure 1.9b, the fatigue load can be described by the maximum and minimum applied stress. The R-ratio given by

$$R = \frac{\sigma_{min}}{\sigma_{max}} \,, \tag{1.5}$$

is the ratio between the minimal stress σ_{min} and maximal stress σ_{max}. By testing at multiple amplitudes and mean stresses, the effect of tension-tension, tension-compression and compression-compression on the fatigue life can be described by a constant life diagram (CLD), as shown in Figure 1.12. However, the CLD does not provide information about the effects of fatigue damage or the active damage mode. As shown in Figure 1.11, the off-axis cracks can be opened or closed depending on the stress state. Especially the slanted cracks that form in Puck mode C acts as a wedge leading to delamination and local buckling [54].

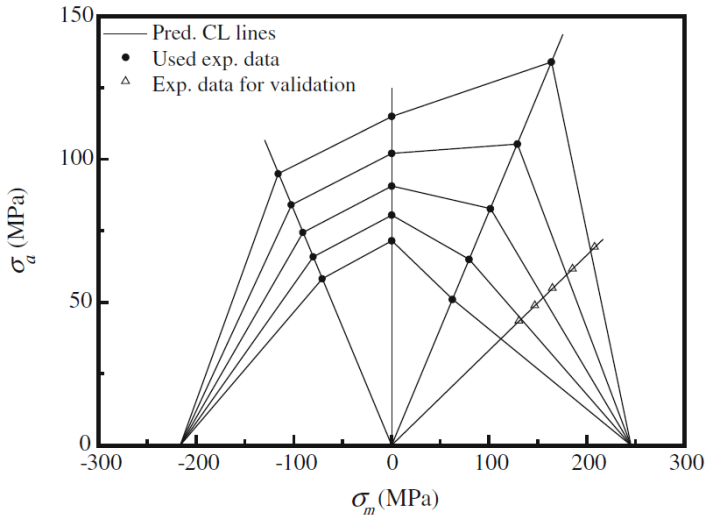

Figure 1.12: Example of a piecewise linear constant life diagram [3].

Quaresimin et al. showed that varying R-ratios have a strong influence on the initiation and propagation of off-axis cracks [55]. Fractographic images for tension-tension tests show several separate damage mechanisms. For tension-compression tests, no specific damage mechanisms could be distinguished because the fracture surface was run-down by the compressive part of the cycles. This shows that the off-axis cracks are temporally closed during compression. Furthermore, they showed that the local hydrostatic and local maximum principal stress can be used as fatigue strength for several R-ratios but only for tension-tension loading, yielding an SN-curve for each R-ratio that is valid for several multiaxial conditions. For tension-compression tests, the local damage mechanisms are not fully understood yet. However, experiments have shown that for tension-compression loading, the compressive part of the cycle has an effect on the initiation of off-axis cracks with higher negative load ratios accelerating the crack formation in cross-ply laminates [56].

During the compression, stiffness is regained because the crack faces are closed and force can be transmitted. This was shown by Brunbauer et al. when they compared the influence of the mean stress on fatigue damage [57]. This effect can be directly observed by looking at the stress-strain hysteresis for individual cycles, as shown in Figure 1.13 where hysteresis cycles at increasing cycle counts are shown for $R = 0.1$ and $R = -1$. For the tension-tension test ($R = 0.1$), the hysteresis cycles show a decrease of the dynamic modulus, which is the slope of the hysteresis cycle, and a shift to higher strains with an increasing cycle count. The tension-compression test ($R = -1$) also shows an increase in strain with the increasing cycle count and a distinctive kink when the stress changes from compression to tension. Similar to [55], Brunbauer et al. also observed smoother fracture surfaces for tension-compression loading compared to tension-tension. In addition, they also observed crushed fibre bundles when compression was applied.

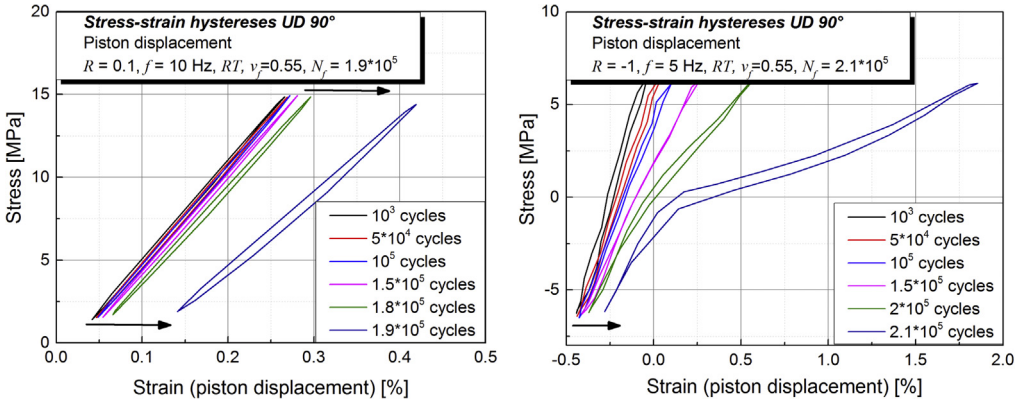

Figure 1.13: Stress-strain hysteresis for UD90° specimens with $R = 0.1$ (left) and $R = -1$ (right) [57]. The hysteresis cycle for $R = 0.1$ shows a shift to higher strains over the fatigue life and a decrease in the dynamic modulus. The cycles for $R = -1$ show a shift to higher strains and a distinctive kink when the stress changes from compression to tension.

Based on the work of Carraro et al. [25, 28] where they showed that the onset of off-axis cracks can be predicted with two master SN-curves for any global multiaxial stress state, Van

Paepegem et al. developed a framework to predict the damage onset for any stress ratio and load level [58]. This phenomenological crack initiation criterion is based on SN diagrams and uses one equation for tension-tension, tension-compression and compression-compression loading, respectively. Damage accumulation is assumed to be linear. Although the micro-damage modes active in the compressive regime are not as well studied and understood as for tension, local maximum principal stress is also used as the fatigue strength for compression. Two parameters, namely the contributions of the cyclic and monotonic part of the stress cycle, are used to compute the allowable cycles. One-parameter approaches like only using the R-ratio or mean stress have been shown to be insufficient [59]. Overall, the model form Paepegem et al. requires seven material parameters. Four parameters are needed for the tension-tension regime, two for compression-compression and one to account for the decreased fatigue life due to tension-compression loading. These parameters can be calibrated with seven SN curves for crack initiation. This model has shown good agreement with experimental results for glass and carbon-reinforced composites.

In addition to models based on SN-diagrams or constant life diagrams for the initiation of off-axis cracks, modified versions of the Paris-Erdogan law are often used [60, 61] to describe the growth of off-axis cracks. These empirical models create a relationship between the crack growth rate and a measure of the loading at the crack tip like the stress intensity factor, as shown in the original Paris-Erdogan law given by

$$\frac{da}{dN} = C(\Delta K)^m \ , \tag{1.6}$$

where da/dN is the crack growth rate, ΔK the range of the stress intensity factor in a cycle and C and m are material coefficients which are obtained by fitting this equation to experimental data. One such model has been developed by Carraro et al. where they used a multiscale strategy to describe the damage evolution [62]. After also using the local hydrostatic and local maximum principal stress to predict crack onset, the crack propagation is described by relating the crack growth rate (CGR) to the energy release rate (ERR). This model also takes the synergistic effects of crack initiation and propagation into account. Since each crack changes the local stress distribution and thereby shields a certain volume of material, new cracks are less likely to initiate near existing ones. The crack density in the non-interactive regime can be directly computed. This is only valid as long as the stress field in a ply does not change from cycle to cycle, i.e. when the crack density is low and the cracks are far enough apart that their effects on the stress field do not overlap. For the interactive regime, which is valid for higher crack densities, an iterative process is used to compute the growth of existing cracks as well as the initiation of new cracks in the vicinity of already existing ones. As shown in Figure 1.14, this model predicts the crack density as a function of cycles for a given loading scenario.

Up to now, no generally accepted model for the evolution of off-axis cracks is available that fully incorporates all effects of load types and load levels for off-axis cracks. Generally, empirical models that are based on SN curves and the Paris-Erdogan law are adapted and fitting parameters are used to describe synergistic effects. In contrast to this phenomenological or empirical approach, a more physical approach to fatigue is developed by Alderliesten [63] with a focus on delamination. The concept of strain energy balance is used for fatigue crack growth where the crack increases with each cycle. This leads to the governing equation for the strain energy release dU to be related to the crack increment da in a cycle N given by

$$\frac{dU}{dN} = \frac{dU}{da}\frac{da}{dN}\,, \tag{1.7}$$

where dU/da is the effective strain energy release rate G_{eff}. In fact, Alderliesten points out a few compelling arguments against using the stress intensity factor K or its range ΔK for fatigue crack growth. Firstly, the relationship between K and G

$$G = \frac{K^2}{E} \tag{1.8}$$

is derived for fixed-grip conditions and not for fatigue cycles. Therefore, the correlation between K and G is only valid for quasi-static conditions and the use of ΔK in fatigue is not automatically justified as the difference between K_{max} and K_{min} does not reflect the energy dissipation during fatigue. Secondly, experimental data for aluminium shows that ΔK is not an appropriate parameter to describe the similitude in fatigue. Thirdly, it is debated if fatigue crack growth is governed by stress or by energy. If it is governed by stress, $\Delta\sigma = \sigma_{max} - \sigma_{min}$ would be sufficient to describe the crack driving force. When considering the applied work to a specimen it is evident that this work is the sum of a monotonic and cyclic part $U_{tot} = U_{mon} + U_{cyc}$, which again, is not reflected in ΔK. It has to be noted that the work of Alderliesten focuses on deriving a physical theory of fatigue crack growth which should not be mistaken for a prediction model. Maybe, a better model for predicting the fatigue

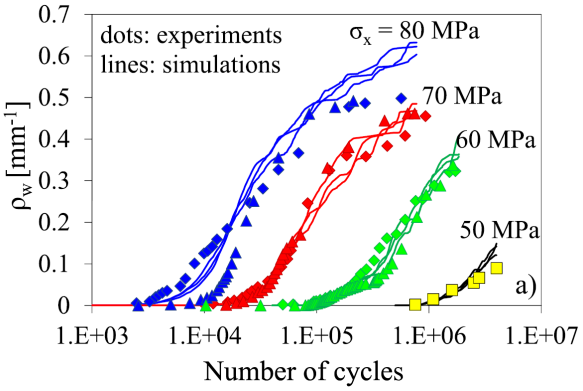

Figure 1.14: Prediction of the crack density by Carraro's model for several load levels.

crack growth can be derived from this work. Also, it has to be shown that this theory is also applicable to matrix cracks, where generally speaking, not one crack but many cracks are considered in a homogenised way and other factors like the fibres restricting the crack path must be accounted for. Nevertheless, this theory already shows promising results in giving the R-ratio effect a more profound physical interpretation [64, 65].

1.4.3 Frequency and hysteretic heating

The frequency of load cycles and hysteretic heating, which is the rise of temperature due to dissipated energy during a hysteresis cycle, are inherently linked. The higher the frequency, the faster the energy is dissipated. Once a certain frequency is reached, the temperature of the material rises due to more heat generated than what the material can dissipate away. The fact that polymers can be considered thermal insulators makes this effect noticeable even at relatively low frequencies [66]. It has been shown that higher frequencies mostly affect the polymer matrix of a composite [66, 67]. Carbon and glass fibres have high melting points compared to the glass transposition temperature of polymers [68]. Therefore, if the temperatures of the material may already get to critical values for the matrix, the fibres are still mostly unaffected. At these temperatures, the stiffness of the matrix is reduced which reduces its ability to transfer loads between fibres.

The energy dissipation is caused by the visco-elasticity of the matrix, damage formation and damage growth as well as internal friction [69]. For sinusoidal cycles without a change in frequency and amplitude, the visco-elastic part of the dissipated energy can be considered to be constant as long as the temperature does not significantly influence the viscous properties of the matrix. Therefore a change in dissipated energy comes from damage formation, damage growth and internal friction. This makes it possible to use the dissipated energy as a measure for damage [70]. The downside of this method is that individual contributions of several damage mechanisms can not be resolved by measuring the dissipated energy alone since the formation of all damage and internal friction contributes to the total dissipated energy. Therefore, it is not a reliable way to quantify damage of a specific damage mode. However, the change in temperature due to hysteretic heating can be used to localise damaged areas [71], as shown in Figure 1.15.

The energy dissipation due to high frequencies is also dependent on the laminate layup. Laminates that are subjected to shear stress show higher dissipated energies than stresses in or transversal to fibre direction [4, 72]. This can be attributed to higher internal friction at crack faces during shear compared to simply opening and closing crack faces for transverse stresses [73]. This leads to problems with tests of laminates that are subjected to mostly shear stresses, like fatigue tests of $[+45/-45]_s$ laminates. Due to the high dissipated energy and subsequent rise of specimen temperature, the comparability of test results between other layups that are

not subjected to shear stresses may be questionable. This was shown by extending the fatigue life of a specimen simply by using a fan for cooling [74]. Therefore, it is important to choose a test frequency where hysteretic heating does not lead to significantly elevated temperatures once damage starts to form. For matrix-dominated laminates, the frequency may be reduced to 5Hz or lower to stay in an acceptable temperature range [75].

The temperature of the material is also influenced by the geometry of the laminate since it influences heat dissipation. The thicker the laminate, the longer it takes to dissipate heat from the middle layer to the surface due to the relatively low thermal conductivity of polymers. This means that the fatigue life is also a function of the shape and size of a composite structure [76]. However, since composite structures are mostly made from relatively thin laminates compared to all other dimensions, this effect may be insignificant compared to the effect of high frequencies on the matrix and other more prominent effects like block loading.

1.4.4 In-situ effect

It is a well-known design rule to avoid stacking plies with the same fibre orientation due to a reduction of strength by doing so [6]. The effect of the ply thickness on the strength of the ply is called the in-situ effect and is shown in Figure 1.16 [77].

Over the past decades, several experimental and analytical models to determine the static in-situ strength have been proposed [77–80]. The in-situ effect can be explained using fracture mechanics. The initial size of a defect cannot be greater than the thickness of the ply. Therefore, thinner plies have automatically smaller defects. After the initiation phase, which is stress-dependent, the crack growth is governed by the energy release rate, which correlates with the square toot of the ply thickness. This means the thinner the ply, the lower the energy release rate and the slower the crack growth [81]. Analytical models usually use

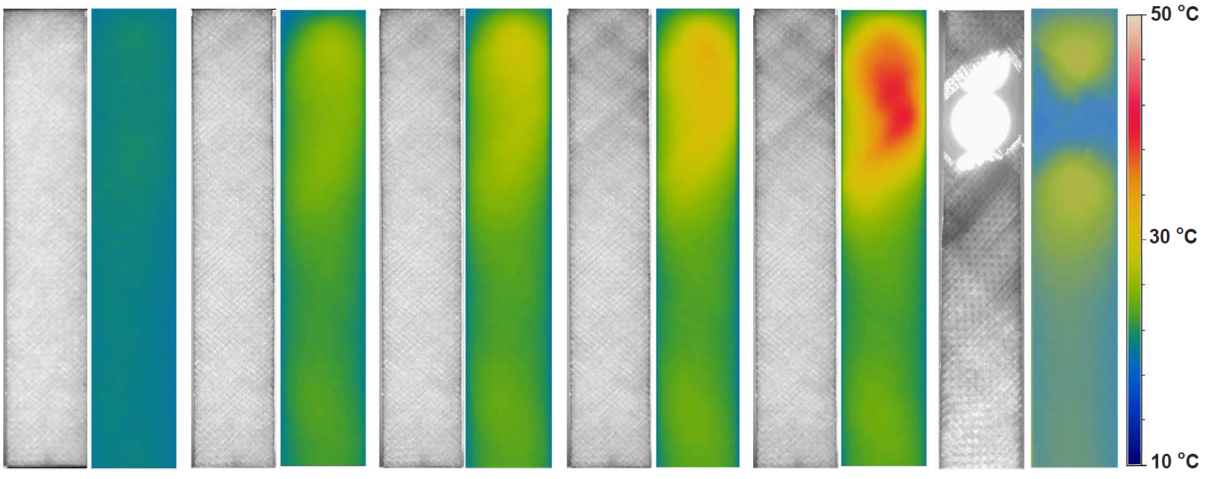

Figure 1.15: Transilluminated white light image and thermal image of a specimen during the fatigue life by [69]. The localised damage is clearly visible in the thermal images.

a fracture mechanics approach to predict the in-situ strength based on the critical energy release rate for crack propagation. The strength of a ply is also affected by the location of the ply in the laminate. Neighbouring plies change the conditions for crack growth and therefore, the in-situ effect is dependent if the ply is embedded between other plies or not [27].

When studying the stress distribution in cracked plies in the vicinity of the cracks, it was found that the maximal reachable crack density is affected by the thickness of a ply, as reported in [78] for static and [46] for fatigue tests. Thinner plies tend to reach higher crack densities than thick plies. The distance between cracks is limited by the stress that can be transmitted from the neighbouring layers, since stresses cannot be transmitted through opened cracks. The maximal crack density can be estimated with shear lag models which have been shown to give good estimations of the saturation crack density [27, 82].

The in-situ effect is well-studied for static loading. For fatigue loads, it has been shown that the ply thickness has an effect on the maximum crack density. It has to be noted, that testing the influence of the R-ratio for multiaxial stress distributions already requires an extensive test campaign. From an engineer's perspective, testing laminates with comparable ply thicknesses as the final structures is an easier solution than incorporating the ply thickness into the test campaign, especially when effects like block loading and the influence of R-ratios, mean stress and other stress measures must be tested due to a lack of a universal theory for fatigue. Nevertheless, a universal fatigue model has to reflect the effect of the ply thickness on the evolution of off-axis cracks.

1.4.5 Environmental influences

A large number of possible environmental influences like temperature, moisture, physical and chemical ageing of the material and other factors are mostly very specific to a particular use case. Temperature, moisture and UV exposure are common problems for components used in

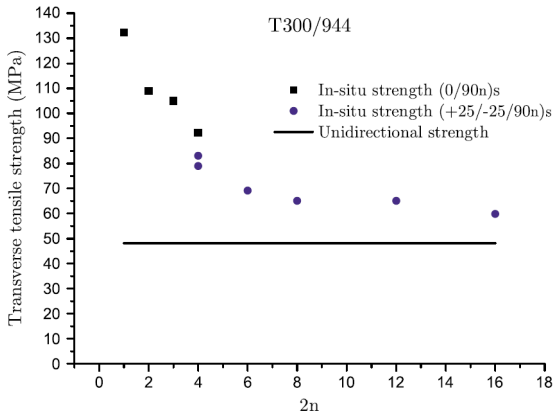

Figure 1.16: In-situ effect in laminates from [77]. The trend towards a minimal strength for thick plies is evident.

outdoor applications like wind turbine blades, aircraft, automotive or outdoor sports-related products. Usually, the matrix and the matrix-fibre interface are affected more than the fibres [4]. This has consequences on the ability of the matrix to transfer loads to the fibres which can lead to a reduction of strength and fatigue life.

Glass and carbon fibres are mostly unaffected by temperatures up to 300°C, which is already above the service temperature of most matrix materials [83]. In general, polymers become softer at high and more rigid and brittle at low temperatures. Therefore, it is usually the polymer matrix that limits the service temperature of the composite. Changing temperatures, especially temperature cycles has shown to cause off-axis matrix cracks which reduce mechanical properties [84, 85]. This is explained by stresses as a result of differing thermal expansion coefficients between the polymer matrix and the fibres. On the micro-scale, this mismatch between the thermal coefficients induces stresses in the fibre-matrix interface. On the mesoscale, thermal stresses are induced by varying fibre orientations because of the anisotropic thermal coefficients of the ply. Thermal stresses can result in a similar crack pattern as mechanical loads with comparable crack densities [86]. The influence of constant elevated temperatures on the fatigue life has been shown by Kawai et al. [87]. They showed that the slope of SN-curves is steeper for higher temperatures but its shape is mostly unaffected. Also, the hysteretic heating adds to the effect of already high temperatures accelerating the damage accumulation and shortening the fatigue life even more. A direct measure of the crack density at the edge of the specimen also showed that the crack growth rate increases with the temperature and that mechanical and thermal cycles lead to comparable crack densities [88]. Miyano et al. proposed a method which uses master curves derived from multiple tests for creep strength, fatigue strength and constant strain rates at varying temperatures to predict the fatigue strength for any combination of temperature, frequency, and tensile load for unidirectional composites [89]. A model with less experimental effort to predict the fatigue life of glass fibre-reinforced composites is presented by Cormier et al. [90]. However, only tension in the fibre direction can be taken into account. Until now, no sophisticated model to predict the effects of the temperature on off-axis damage exists.

Similar to temperature expansion, expansion due to moisture also leads to stresses in the composite laminate. In contrast to temperature, which can rise and fall at relatively high rates, moisture intake usually happens at a much longer timescale [91]. Therefore thermal and hygral stresses are usually unrelated. Like thermal stresses, stresses from hygral expansion on the mesoscale can be accounted for by classical laminate theory by simply adding an extra term for each effect, as given by

$$\left\{\begin{array}{c} n \\ \hline m \end{array}\right\} = \underbrace{\left[\begin{array}{c|c} A & B \\ \hline B & D \end{array}\right]\left\{\begin{array}{c} \varepsilon^\circ \\ \hline \kappa \end{array}\right\}}_{mech} + \underbrace{\left[\begin{array}{c|c} A^h & B^h \\ \hline B^h & D^h \end{array}\right]\left\{\begin{array}{c} h \\ \hline \nabla h \end{array}\right\}}_{hygro} + therm + \dots , \tag{1.9}$$

where n and m denote the in-plane actions and bending moments, A, B and D the tensors of extension, coupling and bending, respectively, ε° and κ the mid-plane extension and curvature tensor as well as h and ∇h the moisture concentration and gradient of moisture concentration. In principle, all effects that add to the strain tensor ε can be accounted for with classical laminate theory. The degree of moisture expansion for a given laminate is highly dependent on the matrix type with epoxy matrices being generally more prone to moisture absorption than vinyl ester or urethane-based matrices [92]. Besides adding stresses on the macro level, moisture also affects the strength of the composite. Generally, moisture reduces the strength of the matrix which leads to damage at lower stress levels for static and fatigue loading. This effect scales directly with the moisture uptake of the matrix up to a saturation value, which is material dependent. After this saturation, additional exposition to water does not further affect the composite [93]. Because the effects of moisture exposure take usually a long time to develop, they are often treated similar to ageing of the material. Even though moisture intake is reversible, it is often linked to irreversible effects caused by the moisture exposure. Ageing can be defined as the entirety of all irreversible chemical and physical processes occurring in the material over time. This has effects on fatigue behaviour, which is the degradation of material properties due to fluctuating loads. For real-world applications, it is important to take both effects into account. For example, in tidal turbine blades, it is essential to account for moisture intake since it has been shown that this severely affects the mechanical properties of the composite and shortens the fatigue life [94]. Fatigue models usually only compute the effects of load cycles at certain stress levels based on the (fatigue-)strength, stiffness and other mechanical properties. For such models, a first estimation of the effects of ageing is possible by using mechanical properties for aged materials. However, this usually does not cover synergistic effects for damage growth. For this, models must be adapted and calibrated, which further adds to the number of needed tests. For practical use, several effects are usually deliberately omitted to keep the complexity of the models and particularly its calibration within reasonable limits [5].

1.5 Cycle counting

Simulating variable amplitude loads as shown in Figure 1.9a in FEM models in detail is only possible for a few cycles. Therefore, methods to compute the combined effect of cycle blocks are commonly used. For this, the variable amplitude time series must be converted into countable cycles which are then categorised into distinct groups. It has to be noted that the definition of a cycle varies with the counting method. The following cycle counting techniques are commonly used [95]:

- *Peak counting*: Peaks and valleys are simply counted. The highest peak is combined with the lowest valley to form the most damaging cycle. Then, the second-highest values are

used and so on. After this, the cycles can be categorised into groups. What counts as a peak or valley is relative to a defined reference load.

- *Mean crossing*: A variation of peak counting where only the highest peak and lowest valley are counted per crossing of the mean value. This reduces small amplitude loads.

- *Level crossing*: A set of load levels is defined that marks the groups for categorising the cycles. The cycles are counted by counting the level crossings of the defined load levels. Crossings when the slope of the time series is positive are marked as positive crossings and the crossings when the slope is negative are marked as negative crossings. Then, the most damaging cycle is created by combining the highest number of successive crossings in the positive and negative directions followed by the second highest number of crossings for the second most dangerous cycle and so on.

- *Rainflow counting*: This algorithm received its name from water falling onto a pagoda, an east-Asian tower with successive roof edges. It extracts closed cycles from a variable amplitude time series by rotating it vertically and mimicking the flow of water down the time series. Each positive peak can be imagined as a water source. The half cycles are counted if the flow of water merges with a flow from an earlier peak or reaches the end of the time series or falls onto another bigger peak. This is repeated for compressive peaks and the half steps with the same magnitude are paired to get full cycles [96].

Up to now, no consensus of which method is best suited for the categorisation of cycles has been reached. One of the most commonly used methods for composite materials is rainflow counting [97]. It has the advantage that hysteresis loops are counted instead of simple crossings of certain stress values. Also, this method always yields closed loops, which can be an important feature for practical applications. For isotropic materials, rainflow counting has been extended to multiaxial load histories by using the relative Mises strain as an indirect measure of damage [98, 99]. Unfortunately, this is not possible for composite materials since the Mises stress or strain is not sufficient to characterise the effort of the material under loading. For composites, the critical plane method is often used for multiaxial load histories [100]. For this, a set of planes are defined in the stress space. The multiaxial stress state is projected onto the defined planes which effectively reduces the stress tensor to a single measure suitable for rainflow counting. Each of the planes yields a separate damage variable. The critical plane is then defined as the plane with the highest damage. An example of the application of this concept is the rainflow counting algorithm for composite materials in the commercial software FEMFAT [101] where it is combined with Puck's failure criterion. For matrix failure, the multiaxial stress is projected onto several predefined planes, which are depicted as lines in the Puck diagram shown in Figure 1.17. These stress values are then used to compute the effort of the material with Puck's failure criterion for each plane. This also allows to differentiate between the three failure modes of Puck's criterion [102].

1.6 Off-axis damage models

When developing a fatigue damage model, the aim is to predict the failure of a structure. The first obstacle to overcome is that failure can mean various things depending on the application. This is true especially for composite materials, since they show a progressive damage profile. For example, damage onset in the form of matrix cracks is already considered to be the point of failure for fuel and pressure vessels, whereas for wind turbine blades, bicycle frames or automotive frames, the stiffness and strength must be kept within certain limits even when damage is present, which allows for a damage tolerant design [103]. This leads to the concept of "design against failure", where failure is defined depending on the application. Over the past decades, many models have been proposed to predict the failure of composite laminates with varying degrees of complexity. It has to be noted that the definition of failure also varies from model to model. Degrieck et al. categorised fatigue models into the following general groups [104], which are summarised here.

- *Fatigue life models:* The number of cycles until failure is predicted based on SN-diagrams or CLD-diagrams. This type of model does not take individual damage modes or damage accumulation into account. Also, stress redistribution due to damage is ignored. In general, these models use empiric equations to directly correlate stresses, strains, energies etc. to the number of allowable cycles. The main advantage is their relative simplicity. However, for each new stacking sequence, new experiments are required.

- *Phenomenological models:* The residual stiffness or strength of a laminate or material is computed based on a proposed evolution law. The model computes the residual properties directly based on macroscopic properties like stress state and the number of cycles without taking actual damage and stress redistribution into account. No information about the damage state in the material can be made with such a model.

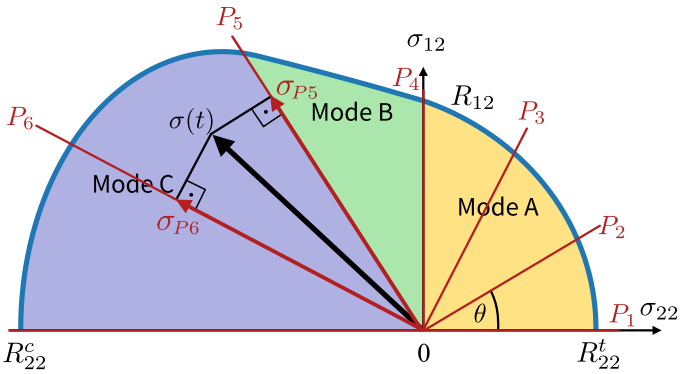

Figure 1.17: Schematic representation of the critical plane concept used in the software FEMFAT. The stress $\sigma(t)$ is projected onto each plane P_1 - P_6. The critical plane is the plane with the most critical stress σ_P according to Puck's failure criterion. Here, only two projected stresses σ_{P5} and σ_{P6} are shown to keep the image simple.

- *Progressive damage models:* A damage variable is used to describe the evolution of each damage mode. Based on this damage, the effect on mechanical properties (strength, stiffness etc.) is computed. This allows to individually track the progression of each damage mode. Due to a drastic increase in computational effort, a multi-scale approach is often applied to simulate effects on several length scales.

Many models are specifically designed for specific stacking sequences. This has advantages because it vastly reduces the complexity of the model. The downside is that these models must be calibrated for each stacking sequence, which can be practically impossible for big structures with many local layup configurations [104]. Therefore, any universal fatigue damage model needs to be ply-based for practical applicability. Ply-based approaches also make multi-scale modelling possible and allow for the optimisation of the stacking sequence.

Progressive damage models are considered to be the best candidates for a universal fatigue model since they compute the evolution of damage and its effect on mechanical properties, which can be done separately for off-axis cracks, diffuse delamination and fibre failure [104]. With this separation of the damage types, synergistic effects between each damage type can be considered separately. This is not possible for fatigue life models, since the evolution of damage is not quantified. Also, progressive damage models allow components to be designed with the premise of damage-tolerant design principles, more so than fatigue life and phenomenological models. As already mentioned, no universal fatigue damage model exists up to now that fully covers the whole fatigue life of an arbitrary composite laminate [105]. This is still an ongoing challenge in the field of mechanical engineering but considerable advancements have been made in the past decade. Most models are empirical in nature as they build on empirical concepts like SN-diagrams or other empirical models to describe damage formation and growth [5]. The current work focuses on off-axis cracks and models to describe their formation and growth. Since there are multiple fatigue damage models, only a few select are presented in greater detail here. Especially the models currently developed at the University of Padova and the University of Ghent, which have been in development for approximately the past decade, show great potential. It has to be mentioned that both models have a high degree of complexity and multiple material parameters must be tested to calibrate them for a new material system. Up to now, these models are not available in commercial programs as they are still in development.

Most progressive fatigue damage models are built from sub-models that perform a specific function. Many modern fatigue damage models use a multiscale approach to accurately predict the effects of damage on mechanical parameters at the micro-scale. These parameters are then used in models at the meso- and macro-scale with the advantage that these meso- and macro models only need sufficient complexity to compute effects on the meso- or macro scale [106]. Most modern fatigue damage models consist of the following sub-models [107]:

- *Damage initiation:* A model for damage initiation based on the stress state is needed. For progressive damage models, SN-diagrams for damage initiation are often used since they give a direct relationship between stress and cycles until initiation.
- *Damage progression:* After initiation, damage progression must be modelled. This is often done by fracture-mechanics-inspired models like da/dN diagrams. Since stresses have a big influence on the growth of damage, stress redistribution in the laminate must be accounted for, which is usually accomplished by a subsequent stress analysis.
- *Damage effect:* The effect of damage on mechanical parameters can be computed with multiple methods. Often analytical micromechanical models are used to compute the effect of a specific damage type on stiffness or strength. Analytical micromechanical models are computationally inexpensive compared to finite element models which is an important requirement for practical usability.
- *Stress analysis:* The stress distribution in each ply is the basis for the sub-models that compute damage formation and growth. However, damage influences the stress distribution in the plies, which must be accounted for. As the stiffness of damaged plies degrades, the stresses in the neighbouring plies rise. This changes the boundary conditions for the sub-models that compute the damage formation and growth. Therefore, fatigue models usually incorporate an iterative computation scheme.

1.6.1 Padova

The Composite Group at DTG-University of Padova is developing a fatigue damage model. This is mostly driven by P. A. Carraro and M. Quaresimin, with the goal to develop a design framework for the prediction of fatigue damage from initiation to final failure [103]. Over the past decade, their advancements and building blocks of the framework have been published in multiple papers [28, 62, 108, 109]. The backbone of the framework is the so called "optimal shear lag model" for computing the effect of off-axis cracks on the stiffness of a laminate. This model combines the *stress analysis* and the *damage effect*. A shear lag model is a model where the stress transfer between an interface is described with shear stresses [110]. In this particular bi-dimensional shear lag model, stresses are transferred between uncracked and cracked plies. The model is applicable to symmetric laminates made from $2n-1$ plies of arbitrary thickness and orientation. Another prerequisite is that all plies are of the same material. Cracks can be introduced into the $2n$ plies and the symmetry condition is applied to the middle layer. The basis is a shear lag analysis of a single cracked ply where the displacement in the plies is assumed to be a parabolic function. The system of equilibrium equations for the stresses results in a system of homogeneous differential equations. It has to be mentioned that the solutions to these equations are not trivial. In the case of a ratio between longitudinal and transverse Young's modulus of 0.1, the solution can be expressed as a linear combination

of the undamaged laminate and the perturbation of the stress field from the cracks. Since this solution is used for further derivations of the stiffness of the damaged laminate, this makes the model only applicable to materials with a longitudinal Young's modulus of at least ten times the transverse Young's modulus. Although this might be not a problem for carbon fibre-reinforced polymers, it could limit its usability for composites with less difference between ´ longitudinal and transverse stiffness. From the solution of the system of differential equations and a set of boundary conditions, the averaged ply stresses are computed. The plane stress compliance matrix is then computed directly from the global strains, which are part of the boundary conditions and therefore known, and from the ply stresses. This allows to directly compute the plane stress stiffness matrix of the laminate as a function of the crack density. For laminates with more than one cracked ply, an interaction model based on the work of Kachanov is used [111]. It is based on the superposition of various configurations of cracked and uncracked laminates. One advantage of the interaction model is that it can be used with any model that can calculate the effect of cracks on the stiffness of a single ply and not only the optimal shear lag model for a single cracked layer [108]. This shear lag model has also been extended to include diffuse delamination by assuming that no shear stress is transferred in the delaminated areas [109]. The resulting system of differential equations is similar to the model without diffuse delaminations and the same prerequisite for Young's moduli applies. The authors report a good agreement between the model and experimental results for $[0_x/90_{2x}]_s$ laminates and finite element models for laminates with 0°, 90° and ±45° plies in various layup configurations.

For the part of *damage initiation*, the damage-based model for crack initiation is used [28], which was already discussed in section 1.4.2. It is based on computing the local hydrostatic stress σ_h and local maximum principal stress σ_I at the micro-scale. With the stresses at the micro-scale, the cycles for crack initiation are determined from SN diagrams for σ_h and σ_I, respectively.

Damage progression is computed with an iterative process. The model is mentioned in section 1.4.2 as an example for computing the evolution of damage based on a Paris-Erdogan relationship [62]. A schematic representation of the model for crack density evolution is shown in Figure 1.18. The crack propagation model is separated into a non-interactive and interactive region. In the non-interactive region, the crack density is low and cracks are on average far enough apart that the perturbation of stresses from one crack does not affect the stress distribution of another. In the interactive region, the influences of the stress perturbations between cracks must be accounted for. The model starts with a representative laminate that is divided into elements. Each element is assigned a strength according to a Weibull distribution. The parameters of the Weibull distribution must be calibrated to the material. This reflects the statistical distribution of strength in a real laminate due to imperfections in the material and ensures that during the iterative procedure, not all elements of the representative laminate crack at exactly the same time. For the non-interactive and an interactive regions, separate

crack propagation laws are used. As shown in Figure 1.18, the damage state for each ply is updated in each iteration, where the damage state of each element and each ply is recomputed. If an element already contains a crack, the growth of this crack into adjacent elements is computed based on the energy release rate. If the element does not contain a crack, it is checked if a crack will initiate. If this is the case, a crack with a defined initial length is added to the element. The authors report a good agreement between the model and experimental results, as shown in Figure 1.14.

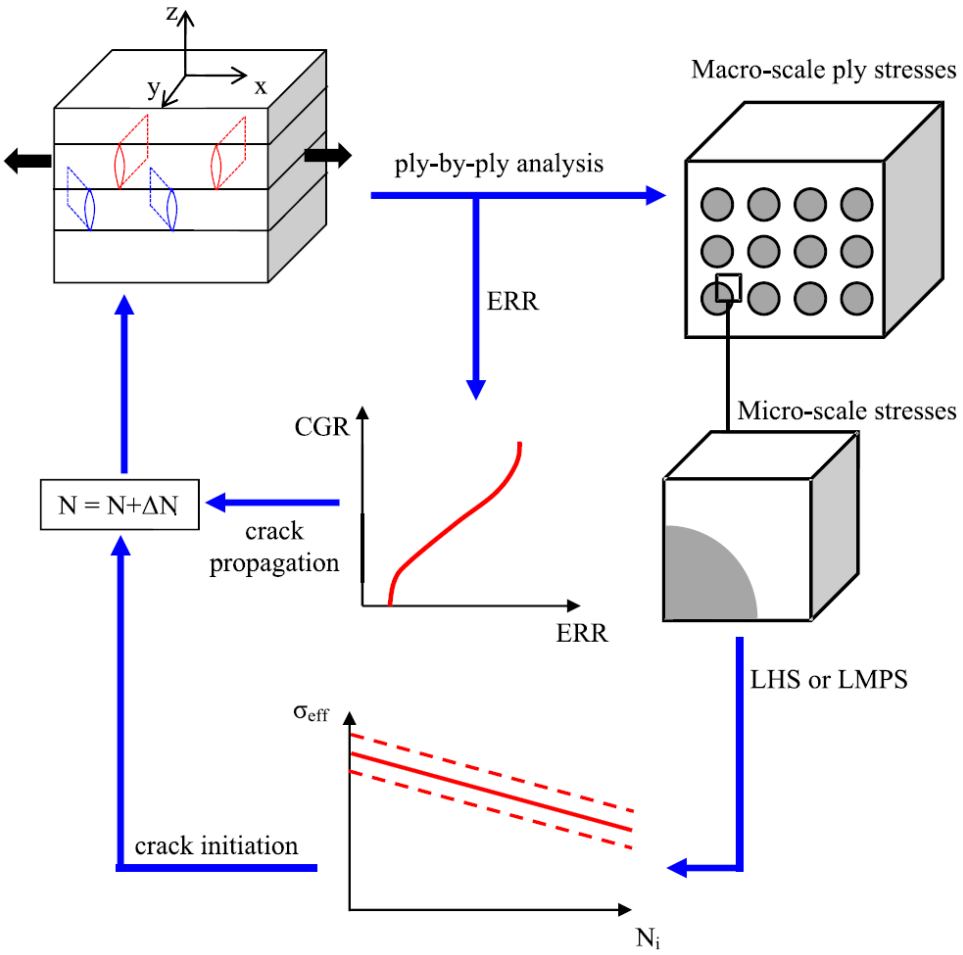

Figure 1.18: Schematic representation of the model for off-axis crack propagation from [62].

Even though the shear lag model is capable of computing the effect of diffuse delamination and off-axis cracks, no model to compute the onset and propagation of diffuse delamination similar to the off-axis cracks is proposed yet. An experimental campaign targeted at the effects of off-axis cracks on diffuse delamination has already been published [112].

Overall, this fatigue damage model focuses on off-axis matrix cracks with the capability to be extended to diffuse delamination. The sub-models for crack initiation and propagation are empirical since SN diagrams and a Paris-Erdogan law is used. Nevertheless, a strong focus is put on modelling physical phenomena in a multi-scale approach. For the computation of the stress concentration factors for local hydrostatic stress and local maximum principal stress, a finite element model is needed. The advantage is that the concentration factors are

only dependent on the material and fibre volume fraction and can therefore be computed in advance [28]. Without this, iterating over multiple elements in multiple plies for multiple time steps and computing the local stresses would be not feasible. The advantages of this model can be summarised as:

- An analytical model to compute the effects of off-axis cracks and diffuse delamination directly from the crack density without any calibration is used.
- The point of crack initiation is computed based on stresses at the micro-scale. Only two master curves for multiaxial laminates with positive transverse stresses are needed, which reduces the number of tests needed for material characterisation.
- The sub-models can be used separately as they have only weak dependencies on each other.

Up to now, the model is only tested against tension-tension fatigue data (R-ratio > 0). In the crack propagation model, the effects of tension-compression or compression-compression are not included and not discussed in the publications. It has to be shown if the model can still predict the effects for other loading scenarios than tension-tension or if the model must be extended. Even with the reduction in necessary tests for the model for crack onset, the testing effort for the calibration of all material parameters is high.

1.6.2 Ghent

At the department of materials science and engineering at the University of Ghent, a variational model to compute the stress and displacement fields in laminates with cracks is under development [113]. A variational approach means that the complementary energy in a system is minimised. Same as the optimal shear lag model discussed in section 1.6.1, this model combines the *stress analysis* and *damage effect*. The basis of the current model was developed by M. Hajikazemi et al. at the Amirkabir University of Technology, Tehran [114]. The goal is to find the stress and strain field in a laminate with a cracked layer. The variational method computes the unknown functions of the perturbation stress from the cracks based on a set of boundary conditions. This results in a set of differential equations for the stress field, which is solved numerically. From the stress field as a function of the load case, the effective engineering constants of the cracked laminate can be computed [115]. The first model was published in 2014, which was only applicable to symmetric laminates and has since been extended to arbitrary, non-symmetric laminates [113], cracks and delamination [116] and the effect of free edges on the stress field [117]. It has to be mentioned, that the extensions for delamination and the free edge effect are only applicable to symmetric laminates. Also, the model is only capable of computing the effect of cracks in one direction. However, compared to the optimal shear lag analysis which can predict the effects of cracks in multiple directions, the variational

model can predict the in-plane and out-of-plane thermo-elastic properties. Another closed-form analytical model has been developed by H. Ahmadi et. al. at Ghent to compute the mechanical properties of a laminate with cracks in multiple plies [118]. Contrary to the shear lag or variational models, this takes a simpler approach by computing the effects of cracks in multiple plies with a finite element model and using these results to fit the curves for the engineering constants of the laminate. However, it is also limited to symmetric laminates and each stacking sequence and configuration of cracks in the plies basically needs a new analysis of the finite element model.

For *damage initiation*, a model for the initiation of off-axis cracks for arbitrary load ratios and load levels has been developed by Van Paepegem et al. [58]. As already discussed in section 1.4.2, this model basically extends the crack initiation approach by Carraro et al. [28].

Recently, a model for *damage progression* was presented by M. Hajikazemi et al. [119], which uses an extended energy-based criterion. However, it was only demonstrated for static loads and no extension to fatigue is available up to now.

1.7 State of Art - summary and conclusion

The Ghent model shows a lot of similarities with the framework currently developed in Padova (see section 1.6.1). Both focus on an analytical model to predict the mechanical properties of a laminate with off-axis cracks and delamination. The restrictions for both are also similar, as the model from Padova is fully restricted to symmetric laminates with damage in both symmetric plies, as most of the models from Ghent. From the published works, it seems that Padova is more focused on a framework designed to be applied at the component level as an extension to currently used engineering software. Overall, both models are not complete, as damage progression, especially for tension-compression and compression-compression is still not fully covered. For both models, it is assumed that the faces of the off-axis cracks do not carry any load. In fact, the condition of a stress-free crack surface is part of the boundary conditions to solve the systems of differential equations for the stress fields. This means that the stress fields for compressive loads can not be predicted, since the load-carrying capacity of the closed cracks (as discussed in section 1.4.2) is neglected. Besides their similarities in general approach, the two models also show similarities in their restrictions and demonstrate, how far progressive fatigue damage models have come in the past decades, but also what is still missing. This is most prominent by their restriction to symmetric laminates with damage in both symmetric plies. Parts of the Ghent model are already extended to arbitrary laminates, but only with damage in a single orientation. The restriction to symmetric laminates with damage in both symmetric plies fundamentally prevents the use of such models for real-world applications, as it not only restricts their use to symmetric laminates but also for laminates subjected to bending loads. As shown in Figure 1.19, a bending load results in a non-symmetric

stress distribution, even if the laminate is symmetric. This means that the stress states in the upper and lower plies are different, which affects the formation of damage. Therefore, damage in the two symmetric plies will develop differently, which is not covered by the model, since both symmetric plies must have the same damage. For non-symmetric laminates, bending loads are unavoidable and therefore, the restriction to symmetric laminates with damage in both symmetric plies is a problem for real-world applicability.

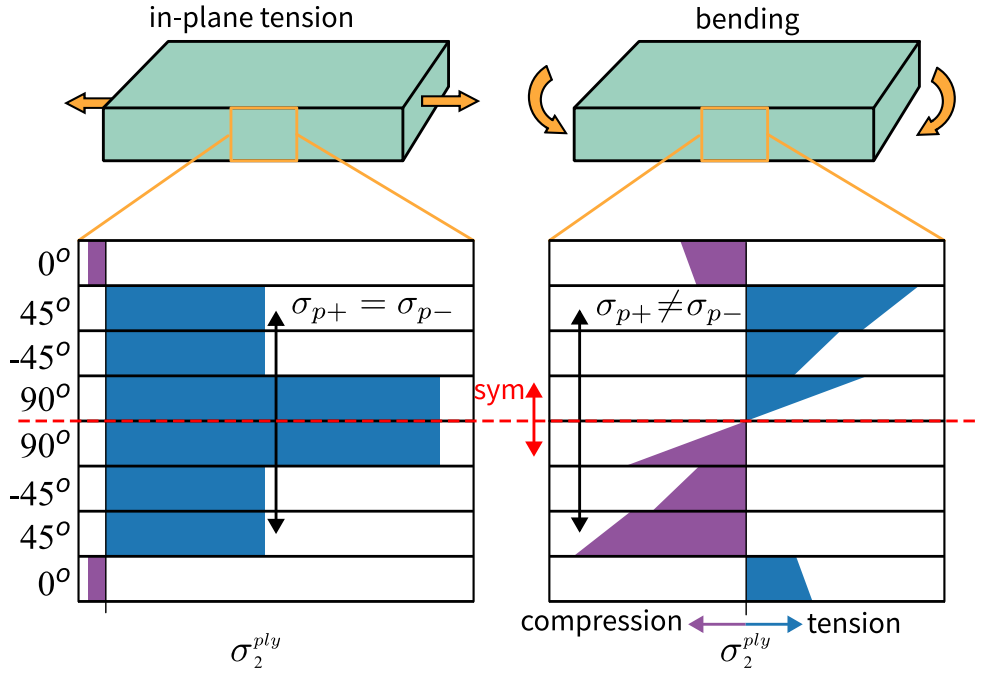

Figure 1.19: Schematic representation of the stress state for a $[0/+45/-45/90]_s$ laminate transverse to fibre direction in the ply-coordinate system for an in-plane tension load and bending. As shown, even for symmetric laminates the stress state is not symmetric for load cases involving bending.

There are other progressive damage models aimed to predict the effect of fatigue on composite laminates, but to the author's knowledge, none of them provide a complete framework for efficient fatigue damage modelling like the two models currently developed in Padova and Ghent. Zhou et al. presented a progressive damage model based on finite element analysis [120]. For each fixed amount of cycles, the whole finite element model must be recomputed, which is feasible for smaller models like specimens, but not for large structures [106]. A similar approach was used by E. N. Eliopoulos, who implemented an algorithm called FADAS, which stands for Fatigue Damage Simulator for various finite element formulations to be used in commercial finite element software [121]. This approach is based on Puck's failure criterion [54] and the degradation of strength and stiffness is computed with empirical formulations. The fatigue life is predicted with CLD diagrams, which requires extensive experimental campaigns to fit all parameters. Another approach often seen is to adapt static progressive damage analysis based on the finite element method to fatigue. Engelstad et al. [122] compared nine analysis methods that are based on discrete damage analysis for static and fatigue loads [123]. For static loads, most methods showed consistent results. The results for fatigue showed sig-

nificant inconsistencies and predictions of incorrect failure modes. The models often needed considerable recalibration with experimental data to reach satisfactory results [124]. The authors of this study concluded that the accuracy of the compared methods is quite low for fatigue. Also, algorithmic errors were found in some methods, which shows that potential users should be cautious with methods that are not well-established and thoroughly verified. It has to be mentioned that this comparison was made for open-hole tension specimens with multiple layup configurations and only for constant amplitude loading at an R-ratio of 0.1, which can be considered one of the simplest fatigue load cases.

This summarises that there is still considerable engineering effort necessary to push progressive fatigue damage models to a point where they can be considered well-established and proven for real-world use. However, promising models are currently under development. Even though they have still major restrictions which will prevent them to become widespread engineering tools in their current form, important progress has been made in the past decade towards multi-scale progressive fatigue damage modelling. This may allow damage-tolerant designs to further optimise components made from composite laminates in the future.

2 Objectives of the thesis

As already discussed, one of the biggest challenges of fatigue damage models for composite laminates is the lack of applicability as universal engineering tools. Many currently used methods rely on extensions of the finite element method to discrete damage. A comparison of such models showed that even for simple fatigue load cases, the predictions resulted in significant errors and wrong damage modes [124]. Other models like the models currently under development in Padova and Ghent show great potential in transferring the computation of the effect of damage to analytical models. However, up to now, they impose restrictions which fundamentally prevent them from being used as engineering tools for real-world applications. The objective of this thesis is to investigate the effects of matrix cracks on the mechanical properties of composite laminates and the development of a general ply-based fatigue damage model for composite materials with a focus on applicability.

The fatigue damage model builds upon the ply-based static damage model for matrix dominated damage in composite laminates from Schuecker et al. [125, 126] and extends it to fatigue loading. The model consists of two parts. In the first part, a measure of damage is computed based on the stress state of each ply and the cycle count. The second part computes the effect of damage on the stiffness based on the current damage. The schematic representation of the model is shown in Figure 2.1.

The main part of this thesis consists of the adaptation of the second part of the model, which computes the stiffness degradation due to fatigue damage. The stiffness degradation is based on the Mori-Tanaka method [127, 128], which is an analytical homogenisation scheme. The presented method uses crack-like inclusions to mimic the effect of matrix cracks. With this, the effect of off-axis cracks on the stiffness of the laminate is computed for each ply. Compared to the optimal shear lag analysis of the model from Padova, this method requires a calibration step. In the author's opinion, the fact that this method does not impose the restriction of symmetric laminates, the calibration step can be seen as a minor drawback. All data necessary for the calibration comes from standard fatigue tests, which must be performed for each new material system anyway. The general layout of the computation of the effect of damage is

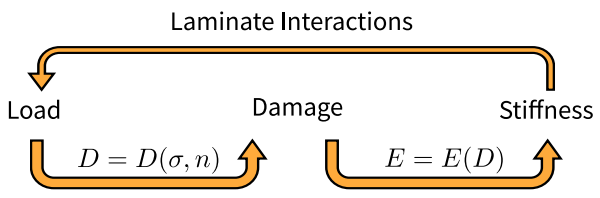

Figure 2.1: The fatigue damage model for off-axis damage. The measure of damage is computed from the stress state and cycle count of each ply and subsequently, the effect of damage on the stiffness. The laminate is updated with a new stiffness for each damaged ply which in turn changes the stress state in the plies.

shown in Figure 2.2. The effect of matrix cracks is computed for each damaged ply. After the homogenization of the damaged plies, the effect on the whole laminate is computed with classical laminate theory. Stress redistribution caused by the weakened plies is automatically accounted for by the laminate theory. In the next step, the new stress state is taken to compute the evolution of damage. It has to be noted that the perturbation of the stress field in plies adjacent to damaged plies due to stress concentrations at the crack tips is currently not accounted for. It has yet to be shown if the simplification to a fully homogenized model at the mesoscale is appropriate. As of now, crack detection is used to quantify the damage which is the base for the computation of effect of damage on the stiffness.

A significant part of the thesis is dedicated to the detection of matrix cracks. For this, an automated crack detection software was developed to help quantify matrix cracks in fatigue experiments. With this information, the correlation between matrix cracks and loss of stiffness could be studied in detail. Also, dissipated energy, secant modulus and dynamic modulus from evaluations of the hysteresis cycles were studied in order to get a deeper insight into the damage process.

The focus of the model is to compute the effect of damage based on evaluations of standard fatigue tests. This underlines the objective of developing a model for practical application, as the model is designed to be incorporated into commercial engineering software. Therefore, it mus be applicable to whole components without extensive test campaigns for each slightly new type of material. On the component level, the complexity of the model must be adequate for its use case. Nevertheless, the model is developed by considering the actual damage mechanisms. For this, the effects of micro-damage on the stiffness loss are studied and implemented with the premise, that the adaptation to new ply materials does not require experiments on the micro-scale. Overall, this work combines existing models from micromechanics, static damage and laminate theory to a fully ply-based fatigue-damage model.

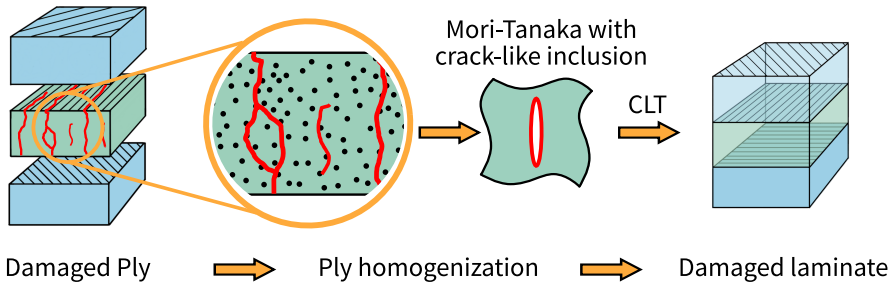

Figure 2.2: Homogenization of a damaged ply. The effect of matrix cracks is computed with the Mori-Tanaka homogenization method. Crack-like voids are used as inclusions to mimic the real cracks. The redistribution of stresses caused by the weakened ply is computed with classical laminate theory.

3 Compilation of thesis

This thesis consists of the following appended papers. Paper A2 is an update to the open-source crack detection package introduced in Paper A. However, it is important as the updated crack detection algorithm is used throughout the following papers. The contributions of the author to each paper are listed in Table 3.1.

Paper A: M. Drvoderic, M. Rettl, M. Pletz, und C. Schuecker, CrackDect: Detecting crack densities in images of fiber-reinforced polymers, SoftwareX, Bd. 16, S. 100832, Dez. 2021, doi: 10.1016/j.softx.2021.100832. published

Paper A2: M. Drvoderic, J. J. Bender, M. Pletz, und C. Schuecker, „Version 0.2 - CrackDect: Detecting crack densities in images of fiber-reinforced polymers“, SoftwareX, Bd. 19, S. 101198, Juli 2022, doi: 10.1016/j.softx.2022.101198. published

Paper B: M. Drvoderic, M. Pletz, und C. Schuecker, Modeling Stiffness Degradation of Fiber-Reinforced Polymers Based on Crack Densities Observed in Off-Axis Plies, J. Compos. Sci., Bd. 6, Nr. 1, S. 10, Dez. 2021, doi: 10.3390/jcs6010010. published

Paper C: M. Drvoderic, M. Pletz, C. Schuecker, Fatigue damage model for composite laminates based on a Mori-Tanaka formulation, Proceedings of the 20th European Conference on Composite Materials (ECCM20). published

Paper D M. Drvoderic, M. Gfrerrer, J. Wiener, G. Pinter, M. Pletz, und C. Schuecker, Comparing crack density and dissipated energy as measures for off-axis damage in composite laminates, Int. J. Fatigue, Bd. 169, S. 107486, Apr. 2023, doi: 10.1016/j.ijfatigue.2022.107486. published

Activity	Paper				
	A	A2	B	C	D
Conceptualisation	80%	100%	60%	60%	70%
Method development & implementation	80%	100%	80%	90%	70%
Numerical and experimental study	100%	100%	100%	100%	50%
Writing - Original Draft	100%	100%	100%	100%	80%

Table 3.1: Contributions of the author to the papers listed in this thesis.

4 Conclusion

This work presents the early stages of the development of a progressive and fully ply-based fatigue damage model, which aims to provide sufficient accuracy at the macro-scale. A multi-level approach is used to include effects at the micro-scale that influence the initiation and progression of off-axis cracks. The effects of these cracks on the stiffness of each ply are homogenised using a micromechanical approach which enables the use of classical laminate theory for computation of the stress state in the plies. The intention of such a model is to provide a usable and efficient solution which can be implemented into bigger numerical models. The proposed model does not impose any restrictions to the stacking sequence which eliminates one of the biggest problems with current progressive fatigue damage models (see section 1.7.

The papers listed in chapter 3 show the progression of the thesis over the course of four years. As already discussed in section 1.3.1, it is essential to quantify the damage in composite materials in order to develop fatigue damage models. For this, *CrackDect* has been developed. It enables efficient and reliable crack detection for the specific case of transilluminated white light images. Due to a lack of open-source tools, the project of crack detection has been developed from its early stages as an in-house tool to an open-source package which provides a modular structure for pre-processing of large image stacks and crack detection algorithms, as described in Paper A. Paper A2 shows the addition of new crack detection algorithms that have been developed after the first version of *CrackDect*. The evaluation of the crack density for whole fatigue test series was only possible due to the investment in efficient crack detection methods early in the thesis. As shown in Figure 1.4, each image of damaged off-axis plies shows multiple cracks. Fatigue tests produce a large number of similar images where the progression of off-axis cracks is evident. It is easy to understand that tracking the progression of the cracks for not only one test but a series of tests quickly becomes infeasible. Besides the new possibilities of automated crack detection, it has to be mentioned that the evaluation of whole test series still requires a certain amount of experience. The algorithms in *CrackDect* are built upon signal processing algorithms and require input parameters, which must be determined manually. Paper B shows the necessary pre-processing of the raw images and the determination of the input parameters.

The necessary calibration of the damage model is shown in Paper B. The effect of damage on the stiffness of the specimens is compared with experimental data. It is shown that the model can predict the effect of damage but effects on the micro-scale must be considered. This shows that a multiaxial approach is necessary to accurately predict the stiffness degradation of a laminate in an analytical fatigue damage model.

The findings of Paper B are used as a starting point for Paper C, where the influence of biaxiality ratio λ on the onset of off-axis crack is studied. A closer look is taken on the dissipated hysteretic energy which reveals that the biaxiality ratio λ of the transversal and in-plane shear stress has a big influence on the amount of dissipated energy. This was interpreted as evidence for the confirmation of Carraro's model for off-axis crack initiation (see section 1.6.1). The explanation is that the two micro-damage driving forces that drive the formation of micro-cracks at an angle between the fibres or fibre-matrix interface fracture, respectively, result in different dissipated energies. In this paper, this hypothesis could not be fully confirmed due to a lack of experimental data. Furthermore, the stiffness degradation model is calibrated to both micro-damage regions which shows a significant improvement in of the predictions.

Paper D is focused on comparing the dissipated energy and the crack density in detail, which directly addresses the questions that arose in Paper C. Also, Carraro's model was used to compute the critical damage driving force at the micro level. The predictions are compared to experimental data and fractographic images which show good agreement. To the knowledge of the authors, this is the first paper where the model proposed by Carraro et al. is verified form a independent group. The hypothesis first formulated in Paper C, namely that the micro-damage modes correlate with the level of dissipated energy is confirmed in this paper. Also, the results show that the formation of off-axis cracks correlates well with the beginning of the stiffness degradation.

The problem of predicting the initiation, progression and effects of fatigue loads on composite laminates will not be tackled in a single thesis due to its complexity and amount of experimental data. Instead, incremental progression has been made over the past decades. This work extends Schuecker's static progressive damage model to fatigue and provides a basis for further development. It shows that the effect of damage on the stiffness of the laminate can be computed with an improved micromechanical model. For the initiation of off-axis cracks, SN diagrams are used. However, the model still lacks a method to predict the progression of damage. For this, the framework from Padova (see section 1.6.1) might be a promising candidate. Combining their model for damage progression with the here presented model for stiffness degradation could potentially yield a fully ply-based framework for a progressive fatigue damage model for off-axis cracks.

5 References

[1] A. Wöhler, Versuche über die Festigkeit der Eisenbahnwagenachsen, Zeitschrift für Bauwesen 10 (1860) 160–161.

[2] K. L. Reifsnider, Fatigue of composite materials, no. 4 in Composite materials series, Elsevier, 1991.

[3] A. P. Vassilopoulos, T. Keller, Fatigue of Fiber-reinforced Composites, Engineering Materials and Processes, Springer London, 2011. doi:10.1007/978-1-84996-181-3.

[4] P. Alam, D. Mamalis, C. Robert, C. Floreani, C. M. Ó Brádaigh, The fatigue of carbon fibre reinforced plastics - a review, Composites Part B: Engineering 166 (2019-06) 555–579. doi:10.1016/j.compositesb.2019.02.016.

[5] A. P. Vassilopoulos, The history of fiber-reinforced polymer composite laminate fatigue, International Journal of Fatigue 134 (2020-05). doi:10.1016/j.ijfatigue.2020.105512.

[6] H. Schürmann, Konstruieren mit Faser-Kunststoff-Verbunden: mit 39 Tabellen, 2nd Edition, VDI-Buch, Springer, 2007. doi:https://doi.org/10.1007/978-3-540-72190-1.

[7] J. Awerbuch, H. Hahn, Off-axis fatigue of graphite/epoxy composite, in: K. Lauraitis (Ed.), Fatigue of Fibrous Composite Materials, ASTM International, 1981-01-01, pp. 243–273. doi:10.1520/STP27624S.

[8] L. Asp, L. Berglund, R. Talreja, A criterion for crack initiation in glassy polymers subjected to a composite-like stress state, Composites Science and Technology 56 (11) (1996-01) 1291–1301. doi:10.1016/S0266-3538(96)00090-5.

[9] L. Asp, L. Berglund, R. Talreja, Prediction of matrix-initiated transverse failure in polymer composites, Composites Science and Technology 56 (9) (1996-01) 1089–1097. doi:10.1016/0266-3538(96)00074-7.

[10] K. Reifsnider, R. Jamison, Fracture of fatigue-loaded composite laminates, International Journal of Fatigue Vol. 4 (1982-10) 187–197. doi:10.1016/0142-1123(82)90001-9.

[11] J. Zangenberg, P. Brøndsted, J. W. Gillespie, Fatigue damage propagation in unidirectional glass fibre reinforced composites made of a non-crimp fabric, Journal of Composite Materials 48 (22) (2014-09) 2711–2727. doi:10.1177/0021998313502062.

[12] K. M. Jespersen, J. A. Glud, J. Zangenberg, A. Hosoi, H. Kawada, L. P. Mikkelsen, Uncovering the fatigue damage initiation and progression in uni-directional non-crimp fabric reinforced polyester composite, Composites Part A: Applied Science and Manufacturing 109 (2018-06) 481–497. doi:10.1016/j.compositesa.2018.03.002.

[13] J. Bartley-Cho, S. Gyu Lim, H. Hahn, P. Shyprykevich, Damage accumulation in quasi-isotropic graphite/epoxy laminates under constant-amplitude fatigue and block loading, Composites Science and Technology 58 (9) (1998-09) 1535–1547. doi:10.1016/S0266-3538(97)00214-5.

[14] A. Plumtree, Fatigue damage evolution in off-axis unidirectional CFRP, International Journal of Fatigue 24 (2) (2002-04) 155–159. doi:10.1016/S0142-1123(01)00068-8.

[15] A. Wharmby, Observations on damage development in fibre reinforced polymer laminates under cyclic loading, International Journal of Fatigue 25 (5) (2003-05) 437–446. doi:10.1016/S0142-1123(02)00118-4.

[16] K. Tohgo, S. Nakagawa, K. Kageyama, Fatigue behavior of CFRP cross-ply laminates under on-axis and off-axis cyclic loading, International Journal of Fatigue 28 (10) (2006-10) 1254–1262. doi:10.1016/j.ijfatigue.2006.02.011.

[17] M. Quaresimin, P. Carraro, Damage initiation and evolution in glass/epoxy tubes subjected to combined tension–torsion fatigue loading, International Journal of Fatigue 63 (2014-06) 25–35. doi:10.1016/j.ijfatigue.2014.01.002.

[18] J. Glud, J. Dulieu-Barton, O. Thomsen, L. Overgaard, Fatigue damage evolution in GFRP laminates with constrained off-axis plies, Composites Part A: Applied Science and Manufacturing 95 (2017-04) 359–369. doi:10.1016/j.compositesa.2017.02.005.

[19] R. Talreja, Transverse cracking and stiffness reduction in composite laminates, Journal of Composite Materials 19 (4) (1985-07) 355–375. doi:10.1177/002199838501900404.

[20] J. Tong, F. Guild, S. Ogin, P. Smith, On matrix crack growth in quasi-isotropic laminates—i. experimental investigation, Composites Science and Technology 57 (11) (1997-01) 1527–1535. doi:10.1016/S0266-3538(97)00080-8.

[21] A. Wharmby, F. Ellyin, Damage growth in constrained angle-ply laminates under cyclic loading, Composites Science and Technology 62 (9) (2002-07) 1239–1247. doi:10.1016/S0266-3538(02)00075-1.

[22] J. Varna, R. Joffe, N. Akshantala, R. Talreja, Damage in composite laminates with off-axis plies, Composites Science and Technology 59 (14) (1999-11) 2139–2147. doi:10.1016/S0266-3538(99)00070-6.

[23] S. Adden, P. Horst, Stiffness degradation under fatigue in multiaxially loaded non-crimped-fabrics, International Journal of Fatigue 32 (1) (2010-01) 108–122. doi:10.1016/j.ijfatigue.2009.02.002.

[24] D. Purslow, Matrix fractography of fibre-reinforced epoxy composites, Composites 17 (4) (1986-10) 289–303. doi:10.1016/0010-4361(86)90746-9.

[25] M. Quaresimin, P. Carraro, L. Maragoni, Early stage damage in off-axis plies under fatigue loading, Composites Science and Technology 128 (2016-05) 147–154. doi:10.1016/j.compscitech.2016.03.015.

[26] A. Puck, Failure analysis of frp laminates by means of physically based phenomenological models, Composites Science and Technology 58 (7) (1998-07) 1045–1067. doi:10.1016/S0266-3538(96)00140-6.

[27] S. Pinho, R. Darvizeh, P. Robinson, C. Schuecker, P. Camanho, Material and structural response of polymer-matrix fibre-reinforced composites, Journal of Composite Materials 46 (19) (2012-09) 2313–2341. doi:10.1177/0021998312454478.

[28] P. Carraro, M. Quaresimin, A damage based model for crack initiation in unidirectional composites under multiaxial cyclic loading, Composites Science and Technology 99 (2014-07) 154–163. doi:10.1016/j.compscitech.2014.05.012.

[29] M. Lafarie-Frenot, C. Hénaff-Gardin, Formation and growth of 90° ply fatigue cracks in carbon/epoxy laminates, Composites Science and Technology 40 (3) (1991-01) 307–324. doi:10.1016/0266-3538(91)90087-6.

[30] D. Zhang, J. Ye, D. Lam, Ply cracking and stiffness degradation in cross-ply laminates under biaxial extension, bending and thermal loading, Composite Structures 75 (1) (2006-09) 121–131. doi:10.1016/j.compstruct.2006.04.048.

[31] M. Quaresimin, P. Carraro, L. Mikkelsen, N. Lucato, L. Vivian, P. Brøndsted, B. Sørensen, J. Varna, R. Talreja, Damage evolution under cyclic multiaxial stress state: A comparative analysis between glass/epoxy laminates and tubes, Composites Part B: Engineering 61 (2014-05) 282–290. doi:10.1016/j.compositesb.2014.01.056.

[32] L. Maragoni, P. Carraro, M. Peron, M. Quaresimin, Fatigue behaviour of glass/epoxy laminates in the presence of voids, International Journal of Fatigue 95 (2017-02) 18–28. doi:10.1016/j.ijfatigue.2016.10.004.

[33] H. Shen, W. Yao, W. Qi, J. Zong, Experimental investigation on damage evolution in cross-ply laminates subjected to quasi-static and fatigue loading, Composites Part B: Engineering 120 (2017-07) 10–26. doi:10.1016/j.compositesb.2017.02.033.

[34] X. Li, J. Kupski, S. Teixeira De Freitas, R. Benedictus, D. Zarouchas, Unfolding the early fatigue damage process for CFRP cross-ply laminates, International Journal of Fatigue 140 (2020-11) 105820. doi:10.1016/j.ijfatigue.2020.105820.

[35] J. Bender, B. Bak, S. Jensen, E. Lindgaard, Effect of variable amplitude block loading on intralaminar crack initiation and propagation in multidirectional GFRP laminate, Composites Part B: Engineering 217 (2021-07) 108905. doi:10.1016/j.compositesb.2021.108905.

[36] X. Li, R. Benedictus, D. Zarouchas, Early fatigue damage accumulation of CFRP cross-ply laminates considering size and stress level effects, International Journal of Fatigue 159 (2022-06) 106811. doi:10.1016/j.ijfatigue.2022.106811.

[37] A. Ayenu-Prah, N. Attoh-Okine, Evaluating pavement cracks with bidimensional empirical mode decomposition, EURASIP Journal on Advances in Signal Processing 2008 (1) (2008-12) 861701. doi:10.1155/2008/861701.

[38] M. Salman, S. Mathavan, K. Kamal, M. Rahman, Pavement crack detection using the gabor filter, in: 16th International IEEE Conference on Intelligent Transportation Systems (ITSC 2013), IEEE, The Hague, Netherlands, 2013-10, pp. 2039–2044. doi:10.1109/ITSC.2013.6728529.

[39] A. Mohan, S. Poobal, Crack detection using image processing: A critical review and analysis, Alexandria Engineering Journal 57 (2) (2018-06) 787–798. doi:10.1016/j.aej.2017.01.020.

[40] H. S. Munawar, A. W. A. Hammad, A. Haddad, C. A. P. Soares, S. T. Waller, Image-based crack detection methods: A review, Infrastructures 6 (8) (2021-08-14) 115. doi:10.3390/infrastructures6080115.

[41] F. Sket, A. Enfedaque, C. Alton, C. González, J. Molina-Aldareguia, J. Llorca, Automatic quantification of matrix cracking and fiber rotation by x-ray computed tomography in shear-deformed carbon fiber-reinforced laminates, Composites Science and Technology 90 (2014-01) 129–138. doi:10.1016/j.compscitech.2013.10.022.

[42] I. Miskdjian, M. Hajikazemi, W. Van Paepegem, Automatic edge detection of ply cracks in glass fiber composite laminates under quasi-static and fatigue loading using multi-scale digital image correlation, Composites Science and Technology 200 (2020-11) 108401. doi:10.1016/j.compscitech.2020.108401.

[43] I. Fogel, D. Sagi, Gabor filters as texture discriminator, Biological Cybernetics 61 (2) (1989-06). doi:10.1007/BF00204594.

[44] N. Otsu, A threshold selection method from gray-level histograms, IEEE Transactions on Systems, Man, and Cybernetics 9 (1) (1979-01) 62–66. doi:10.1109/TSMC.1979.4310076.

[45] J. Glud, J. Dulieu-Barton, O. Thomsen, L. Overgaard, Automated counting of off-axis tunnelling cracks using digital image processing, Composites Science and Technology 125 (2016-03) 80–89. doi:10.1016/j.compscitech.2016.01.019.

[46] G. Just, I. Koch, M. Gude, Experimental analysis of matrix cracking in glass fiber reinforced composite off-axis plies under static and fatigue loading, Polymers 14 (11) (2022-05-26) 2160. doi:10.3390/polym14112160.

[47] B. F. Sørensen, R. Talreja, Analysis of damage in a ceramic matrix composite, International Journal of Damage Mechanics 2 (3) (1993-07) 246–271. doi:10.1177/105678959300200305.

[48] J. N. Yang, D. L. Jones, Effect of load sequence on the statistical fatigue of composites, AIAA Journal 18 (12) (1980-12) 1525–1531. doi:10.2514/3.50912.

[49] B. Harris, N. Gathercole, H. Reiter, T. Adam, Fatigue of carbon-fibre-reinforced plastics under block-loading conditions, Composites Part A: Applied Science and Manufacturing 28 (4) (1997-01) 327–337. doi:10.1016/S1359-835X(96)00131-5.

[50] E. Gamstedt, An experimental investigation of the sequence effect in block amplitude loading of cross-ply composite laminates, International Journal of Fatigue 24 (2) (2002-04) 437–446. doi:10.1016/S0142-1123(01)00099-8.

[51] W. V. Paepegem, J. Degrieck, Effects of load sequence and block loading on the fatigue response of fiber-reinforced composites, Mechanics of Advanced Materials and Structures 9 (1) (2002-01) 19–35. doi:10.1080/153764902317224851.

[52] M. A. Miner, Cumulative damage in fatigue, Journal of Applied Mechanics 12 (3) (1945-09-01) A159–A164. doi:10.1115/1.4009458.

[53] P. Leevers, Fracture of polymeric materials, in: Encyclopedia of Materials: Science and Technology, Elsevier, 2001, pp. 3322–3329. doi:10.1016/B0-08-043152-6/00594-5.

[54] A. Puck, H. Schürmann, Failure analysis of FRP laminates by means of physically based phenomenological models, Composites Science and Technology 62 (12) (2002) 1633–1662. doi:https://doi.org/10.1016/S0266-3538(01)00208-1.

[55] M. Quaresimin, P. Carraro, L. Maragoni, Influence of load ratio on the biaxial fatigue behaviour and damage evolution in glass/epoxy tubes under tension–torsion loading, Composites Part A: Applied Science and Manufacturing 78 (2015-11) 294–302. doi:10.1016/j.compositesa.2015.08.009.

[56] P. Carraro, L. Maragoni, M. Quaresimin, Damage evolution in cross-ply laminates under tension–compression and compression-compression cyclic loads, Composites Part A: Applied Science and Manufacturing 156 (2022-05) 106888. doi:10.1016/j.compositesa.2022.106888.

[57] J. Brunbauer, G. Pinter, Effects of mean stress and fibre volume content on the fatigue-induced damage mechanisms in CFRP, International Journal of Fatigue 75 (2015-06) 28–38. doi:10.1016/j.ijfatigue.2015.01.014.

[58] W. Van Paepegem, R. Sevenois, D. Garoz, F. Gilabert, S. Spronk, Microscale based prediction of matrix crack initiation in UD composite plies subjected to multiaxial fatigue for all stress ratios and load levels, Composites Science and Technology 142 (2017-04) 124–138. doi:10.1016/j.compscitech.2017.02.004.

[59] R. Alderliesten, Critical review on the assessment of fatigue and fracture in composite materials and structures, Engineering Failure Analysis 35 (2013-12) 370–379. doi:10.1016/j.engfailanal.2013.03.022.

[60] P. C. Paris, M. P. Gomez, W. E. Anderson, A rational analytic theory of fatigue, The Trend in Engineering 13 (1961) 9–14.

[61] P. Paris, F. Erdogan, A critical analysis of crack propagation laws, Journal of Basic Engineering 85 (4) (1963-12-01) 528–533. doi:10.1115/1.3656900.

[62] P. Carraro, L. Maragoni, M. Quaresimin, Prediction of the crack density evolution in multidirectional laminates under fatigue loadings, Composites Science and Technology 145 (2017-06) 24–39. doi:10.1016/j.compscitech.2017.03.013.

[63] R. C. Alderliesten, How proper similitude principles could have improved our understanding about fatigue damage growth, in: Proceedings of the 28th ICAF Symposium, Helsinki, 2015.

[64] L. Yao, R. Alderliesten, R. Benedictus, Interpreting the stress ratio effect on delamination growth in composite laminates using the concept of fatigue fracture toughness, Composites Part A: Applied Science and Manufacturing 78 (2015-11) 135–142. doi:10.1016/j.compositesa.2015.08.005.

[65] J. Pascoe, R. Alderliesten, R. Benedictus, On the physical interpretation of the r-ratio effect and the LEFM parameters used for fatigue crack growth in adhesive bonds, International Journal of Fatigue 97 (2017-04) 162–176. doi:10.1016/j.ijfatigue.2016.12.033.

[66] A. Rotem, Load frequency effect on the fatigue strength of isotropic laminates, Composites Science and Technology 46 (2) (1993) 129–138. doi:10.1016/0266-3538(93)90168-G.

[67] V. Barron, M. Buggy, N. H. McKenna, Frequency effects on the fatigue behaviour on carbon fibre reinforced polymer laminates, Journal of Materials Science 36 (7) (2001) 1755–1761. doi:10.1023/A:1017576725885.

[68] AVK – Industrievereinigung Verstärkte Kunststoffe e. V. (Ed.), Handbuch Faserverbundkunststoffe/Composites, Springer Fachmedien Wiesbaden, 2013. doi:10.1007/978-3-658-02755-1.

[69] A. V. Movahedi-Rad, T. Keller, A. P. Vassilopoulos, Fatigue damage in angle-ply GFRP laminates under tension-tension fatigue, International Journal of Fatigue 109 (2018-04) 60–69. doi:10.1016/j.ijfatigue.2017.12.015.

[70] C. K. H. Dharan, T. F. Tan, A hysteresis-based damage parameter for notched composite laminates subjected to cyclic loading, Journal of Materials Science 42 (6) (2007-03-07) 2204–2207. doi:10.1007/s10853-007-1498-9.

[71] J. Montesano, Z. Fawaz, H. Bougherara, Use of infrared thermography to investigate the fatigue behavior of a carbon fiber reinforced polymer composite, Composite Structures 97 (2013-03) 76–83. doi:10.1016/j.compstruct.2012.09.046.

[72] L. Gornet, O. Wesphal, C. Burtin, J.-L. Bailleul, P. Rozycki, L. Stainier, Rapid determination of the high cycle fatigue limit curve of carbon fiber epoxy matrix composite laminates by thermography methodology: Tests and finite element simulations, Procedia Engineering 66 (2013) 697–704. doi:10.1016/j.proeng.2013.12.123.

[73] R. Chandra, S. Singh, K. Gupta, Damping studies in fiber-reinforced composites – a review, Composite Structures 46 (1) (1999-09) 41–51. doi:10.1016/S0263-8223(99)00041-0.

[74] J. Brunbauer, G. Pinter, On the strain measurement and stiffness calculation of carbon fibre reinforced composites under quasi-static tensile and tension-tension fatigue loads, Polymer Testing 40 (2014-12) 256–264. doi:10.1016/j.polymertesting.2014.09.014.

[75] J. M. Hodgkinson, Mechanical testing of advanced fibre composites, CRC Press ; Woodhead, 2000.

[76] D. Perreux, E. Joseph, The effect of frequency on the fatigue performance of filament-wound pipes under biaxial loading: Experimental results and damage model, Composites Science and Technology 57 (3) (1997-01) 353–364. doi:10.1016/S0266-3538(96)00155-8.

[77] P. P. Camanho, C. G. Dávila, S. T. Pinho, L. Iannucci, P. Robinson, Prediction of in situ strengths and matrix cracking in composites under transverse tension and in-plane shear, Composites Part A: Applied Science and Manufacturing 37 (2) (2006-02) 165–176. doi:10.1016/j.compositesa.2005.04.023.

[78] F. Crossman, W. Warren, A. Wang, G. Law, Initiation and growth of transverse cracks and edge delamination in composite laminates part 2. experimental correlation, Journal of Composite Materials 14 (1) (1980-01) 88–108. doi:10.1177/002199838001400107.

[79] F.-K. Chang, M.-H. Chen, The in situ ply shear strength distributions in graphite/epoxy laminated composites, Journal of Composite Materials 21 (8) (1987-08) 708–733. doi:10.1177/002199838702100802.

[80] G. Catalanotti, Prediction of in situ strengths in composites: Some considerations, Composite Structures 207 (2019-01) 889–893. doi:10.1016/j.compstruct.2018.09.075.

[81] J. Varna, Modelling mechanical performance of damaged laminates, Journal of Composite Materials 47 (20) (2013-09) 2443–2474. doi:10.1177/0021998312469241.

[82] A. Parvizi, J. E. Bailey, On multiple transverse cracking in glass fibre epoxy cross-ply laminates, Journal of Materials Science 13 (10) (1978-10) 2131–2136. doi:10.1007/BF00541666.

[83] C. Sauder, J. Lamon, R. Pailler, Thermomechanical properties of carbon fibres at high temperatures (up to 2000 °c), Composites Science and Technology 62 (4) (2002-03) 499–504. doi:10.1016/S0266-3538(01)00140-3.

[84] A. A. Fahmy, T. G. Cunningham, Investigation of thermal fatigue in fiber composite materials., Tech. rep., North Carolina State University at Raleigh Dept of Materials Science and Engineering (1976).

[85] D. S. Adams, D. E. Bowles, C. T. Herakovich, Thermally induced transverse cracking in graphite-epoxy cross-ply laminates, Journal of Reinforced Plastics and Composites 5 (3) (1986-07) 152–169. doi:10.1177/073168448600500301.

[86] S. Kobayashi, K. Terada, N. Takeda, Evaluation of long-term durability in high temperature resistant CFRP laminates under thermal fatigue loading, Composites Part B: Engineering 34 (8) (2003-12) 753–759. doi:10.1016/S1359-8368(03)00099-4.

[87] M. Kawai, T. Taniguchi, Off-axis fatigue behavior of plain weave carbon/epoxy fabric laminates at room and high temperatures and its mechanical modeling, Composites Part A: Applied Science and Manufacturing 37 (2) (2006-02) 243–256. doi:10.1016/j.compositesa.2005.07.003.

[88] C. Henaffgardin, Specificity of matrix cracking development in CFRP laminates under mechanical or thermal loadings, International Journal of Fatigue 24 (2) (2002-04) 171–177. doi:10.1016/S0142-1123(01)00070-6.

[89] Y. Miyano, M. Nakada, H. Kudoh, R. Muki, Prediction of tensile fatigue life for unidirectional CFRP, Journal of Composite Materials 34 (7) (2000-04) 538–550. doi:10.1177/002199830003400701.

[90] L. Cormier, S. Joncas, Modelling the effect of temperature on the probabilistic stress–life fatigue diagram of glass fibre–polymer composites loaded in tension along the fibre direction, Journal of Composite Materials 52 (2) (2018-01) 207–224. doi:10.1177/0021998317704896.

[91] P. Vannucci, Anisotropic Elasticity, Vol. 85 of Lecture Notes in Applied and Computational Mechanics, Springer Singapore, 2018. doi:10.1007/978-981-10-5439-6.

[92] G. Dell'Anno, R. Lees, Effect of water immersion on the interlaminar and flexural performance of low cost liquid resin infused carbon fabric composites, Composites Part B: Engineering 43 (3) (2012-04) 1368–1373. doi:10.1016/j.compositesb.2011.08.037.

[93] R. Selzer, K. Friedrich, Mechanical properties and failure behaviour of carbon fibre-reinforced polymer composites under the influence of moisture, Composites Part A: Applied Science and Manufacturing 28 (6) (1997-01) 595–604. doi:10.1016/S1359-835X(96)00154-6.

[94] P. Alam, C. Robert, C. M. Ó Brádaigh, Tidal turbine blade composites - a review on the effects of hygrothermal aging on the properties of CFRP, Composites Part B: Engineering 149 (2018-09) 248–259. doi:10.1016/j.compositesb.2018.05.003.

[95] E08 Committee, Practices for cycle counting in fatigue analysis, Tech. rep., ASTM International (2017). doi:10.1520/E1049-85R97.

[96] S. Downing, D. Socie, Simple rainflow counting algorithms, International Journal of Fatigue 4 (1) (1982-01) 31–40. doi:10.1016/0142-1123(82)90018-4.

[97] R. Stelzer, B. Carlton, S. Mazzoni, Comparison of cycle counting methods for potential liquefaction and structural fatigue assessment, 17th World Conference on Earthquake Engineering, Sendai, Japan, 2020.

[98] C. H. Wang, M. W. Brown, Life prediction techniques for variable amplitude multiaxial fatigue—part 1: Theories, Journal of Engineering Materials and Technology 118 (3) (1996-07-01) 367–370. doi:10.1115/1.2806821.

[99] M. A. Meggiolaro, J. T. P. de Castro, An improved multiaxial rainflow algorithm for non-proportional stress or strain histories – part II: The modified wang–brown method, International Journal of Fatigue 42 (2012-09) 194–206. doi:10.1016/j.ijfatigue.2011.10.012.

[100] T. Langlais, Multiaxial cycle counting for critical plane methods, International Journal of Fatigue 25 (7) (2003-07) 641–647. doi:10.1016/S0142-1123(02)00148-2.

[101] C. Gaier, H. Dannbauer, Fatigue analysis of multiaxially loaded components with the fe-postprocessor femfat-max, in: Biaxial/Multiaxial Fatigue and Fracture, Vol. 31 of European Structural Integrity Society, Elsevier, 2003, pp. 223–240. doi:https://doi.org/10.1016/S1566-1369(03)80013-4.

[102] C. Gaier, G. Pramhas, W. Steiner, An extended critical plane criterion for general load situations, in: Proceedings of the 8th International Fatigue Conference, Stockholm, Sweden, 2002, pp. 259–266.

[103] P. A. Carraro, M. Quaresimin, Fatigue damage and stiffness evolution in composite laminates: a damage-based framework, Procedia Engineering 213 (2018) 17–24. doi:10.1016/j.proeng.2018.02.003.

[104] J. Degrieck, W. Van Paepegem, Fatigue damage modeling of fibre-reinforced composite materials: Review, Applied Mechanics Reviews 54 (4) (2001-07-01) 279–300. doi:10.1115/1.1381395.

[105] R. D. B. Sevenois, W. Van Paepegem, Fatigue damage modeling techniques for textile composites: Review and comparison with unidirectional composite modeling techniques, Applied Mechanics Reviews 67 (2) (2015-03-01) 020802. doi:10.1115/1.4029691.

[106] A. P. Vassilopoulos (Ed.), Fatigue life prediction of composites and composite structures, Woodhead Publishing in materials, CRC Press ; Woodhead Publishing, 2010. doi:https://doi.org/10.1016/C2017-0-02509-0.

[107] M. M. Shokrieh, L. B. Lessard, Progressive fatigue damage modeling of composite materials, part i: Modeling, Journal of Composite Materials 34 (13) (2000-07) 1056–1080. doi:10.1177/002199830003401301.

[108] P. Carraro, M. Quaresimin, A stiffness degradation model for cracked multidirectional laminates with cracks in multiple layers, International Journal of Solids and Structures 58 (2015-04) 34–51. doi:10.1016/j.ijsolstr.2014.12.016.

[109] P. Carraro, L. Maragoni, M. Quaresimin, Stiffness degradation of symmetric laminates with off-axis cracks and delamination: an analytical model, International Journal of Solids and Structures 213 (2021-03) 50–62. doi:10.1016/j.ijsolstr.2020.12.013.

[110] J. Nairn, D. Mendels, On the use of planar shear-lag methods for stress-transfer analysis of multilayered composites, Mechanics of Materials 33 (6) (2001-06) 335–362. doi:10.1016/S0167-6636(01)00056-4.

[111] M. Kachanov, Elastic solids with many cracks: A simple method of analysis, International Journal of Solids and Structures 23 (1) (1987) 23–43. doi:10.1016/0020-7683(87)90030-8.

[112] P. A. Carraro, L. Maragoni, M. Quaresimin, Characterisation and analysis of transverse crack-induced delamination in cross-ply composite laminates under fatigue loadings, International Journal of Fatigue 129 (2019-12) 105217. doi:10.1016/j.ijfatigue.2019.105217.

[113] M. Hajikazemi, L. McCartney, H. Ahmadi, W. Van Paepegem, Variational analysis of cracking in general composite laminates subject to triaxial and bending loads, Composite Structures 239 (2020-05) 111993. doi:10.1016/j.compstruct.2020.111993.

[114] M. Hajikazemi, M. Sadr, A variational model for stress analysis in cracked laminates with arbitrary symmetric lay-up under general in-plane loading, International Journal of Solids and Structures 51 (2) (2014-01) 516–529. doi:10.1016/j.ijsolstr.2013.10.024.

[115] M. Hajikazemi, M. Sadr, Stiffness reduction of cracked general symmetric laminates using a variational approach, International Journal of Solids and Structures 51 (7) (2014-04) 1483–1493. doi:10.1016/j.ijsolstr.2013.12.040.

[116] M. Hajikazemi, H. Ahmadi, L. McCartney, W. Van Paepegem, A variational approach for accurate prediction of stress and displacement fields and thermo-elastic constants in general symmetric laminates containing ply cracking and delamination under general triaxial loading, International Journal of Solids and Structures 254-255 (2022-11) 111917. doi:10.1016/j.ijsolstr.2022.111917.

[117] M. Hajikazemi, W. Van Paepegem, A variational model for free-edge interlaminar stress analysis in general symmetric and thin-ply composite laminates, Composite Structures 184 (2018-01) 443–451. doi:10.1016/j.compstruct.2017.10.012.

[118] H. Ahmadi, M. Hajikazemi, W. Van Paepegem, Closed-form formulae for prediction of homogenized ply-properties and laminate thermo-elastic constants in symmetric laminates containing ply cracks in multiple orientations, Composite Structures 241 (2020-06) 112061. doi:10.1016/j.compstruct.2020.112061.

[119] M. Hajikazemi, L. McCartney, W. Van Paepegem, Matrix cracking initiation, propagation and laminate failure in multiple plies of general symmetric composite laminates, Composites Part A: Applied Science and Manufacturing 136 (2020-09) 105963. doi:10.1016/j.compositesa.2020.105963.

[120] S. Zhou, Y. Li, K. Fu, X. Wu, Progressive fatigue damage modelling of fibre-reinforced composite based on fatigue master curves, Thin-Walled Structures 158 (2021-01) 107173. doi:10.1016/j.tws.2020.107173.

[121] E. N. Eliopoulos, T. P. Philippidis, A progressive damage simulation algorithm for GFRP composites under cyclic loading. part i: Material constitutive model, Composites Science and Technology 71 (5) (2011-03) 742–749. doi:10.1016/j.compscitech.2011.01.023.

[122] S. P. Engelstad, S. B. Clay, Comparison of composite damage growth tools for static behavior of notched composite laminates, Journal of Composite Materials 51 (10) (2017-05) 1493–1524. doi:10.1177/0021998316675945.

[123] S. B. Clay, S. P. Engelstad, Benchmarking of composite progressive damage analysis methods: The background, Journal of Composite Materials 51 (10) (2017-05) 1325–1331. doi:10.1177/0021998316672520.

[124] S. Engelstad, S. Clay, Comparison of composite damage growth tools for fatigue behavior of notched composite laminates, Journal of Composite Materials 51 (15) (2017-06) 2227–2249. doi:10.1177/0021998317694948.

[125] C. Schuecker, H. Pettermann, A continuum damage model for fiber reinforced laminates based on ply failure mechanisms, Composite Structures 76 (1) (2006-10) 162–173. doi:10.1016/j.compstruct.2006.06.023.

[126] C. Schuecker, H. Pettermann, Constitutive ply damage modeling, FEM implementation, and analyses of laminated structures, Computers & Structures 86 (9) (2008-05) 908–918. doi:10.1016/j.compstruc.2007.04.021.

[127] T. Mori, K. Tanaka, Average stress in matrix and average elastic energy of materials with misfitting inclusions, Acta Metallurgica 21 (5) (1973-05) 571–574. doi:10.1016/0001-6160(73)90064-3.

[128] Y. Benveniste, A new approach to the application of mori-tanaka's theory in composite materials, Mechanics of Materials 6 (2) (1987-06) 147–157. doi:10.1016/0167-6636(87)90005-6.

6 Papers

Paper A

CrackDect: Detecting crack densities in images of fiber-reinforced polymers

Authors: Drvoderic, Matthias
Rettl, Matthias
Pletz, Martin
Schuecker, Clara

SoftwareX
DOI: 10.1016/j.softx.2021.100832

SoftwareX 16 (2021) 100832

Contents lists available at ScienceDirect

SoftwareX

journal homepage: www.elsevier.com/locate/softx

Original software publication

CrackDect: Detecting crack densities in images of fiber-reinforced polymers

Matthias Drvoderic, Matthias Rettl, Martin Pletz *, Clara Schuecker

Chair of Designing Plastics and Composite Materials, Department of Polymer Engineering and Science, Montanuniversitaet Leoben, Austria

ARTICLE INFO

Article history:
Received 11 June 2021
Received in revised form 27 September 2021
Accepted 28 September 2021

MSC:
68U10

Keywords:
Crack detection
Image processing
Fiber-reinforced polymers
Crack density
Python

ABSTRACT

CrackDect is a tool to detect cracks in a given direction from a series of images. It is specialized to detect multiple matrix cracks in composite laminates to yield the crack density but can also be used as a general line detection. The package is written in Python, and includes classes and functions to efficiently handle large image stacks, pre-process images and perform the crack detection. Due to its modular structure it is easily expandable to other crack detection or feature recognition algorithms. Pre-processing of whole image stacks can be customized to account for different image capturing techniques. Since image processing tends to be computational and memory expensive, special focus is put on efficiency.

Code metadata

Current code version	v0.1.1
Permanent link to code/repository used for this code version	https://github.com/ElsevierSoftwareX/SOFTX-D-21-00109
Code Ocean compute capsule	–
Legal Code License	MIT
Code versioning system used	GIT
Software code languages, tools, and services used	Python, Scikit-image, SciPy, NumPy, SQLAlchemy, Numba, Matplotlib, PyQt5
Compilation requirements, operating environments	Python 3.8.x and higher, cross platform
If available Link to developer documentation/manual	https://crackdect.readthedocs.io/en/latest/
Support email for questions	kkv.leoben@gmail.com

1. Motivation and significance

The increasing use of unidirectional fiber-reinforced polymers in structural components requires models that predict not only their static failure but also fatigue damage. Due to their complex micro-structure, different damage modes may occur in their service life [1]. One of the most common and earliest damage modes is the development of through-the-thickness matrix cracks. These cracks propagate along fibers of one ply and are called tunneling or off-axis cracks. Over the past decades, much research has been conducted on initiation, growth, and the effect of this damage mode since it is responsible for the first big drop in the stiffness of a laminate [2–8]. The accumulation and effect of these off-axis cracks is schematically shown in Fig. 1. Often, the observed off-axis cracks are counted manually to calculate the crack density [6,8], which is then used as a measure for damage. This is not only a very tedious process but also prone to human errors. Phenomenological models that predict the stiffness degradation due to off-axis cracks for static and fatigue loading have been proposed [9–11], but to use them, calibration parameters related to the crack state are required. This step is labor-intensive when

* Corresponding author.
E-mail address: martin.pletz@unileoben.ac.at (Martin Pletz).

https://doi.org/10.1016/j.softx.2021.100832

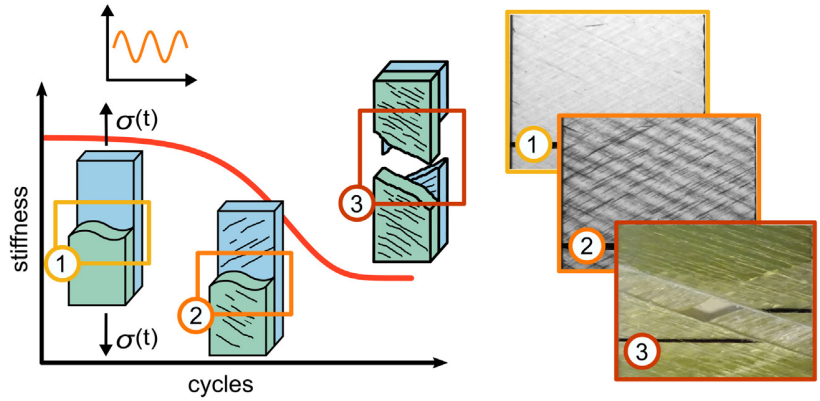

Fig. 1. Off-axis cracks initiate due to dynamic loading (1) and accumulate along the service live (2). The stiffness drops with the accumulation of damage and eventually, these cracks and a combination of other damage mechanisms lead to final failure (3).

cracks are counted manually. Therefore, the development of phenomenological models is limited by the difficulty of evaluating large experimental campaigns.

The prerequisites for counting off-axis cracks can range from a simple camera setup to extensive imaging techniques like computed tomography (CT), depending on the material of the specimen. Transmitted or transilluminated white light imaging (TWLI) is an option for transparent composites like glass fiber-reinforced polymers (GFRPs). The TWLI setup consists of a light source placed behind a transparent specimen and the light that is transmitted through the specimen is captured with a camera. Since cracks in the specimen scatter the transmitted light, they appear as dark lines in the images [6,12]. For non-transparent composites, CrackDect can be used for images obtained by a suitable imaging technique such as computed tomography. Considering that the manual evaluation of multiple images for each specimen in the experimental campaign is labor-intensive, a few attempts on developing an automated algorithm for crack detection using images of the cracked specimen can be found in literature but they are either limited to special and expensive imaging techniques like x-ray [13], poorly documented, or the software is not publicly available. An advanced and broadly applicable automated crack detection algorithm for off-axis cracks was presented by Glud et al. [14]. Up to now, however, no software is publicly available for this specialized crack detection algorithm.

The CrackDect package provides this algorithm and the necessary framework for pre-processing whole image stacks. It is meant as an automated evaluation tool for fatigue experiments to determine increasing crack densities. CrackDect thus aids in the development, validation and calibration of new and better damage or fatigue models for composite materials. The package can be implemented in evaluation processes where, generally, only the paths to the image storage location needs to be changed. CrackDect is not limited to one class of materials or imaging technique. The only prerequisite is an imaging technique where cracks appear with a different intensity than uncracked regions. The method is independent of mechanical properties since it only relies on the images of the cracked material. To compute the crack density, the scale of the image is needed in the post-processing to compute the crack density as crack length per area instead of cracks per pixel.

2. Software description

CrackDect provides high level classes and functions to handle large image stacks and pre-process them to meet the prerequisites to finally apply the crack detection algorithm. The focus is to provide a modular and expandable framework for crack detection but it can also be used as an image processing tool only. Its strength is the efficient handling of large image stacks. Since loading a lot of images can lead to excessive RAM usage, it provides container objects dedicated to track used RAM of loaded images and manage loading and unloading of preliminary results to out-of-memory databases. The pre-processing for the crack detection is designed such that other image processing libraries and custom functions can be easily applied to a whole image stack.

2.1. Software architecture and functionalities

CrackDect is divided into independent modules. The processing pipeline is linear for nearly all cases. The user loads images, processes them and at the end performs the crack detection. Fig. 2 shows a typical example of the process pipeline. The main modules are:

- *imagestack*: Classes to efficiently handle large image collections.
- *stack_operations*: Processing image stacks, coordinate transformations and the detection of changes in image series.
- *crack_detection*: Core functionality of the crack detection and implementation of the automated crack detection algorithm.

An *_io* module with convenience functions as well as a viewer for image stacks (*visualization*) is included. Bottom-level functions to process single images are collected in *image_functions*. Fig. 3 shows the structure of the package with functions and classes of the main modules. The package builds on the functionality of NumPy [15], SciPy [16], Scikit-image [17] and Numba [18]. Matplotlib [19] is used for visualization.

2.2. The ImageStack

Image stacks behave like Python lists for accessing and manipulating images. The only difference is that there is no such thing as nested image stacks and addition, subtraction, and other comparison methods (e.g. greater than) are not implemented. The images of a stack are represented as NumPy arrays. Currently, two classes handle image stacks:

- *ImageStack*: Light wrapper around a Python list with additional methods for image processing.
- *ImageStackSQL*: Connects to a database to store and load images. This is done fully automated by taking advantage of lazy loading from the object-relational mapper SQLAlchemy [20]. It tracks allocated RAM of the images and starts to save

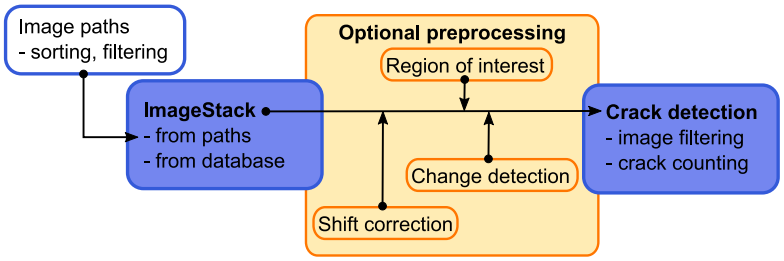

Fig. 2. Pipeline example for the crack detection. The pre-processing is optional and modular so custom image processing functions can be used on the image stack.

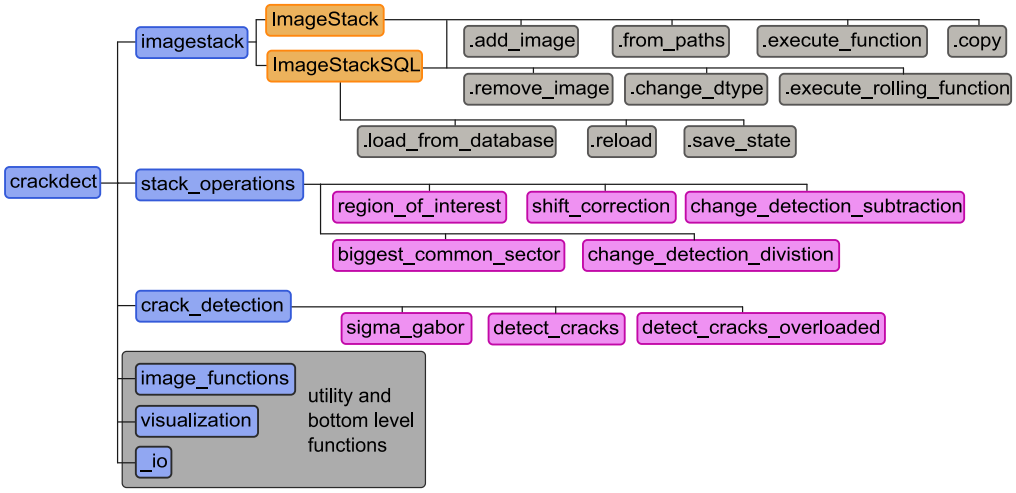

Fig. 3. Structure of the main modules. (Sub)modules are blue, classes yellow, class methods gray and functions pink. (For interpretation of the references to color in this figure legend, the reader is referred to the web version of this article.)

all changes in the connected database when a set RAM limit is exceeded. Images persist in RAM until RAM is needed and expired images are only loaded the next time they are directly accessed. This allows to create and manipulate image stacks that exceed the available RAM. It can also be used to save preliminary results or for data transfer since an image stack object can be created from previously saved stacks.

All these classes have the same base methods for accessing and setting images. Therefore it does not matter from which class the image stack object originates when using pre-processing functions on an image stack. All images in one stack must have the same data type (e.g. *np.float32*) which can be selected by the user. If an image is added to the stack or modified, the data type is automatically adjusted if it does not fit. This ensures similar behavior of image processing functions for all images in the stack.

2.3. Stack operations

All stack operations can act on an image stack or a simple list of images. The basic pre-processing for images captured with TWLI is included. All the functions change the images in the stack they act upon. If the state prior to a stack operation should be preserved, the image stack can be copied before the stack operation. Currently, there are functions to detect the change between two images, shift corrections and cropping to desired regions implemented.

2.4. Crack detection

The *crack_detection* module provides all parts of the crack detection algorithm as well as top-level functions for convenient access. The algorithm searches for cracks only in one given direction at a time. Therefore it is possible to detect the cracks for plies with fibers in one direction without detecting the cracks of other plies. The crack detection module performs the following steps:

1. Gabor filter: The Gabor filter is applied to an image. This recognizes edges in a given direction [21].
2. Threshold: The result of the Gabor filter is divided into foreground and background. Foreground is considered as cracked area. The default in this package is Yen's method [22]. Glud's algorithm uses Otsu's threshold [14,23] but for images with blurry areas, artifacts and high crack densities, Yen's threshold has been found to give better results and less false detections in the examples tested.
3. Skeletonizing: The resulting pattern is then reduced to lines of 1 pixel width by a skeletonizing algorithm [24].
4. Crack detection: The skeletonized image is then rotated until the cracks point in the vertical direction. Then an algorithm scans each row of pixels. Upon finding a crack (white pixel) it follows the crack to the end, deletes it from the pattern and saves start and endpoint of the crack. This is repeated until all cracks are detected. Based on the coordinates of start and endpoints, the crack density is calculated as

$$\rho_c = \frac{\sum_{i=1}^{n} L_i}{A} \tag{1}$$

with L_i denoting the length of crack i and A denoting the area of the input image.

An example of what these steps look like for a real image with cracks is shown in Fig. 4. It shows the steps from the original

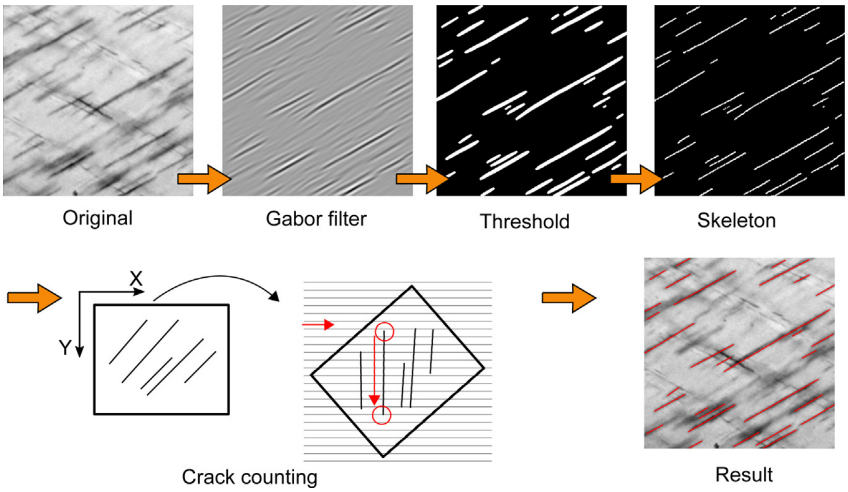

Fig. 4. The filtering steps and final result of the crack detection algorithm. The result shows the detected cracks with the original image in the background.

image to the resulting detected cracks for an example image. Intermediate steps after applying a Gabor filter, using a threshold, and skeletonizing are shown for this image.

3. Illustrative examples

The CrackDect tool is here used for detecting cracks in a set of example images that had been taken during fatigue experiments of glass fiber-reinforced composite laminates (see Fig. 5). The laminates consist of 12 layers with orientations of $\pm 60°$ relative to the (vertical) loading direction. Details about the tests are reported in [25]. The folder *example_images* in the repository contains all images for this example. This is the complete script for producing the results shown in Fig. 5(b):

```
import numpy as np
import crackdect as cr

# read image paths for *.bmp images
paths = cr.image_paths('example_images',
    image_types=['bmp'])
# create image stack from paths
stack = cr.ImageStack.from_paths(paths, dtype=np.
    float32, as_gray=True)

# align the images in a global coordinate system
cr.shift_correction(stack)
# cut to desired region
cr.region_of_interest(stack, x0=100, x1=1400, y0
    =20, y1=850)

# crack detection for the pre-processed images
rho, cracks, _ = cr.detect_cracks(stack, theta=60,
     crack_width=10, ar=2, min_size=20)
```

In this script, all images are bulk-loaded into an *ImageStack*. The last image of the stack is shown in Fig. 5(a) and the detected cracks in Fig. 5(b). The images of the stack are not aligned perfectly so a shift correction is necessary. Furthermore, the region of interest is defined as the area of the specimen above the black bar because such markings or artifacts could lead to false detections. White background must not be included in the crack detection since the computation of the crack density is based on the area of the input image. As shown in Fig. 5(b), only cracks aligned with the specified orientation are detected. The crack detection does not alter the image so that cracks in a range of directions (defined by θ_i) can be detected by repeatedly running the detection tool with the angle θ_i as input.

Since the crack detection relies on the Gabor filter, a few settings are needed to create a suitable filter kernel. The following parameters are set to default values but should be adjusted to reliably detect cracks in a given image:

- *theta*: The angle θ between the search direction and a vertical line.
- *crack_width*: Approximate width of the cracks to be detected in pixels. This value is taken as the wavelength of the Gabor kernel.
- *ar*: The aspect ratio of the Gabor kernel. Since cracks are usually long and thin, an aspect ratio larger than 1 should be chosen, howerver, choosing the aspect ratio too high may lead to false detection. A good compromise between speed and accuracy has been found to be a value of 2.
- *min_size*: The minimum length of detected cracks in pixels. Since small artifacts or noise can lead to false detection, this parameter provides an additional filter to exclude unrealistically small detections.

The accuracy of the crack detection is determined by the quality of the input images. A clear image in terms of focus and contrast will result in fewer false detections or missed cracks. The prerequisite for a successful crack detection is always a crack that has contrast to the background. Delamination interferes with the crack detection since it also appears as dark areas in the images. Also, the cracks in the image must be separated by at least a few pixels. Otherwise, two cracks will only get detected as one crack. This can lead to an underestimation of the crack density for images with very high crack densities and delamination.

4. Impact

Characterization of the fatigue behavior of fiber-reinforced polymers and the development of phenomenological damage models is an increasingly growing research topic. This package aims to provide an efficient and easy-to-use toolkit to quantify off-axis cracks based on an automated crack detection algorithm. The main advantages are:

- The evaluation of off-axis cracks is easy to set up. Only a few lines of code (see the example in Section 3) will provide the user with an accurate and reproducible crack density. This speeds up the process enormously compared to manual crack counting and enables the evaluation of large experimental campaigns.

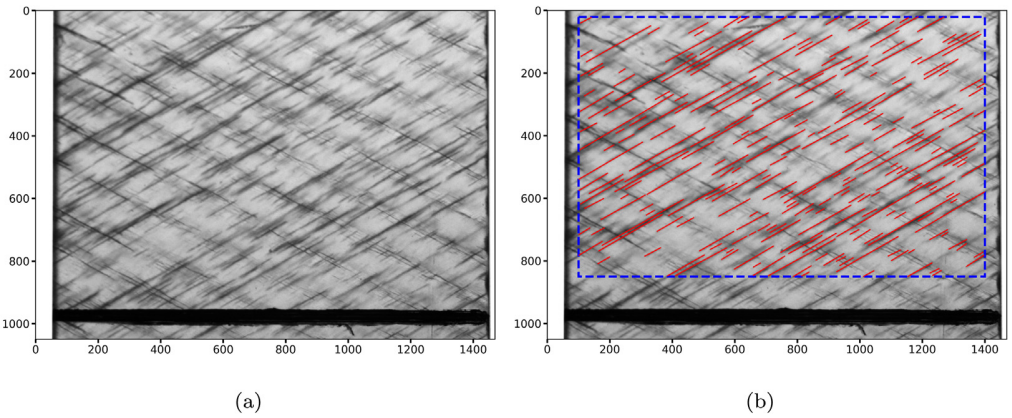

Fig. 5. Original image (a) and the detected cracks (b) with an angle of 60° to the vertical direction. The dashed blue line indicates the selected region of interest, where the white background and black bar are excluded to avoid artifacts in the crack detection. The shown cracks are the result of the parameters shown in the code example in line 15.

- CrackDect not only provides a powerful crack detection algorithm but also tools to efficiently handle image stacks that would overload RAM when loaded at once. The container objects presented in Section 2.2 can be used in all sorts of image processing applications. Batch image processing with complex functions that take the information of multiple images and require several steps can be implemented without needing to worry about memory limits. Multiple image stacks can be stored in one database for easy data transfer.
- CrackDect is developed for scientific use. With a free license model and fully written in Python, the package is accessible for everyone but especially reaches out to the composite fatigue community. The used crack detection algorithm has been described before [14]. CrackDect, however, is the first free and open-source crack density detection tool that efficient handles large image stacks. This efficiency is crucial for large experimental campaigns.

Even if designed and optimized for the specific case of crack detection, CrackDect can be used as a general line detection tool. The modular pre-processing pipeline can be adapted to other image capturing techniques or completely different applications where multiple line-shaped objects with distinct orientations should be detected in images.

5. Conclusions

In this work, a modular crack detection and batch image processing toolkit is introduced. It is optimized for the detection of matrix cracks in transparent composite laminates to obtain crack densities. The tool is implemented in an efficient way for the evaluation of large experimental campaigns. The package puts special focus on efficiency and easy implementation for other researchers. The authors intend to motivate others to use automated crack detection since the extra effort in experiments is low and it provides an direct measure of damage. With this we hope to further accelerate the development of fatigue damage models for composites.

Declaration of competing interest

The authors declare that they have no known competing financial interests or personal relationships that could have appeared to influence the work reported in this paper.

Acknowledgments

Part of this work has been performed within the COMET-project *Experimental and numerical analysis of the damage tolerance behavior of manufactured induced defects and bonded repairs in structural aerospace composite parts* (project-no.: VI-3.04) at the Polymer Competence Center Leoben GmbH (PCCL, Austria) within the framework of the COMET-program of the Federal Ministry for Transport, Innovation and Technology and the Federal Ministry for Digital and Economic Affairs with contributions by Montanuniversität Leoben (Chair of Designing Plastics and Composite Materials) and MAGNA Powertrain Engeneering Center Steyr GmbH CO KG. The PCCL is funded by the Austrian Government and the State Governments of Styria, Lower Austria and Upper Austria.

References

[1] Reifsnider K. In: Reifsnider KL, editor. Fatigue of composite materials. Composite materials series, (4). Amsterdam ; New York: Elsevier; 1991.

[2] Tong J, Guild F, Ogin S, Smith P. On matrix crack growth in quasi-isotropic laminates—I. Experimental investigation. Compos Sci Technol 1997;57(11):1527–35. http://dx.doi.org/10.1016/S0266-3538(97)00080-8, URL https://linkinghub.elsevier.com/retrieve/pii/S0266353897000808.

[3] Bartley-Cho J, Gyu Lim S, Hahn H, Shyprykevich P. Damage accumulation in quasi-isotropic graphite/epoxy laminates under constant-amplitude fatigue and block loading. Compos Sci Technol 1998;58(9):1535–47. http://dx.doi.org/10.1016/S0266-3538(97)00214-5, URL https://linkinghub.elsevier.com/retrieve/pii/S0266353897002145.

[4] Wharmby A, Ellyin F. Damage growth in constrained angle-ply laminates under cyclic loading. Compos Sci Technol 2002;62(9):1239–47. http://dx.doi.org/10.1016/S0266-3538(02)00075-1, URL https://linkinghub.elsevier.com/retrieve/pii/S0266353802000751.

[5] Tohgo K, Nakagawa S, Kageyama K. Fatigue behavior of CFRP cross-ply laminates under on-axis and off-axis cyclic loading. Int J Fatigue 2006;28(10):1254–62. http://dx.doi.org/10.1016/j.ijfatigue.2006.02.011, URL https://linkinghub.elsevier.com/retrieve/pii/S0142112306000466.

[6] Adden S, Horst P. Stiffness degradation under fatigue in multiaxially loaded non-crimped-fabrics. Int J Fatigue 2010;32(1):108–22. http://dx.doi.org/10.1016/j.ijfatigue.2009.02.002, URL https://linkinghub.elsevier.com/retrieve/pii/S0142112309000334.

[7] Quaresimin M, Carraro P. Damage initiation and evolution in glass/epoxy tubes subjected to combined tension–torsion fatigue loading. Int J Fatigue 2014;63:25–35. http://dx.doi.org/10.1016/j.ijfatigue.2014.01.002, URL https://linkinghub.elsevier.com/retrieve/pii/S0142112314000036.

[8] Quaresimin M, Carraro P, Mikkelsen L, Lucato N, Vivian L, Brøndsted P, Sørensen B, Varna J, Talreja R. Damage evolution under cyclic multiaxial stress state: A comparative analysis between glass/epoxy laminates and tubes. Composites B 2014;61:282–90. http://dx.doi.org/10.1016/j.compositesb.2014.01.056, URL https://linkinghub.elsevier.com/retrieve/pii/S1359836814000663.

[9] Schuecker C, Pettermann H. A continuum damage model for fiber reinforced laminates based on ply failure mechanisms. Compos Struct 2006;76(1–2):162–73. http://dx.doi.org/10.1016/j.compstruct.2006.06.023, URL https://linkinghub.elsevier.com/retrieve/pii/S0263822306002625.

[10] Singh CV, Talreja R. A synergistic damage mechanics approach for composite laminates with matrix cracks in multiple orientations. Mech Mater 2009;41(8):954–68. http://dx.doi.org/10.1016/j.mechmat.2009.02.008, URL https://linkinghub.elsevier.com/retrieve/pii/S0167663609000490.

[11] Carraro P, Quaresimin M. A stiffness degradation model for cracked multidirectional laminates with cracks in multiple layers. Int J Solids Struct 2015;58:34–51. http://dx.doi.org/10.1016/j.ijsolstr.2014.12.016, URL https://linkinghub.elsevier.com/retrieve/pii/S0020768314004843.

[12] Tong J, Guild F, Ogin S, Smith P. Off-axis fatigue crack growth and the associated energy release rate in composite laminates. Appl Compos Mater 1997;4(6):349–59. http://dx.doi.org/10.1007/BF02481399, URL http://link.springer.com/10.1007/BF02481399.

[13] Sket F, Enfedaque A, Alton C, González C, Molina-Aldareguia J, Llorca J. Automatic quantification of matrix cracking and fiber rotation by X-ray computed tomography in shear-deformed carbon fiber-reinforced laminates. Compos Sci Technol 2014;90:129–38. http://dx.doi.org/10.1016/j.compscitech.2013.10.022, URL https://linkinghub.elsevier.com/retrieve/pii/S0266353813004223.

[14] Glud J, Dulieu-Barton J, Thomsen O, Overgaard L. Automated counting of off-axis tunnelling cracks using digital image processing. Compos Sci Technol 2016;125:80–9. http://dx.doi.org/10.1016/j.compscitech.2016.01.019, URL https://linkinghub.elsevier.com/retrieve/pii/S0266353816300197.

[15] Harris CR, Millman KJ, van der Walt SJ, Gommers R, Virtanen P, Cournapeau D, et al. Array programming with NumPy. Nature 2020;585(7825):357–62. http://dx.doi.org/10.1038/s41586-020-2649-2, URL http://www.nature.com/articles/s41586-020-2649-2.

[16] SciPy 10 Contributors, Virtanen P, Gommers R, Oliphant TE, Haberland M, Reddy T, et al. SciPy 1.0: fundamental algorithms for scientific computing in Python. Nature Methods 2020;17(3):261–72. http://dx.doi.org/10.1038/s41592-019-0686-2, URL http://www.nature.com/articles/s41592-019-0686-2.

[17] van der Walt S, Schönberger JL, Nunez-Iglesias J, Boulogne F, Warner JD, Yager N, et al. Scikit-image: image processing in Python. PeerJ 2014;2:e453. http://dx.doi.org/10.7717/peerj.453, URL https://peerj.com/articles/453.

[18] Lam SK, Pitrou A, Seibert S. Numba: a LLVM-based Python JIT compiler. In: Proceedings of the second workshop on the llvm compiler infrastructure in HPC. Austin, Texas: ACM Press; 2015, p. 1–6. http://dx.doi.org/10.1145/2833157.2833162, URL http://dl.acm.org/citation.cfm?doid=2833157.2833162.

[19] Hunter JD. Matplotlib: A 2D graphics environment. Comput Sci Eng 2007;9(3):90–5. http://dx.doi.org/10.1109/MCSE.2007.55.

[20] Bayer M. SQLAlchemy. In: Brown A, Wilson G, editors. The architecture of open source applications volume II: structure, scale, and a few more fearless hacks. aosabook.org; 2012, URL http://aosabook.org/en/sqlalchemy.html.

[21] Fogel I, Sagi D. Gabor filters as texture discriminator. Biol Cybernet 1989;61(2). http://dx.doi.org/10.1007/BF00204594, URL http://link.springer.com/10.1007/BF00204594.

[22] Jui-Cheng Yen, Fu-Juay Chang, Shyang Chang. A new criterion for automatic multilevel thresholding. IEEE Trans Image Process 1995;4(3):370–8. http://dx.doi.org/10.1109/83.366472.

[23] Otsu N. A threshold selection method from gray-level histograms. IEEE Trans Syst Man Cybern 1979;9(1):62–6. http://dx.doi.org/10.1109/TSMC.1979.4310076, URL http://ieeexplore.ieee.org/document/4310076/.

[24] Lee T, Kashyap R, Chu C. Building skeleton models via 3-D medial surface axis thinning algorithms. CVGIP: Graph Models Image Process 1994;56(6):462–78. http://dx.doi.org/10.1006/cgip.1994.1042, URL https://linkinghub.elsevier.com/retrieve/pii/S104996528471042X.

[25] Rieser R. Damage mechanics of composites under fatigue loads [Master's thesis], Austria: Montanuniversität Leoben; 2016.

Paper A2

Version 0.2 - CrackDect: Detecting crack densities in images of fiber-reinforced polymers

Authors: Drvoderic, Matthias
Bender, Jens J.
Pletz, Martin
Schuecker, Clara

SoftwareX
DOI: 10.1016/j.softx.2022.101198

SoftwareX 19 (2022) 101198

Contents lists available at ScienceDirect

SoftwareX

journal homepage: www.elsevier.com/locate/softx

Software update

Version 0.2 - CrackDect: Detecting crack densities in images of fiber-reinforced polymers

Matthias Drvoderic [a], Jens J. Bender [b], Martin Pletz [a,*], Clara Schuecker [a]

[a] Chair of Designing Plastics and Composite Materials, Department of Polymer Engineering and Science, Montanuniversitaet Leoben, Austria
[b] CraCS Research Group, Department of Materials and Production, Aalborg University, Fibigerstraede 16, DK-9220, Aalborg East, Denmark

ARTICLE INFO

Article history:
Received 15 July 2022
Accepted 22 August 2022

MSC:
68U10

Keywords:
Crack detection
Image processing
Fiber-reinforced polymers
Crack density
Python

ABSTRACT

The new and improved crack detection algorithm from J.J. Bender for the detection of off-axis cracks in composite materials, as well as a general shift-distortion correction for coherent image series is added to *CrackDect*.

Code metadata

Current code version	v0.2
Permanent link to code/repository used for this code version	https://github.com/ElsevierSoftwareX/SOFTX-D-22-00198
Code Ocean compute capsule	–
Legal Code License	MIT
Code versioning system used	GIT
Software code languages, tools, and services used	Python, Scikit-image, SciPy, NumPy, SQLAlchemy, Numba, Matplotlib, PyQt5
Compilation requirements, operating environments	Python 3.8.x and higher, cross platform
If available Link to developer documentation/manual	https://crackdect.readthedocs.io/en/latest/
Support email for questions	kkv.leoben@gmail.com

1. Description of the software-update

The main additions to *CrackDect* are:

- Implementation of J.J. Bender's crack detection method [1].
- General shift-distortion correction as addition to the existing shift correction methods for coherent image series.

The crack detection method from J.J. Bender is added to *CrackDect*. It is optimized for crack detection of straight off-axis cracks in images of semi-transparent specimen. Originally, it was developed for images captured with transilluminated white light imaging (TWLI), but can be applied to any image as long as there is sufficient contrast between cracks and background. Same as the already implemented algorithm, the purpose is to detect multiple straight cracks in an image. The prerequisites are an image series of a specimen where the first image is used as the reference/background image. This method relies on the history of the images (difference with the prior and reference image) and therefore, it is only applicable to a whole series of images and not to a single image. The main advantage is the capability of an improved crack detection at already high crack densities. It also shows improvements in terms of reduced

DOI of original article: https://doi.org/10.1016/j.softx.2021.100832.
* Corresponding author.
E-mail address: martin.pletz@unileoben.ac.at (Martin Pletz).

https://doi.org/10.1016/j.softx.2022.101198

false-detections and can handle images without any cracks. Compared to the already implemented crack detection algorithm, it is also more robust to changes in illumination and general image noise. This robustness mainly originates in incorporating the history of each image and subsequent elimination of image noise.

Since Bender's crack detection method is only applicable to image series with perfectly aligned images, a general shift and distortion correction is added to *CrackDect*. This allows to correct images where the specimen shows significant shift and/or distortion throughout the series. The prerequisite are features on the specimen that can be used as markers to trace their relative movement.

The detailed documentation of the new crack detection method as well as the shift-distortion correction with examples is available in the official documentation https://crackdect.readthedocs.io/en/latest.

Declaration of competing interest

The authors declare that they have no known competing financial interests or personal relationships that could have appeared to influence the work reported in this paper.

Data availability

No data was used for the research described in the article.

References

[1] Bender J, Bak B, Jensen S, Lindgaard E. Effect of variable amplitude block loading on intralaminar crack initiation and propagation in multidirectional GFRP laminate. Composites B 2021;217. http://dx.doi.org/10.1016/j.compositesb.2021.108905, URL https://linkinghub.elsevier.com/retrieve/pii/S135983682100295X.

Paper B

Modeling Stiffness Degradation of Fiber-Reinforced Polymers Based on Crack Densities Observed in Off-Axis Plies

Authors: Drvoderic, Matthias
Pletz, Martin
Schuecker, Clara

Journal of Composites Science
DOI: 10.3390/jcs6010010

Journal of
Composites Science

MDPI

Article

Modeling Stiffness Degradation of Fiber-Reinforced Polymers Based on Crack Densities Observed in Off-Axis Plies

Matthias Drvoderic, Martin Pletz and Clara Schuecker *

Chair of Designing Plastics and Composite Materials, Department of Polymer Engineering and Science, Montanuniversitaet Leoben, 8700 Leoben, Austria; matthias.drvoderic@unileoben.ac.at (M.D.); martin.pletz@unileoben.ac.at (M.P.)
* Correspondence: clara.schuecker@unileoben.ac.at

Abstract: A model that predicts the stiffness degradation in multidirectional reinforced laminates due to off-axis matrix cracks is proposed and evaluated using data from fatigue experiments. Off-axis cracks are detected in images from the fatigue tests with automated crack detection to compute the crack density of the off-axis cracks which is used as the damage parameter for the degradation model. The purpose of this study is to test the effect of off-axis cracks on laminate stiffness for different laminate configurations. The hypothesis is that off-axis cracks have the same effect on the stiffness of a ply regardless of the acting stress components as long as the transverse stress is positive. This hypothesis proves to be wrong. The model is able to predict the stiffness degradation well for laminates with a ply orientation similar to the one used for calibration but deviates for plies with different in-plane shear stress. This behavior can be explained by the theory that off-axis cracks develop by two different micro damage modes depending on the level of in-plane shear stress. It is found that besides influencing the initiation and growth of off-axis cracks, the stiffness degradation is also mode dependent.

Keywords: crack detection; fiber-reinforced polymers; fatigue damage model; composite fatigue; off-axis cracks

Citation: Drvoderic, M.; Pletz, M.; Schuecker, C. Modeling Stiffness Degradation of Fiber-Reinforced Polymers Based on Crack Densities Observed in Off-Axis Plies. *J. Compos. Sci.* **2022**, *6*, 10. https://doi.org/10.3390/jcs6010010

Academic Editor: Stelios K. Georgantzinos

Received: 7 December 2021
Accepted: 23 December 2021
Published: 29 December 2021

Publisher's Note: MDPI stays neutral with regard to jurisdictional claims in published maps and institutional affiliations.

1. Introduction

Components made from multidirectional fiber-reinforced composite laminates experience several distinct damage mechanisms when exposed to fatigue loads. The macroscopic damage mechanisms are matrix cracks, delamination, and fiber failure. This sequence of damage mechanisms during fatigue loading can be categorized into characteristic damage states [1]. The first fatigue-damage state of multi-axial laminates is matrix cracking in off-axis plies where multiple matrix cracks develop and grow in number and length. These so-called off-axis cracks typically span the whole thickness of a ply and propagate along the fiber direction. One of the main effects of off-axis cracks is a significant stiffness reduction of the laminate but not immediate failure of the component [2–8].

Since multiple similar cracks form under fatigue loading, the crack density is used as a measure for the amount of damage in the material in many progressive damage models [9–17]. These models describe the evolution of off-axis cracks as well as their effect on the stiffness of a laminate. Therefore, off-axis crack densities are often used in the development and calibration of these models or to compare their predictions to experimental data. Transmitted or transilluminated white light imaging (TWLI) can be used for transparent composites like glass fiber-reinforced polymers (GFRPs). It is an efficient, reliable and relatively simple method to capture off-axis cracks [2,10,18–20]. TWLI uses a light source placed behind a transparent specimen and a camera on the other side. An undamaged specimen appears bright as it only absorbs a small portion of the light. Cracks, on the other hand, scatter the light and therefore appear as dark lines in the images. For non-transparent laminates, more sophisticated techniques like computed tomography

may be used [21]. Up to now, a few methods have been developed to compute the crack density from TWLI images. The simplest is to count all cracks along a straight line normal to the fiber direction and divide the number of counted cracks by the length of the line. This method only takes the number of counted cracks and not their length into account and the results are influenced by the selection of the path. As shown in Refs. [17,22,23], including the crack length results in an improved description of the average damage state of the material. A better approach that includes some information of the crack length is the weighted crack density used by Quaresimin et al. [7]. It clusters the cracks into eight groups of crack lengths and then computes a weighted average. Still, manually counting and categorizing the cracks is labor intensive and prone to human errors. An automated algorithm that takes the images as input and detects all cracks in a given direction has been developed by Glud et al. [24]. Based on this algorithm, we have developed *CrackDect*, an open-source package for evaluating crack densities [25]. With this package, even large fatigue test series can be evaluated efficiently. Figure 1 qualitatively shows the evolution of off-axis cracks and the associated stiffness degradation as well as examples of images taken during fatigue tests. CrackDect takes these images and computes the crack density.

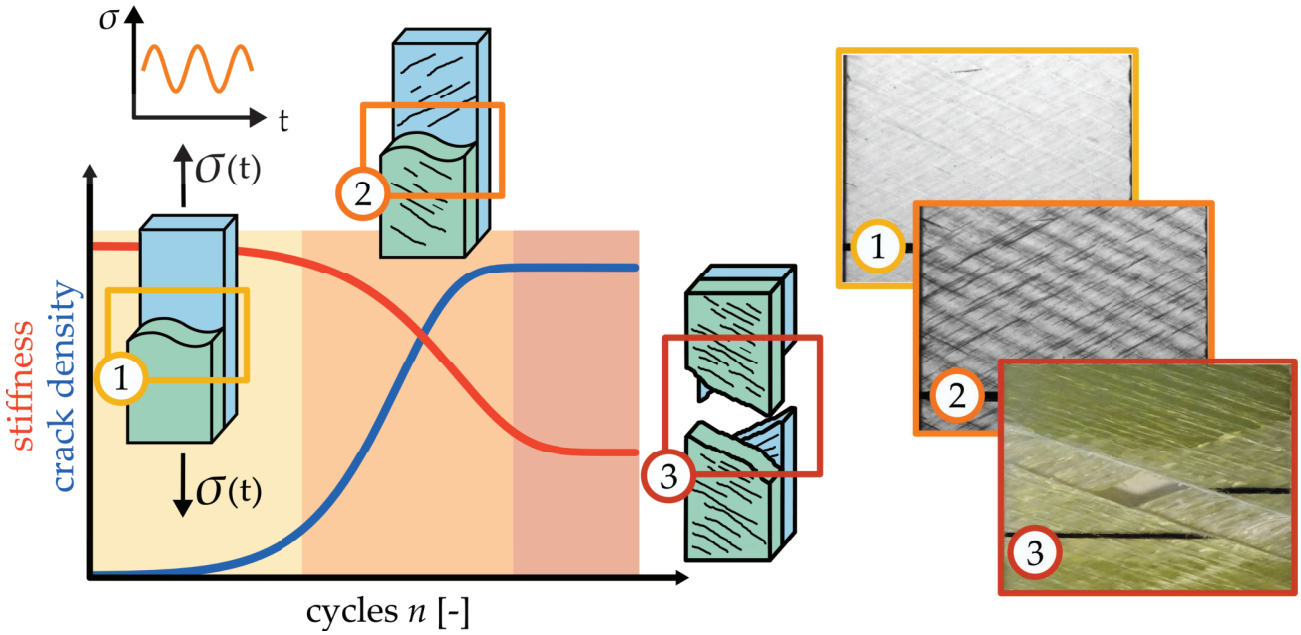

Figure 1. Evolution of off-axis cracks during fatigue tests. The stiffness stays constant as long as there are no cracks (1). After the onset of matrix cracking (2), the cracks grow in number and size and the stiffness starts to decrease due to the damage. (3) The last stage of matrix damage in composites is crack saturation and finally total failure usually due to other damage mechanisms like fiber failure and delamination.

Many fatigue models have been developed to describe the effect of fatigue damage in composite laminates. Degrieck and Van Paepegem [26] sorted them into three categories: fatigue life models, phenomenological models, and progressive damage models. To accurately describe the effect of distinct damage modes, progressive damage models are the most promising candidates since they take the actual cause of the degradation of a mechanical property—the damage—into account. Usually, this is done in a two step approach. In the first step, a damage model describes the evolution of a damage variable with respect to the undamaged material. The second step computes the effect of this damage on mechanical properties. Many models have been developed that establish a connection between off-axis cracks and laminate stiffness [9–17,27]. Often, the Finite Element Method (FEM) is used to compute the elastic response of a laminate. One widely-used approach is to model a representative volume element of the laminate with cracks in one or more plies [17,19].

Resolving the laminate into its plies and computing the effect of cracks on the ply-level has the advantage that the elastic response of any laminate can be computed. The drawback of FEM is that it is time-consuming when implemented as a sub-model for evaluation of large composite structures. Carraro et al. [9] further compared several modeling techniques and developed an analytical model based on shear lag analysis with the capability to compute the elastic response of any symmetric laminate. One drawback of this model is that the laminate must be symmetric and the elastic response is computed for cracks in both symmetric plies. This means that bending loads which yield unsymmetrical stress distributions in the laminate cannot be accounted for. Schuecker et al. [27] proposed a static damage model that computes the stiffness degradation based on the Mori-Tanaka method. The Mori-Tanaka method is a micro-mechanical approach to compute homogenized material properties of a material consisting of a matrix and an embedded inclusion [28]. This allows to compute the stiffness degradation for each ply separately and then combine all plies using classical laminate theory to compute the overall stiffness of the damaged laminate. In Schuecker's approach, the effect of crack-like void inclusions on the stiffness of a ply is computed. Even though this model has been developed for static load cases, it should also be applicable to fatigue since the stiffness degradation is only dependent on the amount of cracks. The main advantages of this model are:

1. The Mori-Tanaka homogenization scheme computes the effect of damage on the stiffness. The resulting stiffness tensor is positive, definite and symmetric. Therefore it meets the thermodynamic limits of the engineering constants of the damaged material without having to develop individual correlations for all the independent engineering constants [29].
2. The model can be calibrated easily to a new material. All data to calibrate the model can be obtained with standard static and fatigue tests.
3. The stiffness degradation is ply-based. Classical laminate theory is used to compute the overall stiffness of the laminate. Therefore, stress-redistribution to other plies is automatically accounted for. The model builds on well-established methods and focuses on efficiency.

Naturally, the model has limitations and prerequisites arising from classical laminate theory and the Mori-Tanaka method, but it has proven to provide an overall relatively simple yet effective approach to compute stiffness degradation of laminates due to cracks. Also, it does not consider delaminations or other damage mechanisms of composite laminates [27,30].

In this work, Schuecker's degradation model is combined with crack detection by replacing the evolution function for static loads by the crack evolution detected from experimental data. Based on the off-axis crack density from experiments, the stiffness degradation computed by the degradation model is compared to experimental stiffness data. Opposed to other works like [31], where crack densities of similar specimens have been averaged, we take the crack density of each individual test and compute the resulting stiffness degradation. This enables a comparison of experimental stiffness data and predictions based on experimental crack density data for individual specimens. Also, a mostly-automated procedure to fit experimental crack density data from the automated crack detection is presented.

2. Methods

2.1. Experimental Fatigue Data

Experimental data from fatigue tests of $\pm\theta_s$ GFRP laminates from [32] is used for comparison with computations of the damage model. The specimens with a gauge length of 100 mm, a width of 20 mm, and a thickness of 2 mm (12 layers) had been cut from GFRP laminate plates produced from a unidirectional glass fiber weave and epoxy resin. The plates had been produced by vacuum pressing manually-impregnated glass fiber layers. The stacking sequence of the laminates is $[+\theta_3/-\theta_3]_s$. For the fatigue tests, stress-controlled sinusoidal load cycles with an R-ratio of 0.1 and a frequency of 5 Hz had been

periodically interrupted to perform displacement-controlled quasi-static tensile tests. The servo-hydraulic material testing system MTS 810 by MTS Systems Corporations had been used for all tests with an optical displacement measurement system (CV-X100 by Keyence) to provide a free field of few for the images taken during the tests. This procedure allows to track the change in stiffness as a function of the number of cycles and take images for the crack detection. For a more detailed description of the experimental setup, the reader is refered to [32]. In addition to the stiffness of the laminates, the crack density is evaluated from TWLI images with crack detection. For this work, the results of the fatigue tests for ±45°, ±60°, and ±75° laminates are used. Laminates with a ply orientation of less than ±45° show delamination as the main damage mode and only little off-axis cracks. The unidirectional 90° laminates show hardly any cracks before final failure.

For each laminate type, two fatigue tests had been conducted. Table 1 lists the static stiffness, transverse strength R_2, and in-plane shear strength R_{12} of the material. In the referenced data from [32], a miscalculation had happened in the evaluation of the in-plane shear strength and in-plane shear modulus G_{12}, which is corrected in this work. Additionally, the static ply properties are corrected with respect to the fiber volume fraction of the individual specimens. The procedure is described in Appendix A. The aforementioned miscalculation does not effect the validity of the tests since only the evaluation had to be redone. The load level of the fatigue tests, which is the ratio of the maximum load in the fatigue test to the static strength of the laminate, is computed by the Puck failure criterion [33]. The exact computation is given in Appendix B. The load levels of the tests are 75% for ±45°, 78% for ±60°, and 74% for ±75° laminates. The slight differences between load levels arise from the corrections done in the evaluation.

Table 1. Elastic constants of the composite ply material from static tests.

E_1 [GPa]	E_2 [GPa]	ν_{12} [−]	G_{12} [GPa]	R_2 [MPa]	R_{12} [MPa]
35.6	10.9	0.27	3.2	57.9	58.3

2.2. Crack Detection

The Python package *CrackDect* is used to to automatically evaluate the crack density from the TWLI images [25]. This package includes a sightly modified crack detection algorithm compared to [24]. Example pictures of a specimen at the beginning, during, and at the end of the fatigue test prior to image processing are shown in Figure 2. The processing pipeline of the images is as follows:

1. **Shift correction:** Since the individual images from a fatigue test are not aligned perfectly due to increasing strain and unavoidable inaccuracies of the test rig (see Figure 2), the shift of the specimen in the images must be corrected.
2. **Region of interest:** Only the area of the specimen without edges or other features like the black line that is used for optical strain measurement (see Figure 2), is evaluated by the crack detection since they might cause false detections.
3. **Crack detection:** Cracks are detected in a cumulative way. Cracks detected in the nth image are added to the n + 1st image.

The exact procedure of this processing pipeline is explained in [25] where the open-source code of all functions can be obtained. The input parameters are listed in Table 2 for each test series. It is observed that the crack width of the first major visible cracks varies slightly with the fiber orientation. Cracks in the ±45° specimens appear to be thinner than in ±75° specimens. Therefore, the average width of cracks that should be detected by the crack detection is set individually for each test series to get comparable results between the test series. To avoid artifacts in the crack detection or false detection due to inherent noise in the images, cracks of less than 50 pixels (0.7 mm) in length are excluded from the evaluation. The crack density is defined as

$$\rho_c = \frac{\sum_{i=1}^{n} L_i}{A} \quad , \tag{1}$$

with L_i as the length of crack i and A as the area of the region of interest (evaluation area). Since the crack detection only computes the crack density based on pixels, the conversion from pixel to millimeter is also listed in Table 2.

Table 2. Input parameters for CrackDect. The coordinates of the region of interest x_0 to y_1 are given in pixel.

Test	Ply Angle [°]	Crack Width [px]	Pixel per mm	x_0	x_1	y_0	y_1
±45° T1	45	8	69.2	200	1500	0	900
±45° T2	45	8	70.3	200	1500	0	950
±60° T1	60	8	68.8	100	1400	0	850
±60° T2	60	10	70.2	100	1400	0	1000
±75° T1	75	15	69.6	200	1400	0	1000
±75° T2	75	12	70.2	200	1450	0	900

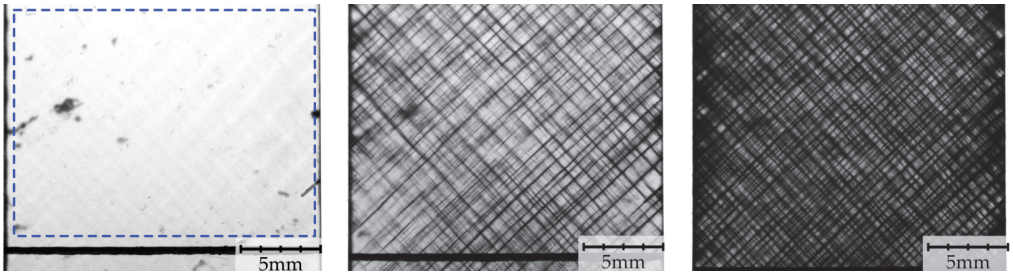

(**a**) (**b**) (**c**)

Figure 2. Example of TWLI images taken from a ±45° specimen with a load level of 75% before the test (**a**), after 254 cycles (**b**), and and after 4013 cycles (**c**). In (**a**), the evaluation area is shown for the crack density (region of interest) marked with the blue rectangle. In (**b**), a typical crack pattern for a ±45° is laminate shown and (**c**) shows the last image taken before failure. The shift of the specimen can easily be observed by the drift of the black line at the bottom from (**a**–**c**). In (**c**), delamination between the plies can be spotted as dark areas.

Instead of using the extracted densities directly, a crack density function is defined by fitting a cumulative Weibull distribution function to the experimental crack density data. The Weibull function is used since it has a form similar to the experimental crack density plotted over the number of cycles in logarithmic space. A direct fit of such a crack density function to the experimental data resulted in convergence problems, even with non-linear least squares algorithms (scipy.optimize.curve_fit) [34]. Therefore, a two-step approach was used to achieve a satisfactory quality of the fit. This fitting process is qualitatively illustrated in Figure 3. The first step is a linear regression in the region where the crack density increases linearly. For experiments that reach crack saturation, the linear fit is done from 30% to 85% of the maximal crack density. If crack saturation is not reached because the specimen fails prior to that, the region for the linear regression extends to 100%. In the second step, the following three-parameter cumulative Weibull distribution function is fitted to the linear regression

$$\rho_c^{fit}(n) = \left[1 - exp\left(-\left(\frac{n - n_0}{\lambda}\right)^k\right)\right] \cdot \rho_c^{sat} \quad , \tag{2}$$

with λ and k as scale and shape parameters respectively, and n_0 to shift the fitted curve along the x-axis. Note that n_0 is a fitting parameter and does not correlate with the cycles to damage initiation n^{init} defined later in Section 3.1. Since the Weibull distribution function has a span of 0–1, the fitted crack density function is scaled with the saturation crack density ρ_c^{sat}.

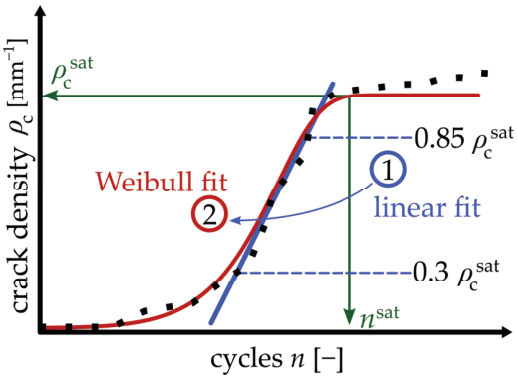

Figure 3. The experimentally obtained crack densities are fitted with a two-step approach. The first step is a linear regression from 30% to 85% of the saturation crack density. In the second step, a cumulative Weibull distribution function is fitted to the linear regression.

2.3. Damage Model

To compute the stiffness degradation of a laminate for a given damage state, Schuecke's damage model is used [27]. Like most progressive damage models, it consists of a part that describes the evolution of a damage variable and a part that computes the effect of this damage on the stiffness of the material. The first part computes the damage variable as a function of the loads for each ply. Then, in the second part, the degradation of stiffness based on the damage variable is computed using the Mori-Tanaka method. Here, only the second part of the model is used since the evolution of the damage variable is obtained by calibration to the fitted crack density functions. The damage variable in the model represents the volume fraction of crack-like inclusions in the Mori-Tanaka formulation, which for void inclusions, is given by

$$\boldsymbol{E}_{MTM,void} = \boldsymbol{E}^{(m)} \left[\boldsymbol{I} + \frac{V}{1-V} (\boldsymbol{I} - \boldsymbol{S})^{-1} \right]^{-1}, \tag{3}$$

where V is the inclusion volume fraction, $\boldsymbol{I}$ is the identity tensor, $\boldsymbol{E}^{(m)}$ is the initial stiffness tensor of the ply, and $\boldsymbol{S}$ is the Eshelby tensor [35,36]. To compute the Eshelby tensor for transversely isotropic materials, the numerical computation scheme by Gavazzi et al. [37] is used.

The Eshelby tensor for an inclusion depends on the surrounding material and the shape of the inclusion. It is assumed that the inclusion geometry is the same for all cracks and independent of the orientation of the ply. Often, an extremely sharp or disk-like inclusion geometry is used when the effect of cracks in a material is computed by the Mori-Tanaka method. Experimental evidence shows that off-axis cracks are often not straight but have a crooked path since the crack has to find the way of least resistance between the fibers. Cracks sometimes even split and merge on the way through the ply [20,38]. Here, the introduction of an orientation tensor to give idealized penny shaped cracks an orientation distribution similar to the crooked paths of the real cracks is avoided. Instead, one oblate ellipsoidal pore that represents the homogenized effect of these cracks qualitatively is used. It has been reported in [39,40] that this approach gives satisfactorily results. In this work, an aspect ratio of 100,1,10 in the 1,2,3-direction of the ply is chosen. The reasoning is as follows: The cracks are substantially longer in fiber direction than in out of plane direction so the 1-direction is set to 10 times the 3-direction. Also, cracks are relatively flat compared to the thickness of the ply so the 3-direction is 10 times the 2-direction. A schematic representation of this idealized inclusion is shown in Figure 4a and its effect on the ply properties is shown in Figure 4b. The curves of E_1, E_2, ν_{12} and G_{12} as function of to the inclusion volume show that E_2 is reduced the most relative to its initial value. The stiffness in fiber direction E_1 is reduced only slightly up to an inclusion volume fraction of 0.1. This behavior qualitatively agrees well with the stiffness degradation of a ply due to off-axis cracks. The degradation

of E_1, E_2, ν_{12} and G_{12} could be fine-tuned by adjusting the aspect ratios if additional data from static tensile tests were available that allows to relate the engineering constants of a ply directly to off-axis cracks.

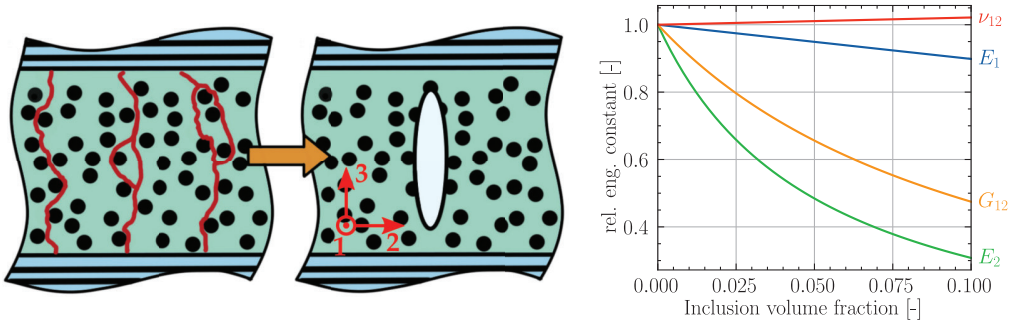

(**a**) (**b**)

Figure 4. Representation of off-axis cracks in one ply (**a**) looking in fiber direction. The crack path is often not straight and can branch or merge. Therefore, an oblate ellipsoid is chosen as a single inclusion shape to compute the homogenized effect of these cracks. The effect of this inclusion is shown in (**b**) with the aspect ratios of 100,1,10 in 1,2,3-direction, respectively.

2.4. Calibration

The Mori-Tanaka method uses inclusion volume fractions to compute the effect of an inclusion in a surrounding matrix material, but since the crack density is analyzed, the model needs to be calibrated to experimental data. A link between the crack density and the inclusion volume fraction for the analyzed stiffness degradation must be established. For this, the ±45° tests are used to calibrate the model. The following equation links the crack density (ρ_c) to the inclusion volume fraction (V) with a simple correlation factor (μ).

$$V = \mu \cdot \rho_c \tag{4}$$

The calibration process is illustrated in Figure 5. First, the experimental stiffness data is smoothed to reduce scatter using a lowess filter [41] with a window length of 40% the range of cycles. Then, the stiffness degradation relative to its initial value up to crack saturation (see Table 3) is calculated from this smoothed curve. Parallel to this, a model of the laminate is built with classical laminate theory. For each ply, the stiffness is reduced according to the damage model (see Equation (3)) as a function of the inclusion volume fraction. The inclusion volume fraction to reach the experimental stiffness degradation is optimized with the minimization algorithm from SciPy (*scipy.optimize.minimize*) [34]. From this, the correlation factor μ can easily be computed from Equation (4). This procedure is carried out for the two ±45° tests and the average is used as the global calibration constant for the material.

Table 3. Results of the crack detection. The cycle number to damage initiation n^{init}, saturation n^{sat}, and crack density growth rate in semi-logarithmic space $d\rho_c/d(log(n))$ are listed to compare the laminates.

Test	ρ_c^{sat} [mm^{-1}]	n^{init}	n^{sat}	$d\rho_c/d(log(n))$ [mm^{-1}]
±45° T1	3	140	4000	2.8
±45° T2	3	30	1500	2.7
±60° T1	2.1	304	2100	3.2
±60° T2	1.7	487	2200	2.3
±75° T1	1.3	93,086	-	2.9
±75° T2	1.3	68,314	-	2.7

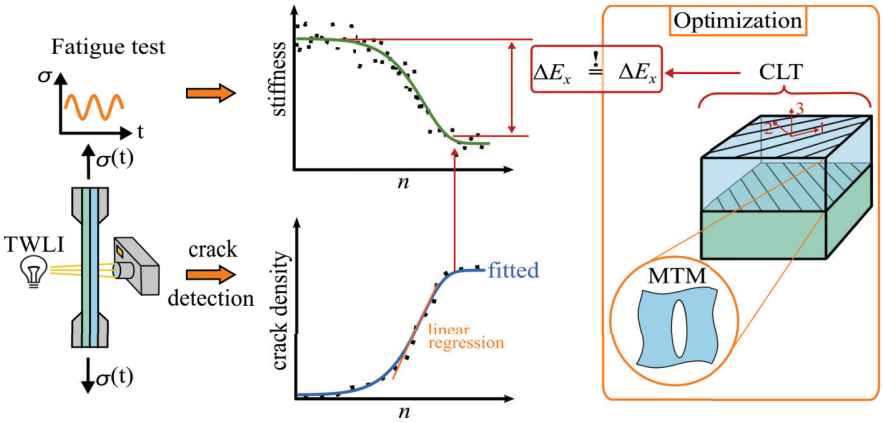

Figure 5. A schematic representation of the correlation process. The stiffness and crack density is evaluated in fatigue tests. The needed inclusion volume fraction is optimized to yield the same stiffness degradation as observed in the experiment. With Equation (4), the correlation constant is then computed from the experimental saturation density.

3. Results and Discussion

3.1. Crack Detection Results

The results of the crack detection are shown in Figure 6. An example of the cracks detected in +60° direction for the ±60° T1 specimen after 759 load cycles is shown in Figure 6a. At this state, the crack density is 0.8 mm/mm^2. The bigger cracks are detected well while cracks smaller than 50 pixel or 0.7 mm in length are filtered out. Since the laminate consists of 12 plies, cracks in the bottom layer will appear fainter and not as sharp as cracks in the top layer. Therefore, the detection is less reliable for cracks in the bottom layer. Cracks in negative fiber-direction are not included because the noise, blur and overlap with cracks in positive fiber direction from the top plies resulted in too many false detections. Since the plies in negative direction develop approximately the same amount of cracks as in positive direction (see Figure 2), only the positive direction is analyzed.

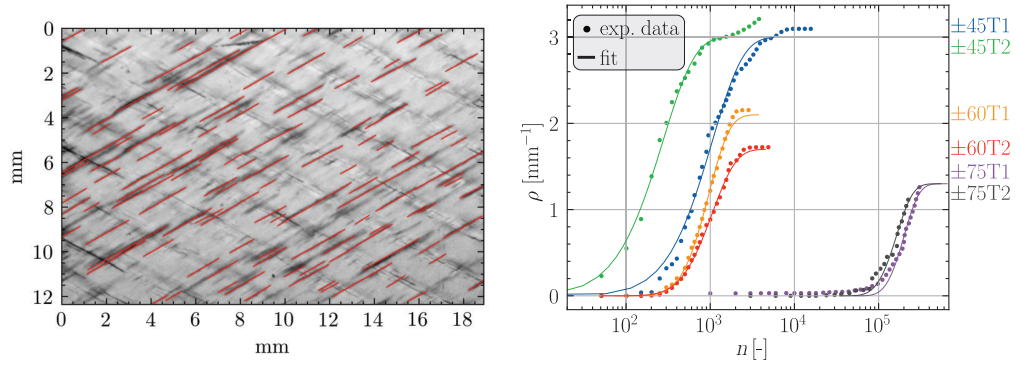

(**a**) (**b**)

Figure 6. Results of the crack detection. An example of the detected cracks for ±60° T1 is shown at 759 cycles (**a**). Cracks are only detected in the chosen direction of +60°. (**b**) shows the crack density results for all tests and the crack density functions.

Figure 6b shows the evolution of the crack density over loading cycles and the corresponding fitted crack density functions for all specimens. In the ±45° laminates, off-axis cracks initiate earlier than in ±60° and ±75° laminates. The ±45° laminates also show the highest crack saturation density. The ±75° laminates do not reach the state of crack saturation because they fail before. The growth rate of the crack density seems to be approximately constant for all tests when plotted on a logarithmic scale.

The results of the crack detection are listed in Table 3. The point of damage initiation n^{init}, crack saturation n^{sat} and the crack density growth rate of the linear region are used to compare the crack detection results. The saturation density ρ_c^{sat} is taken manually at the point where the crack accumulation reaches a plateau. Since the ±75° laminates do not reach crack saturation, the maximum crack density of ±75° T1 is used for the fitted curves. In the ±45° tests, the crack density increases again after reaching a first plateau due to delaminations that cause problems with the crack detection. Therefore, the saturation density is taken at the first plateau. The point of damage initiation n^{init} is defined as the first point with a crack density above 0.1 mm^{-1} and the point of crack saturation n^{sat} are the cycles needed to reach the saturation crack density ρ_c^{sat}. For ±75° tests, crack saturation is not reached. The crack density growth rate is the slope of the linear regression, the first step of the fitting process.

These results show that the automated crack detection is suited to efficiently obtain off-axis crack densities of multidirectional GRFP laminates. Damage initiation is easily detected and the crack density function can be modeled by a three-parameter cumulative Weibull distribution by fitting it to the linear regression of the region of constant crack density increase in semi-logarithmic space (see Figure 6b). The number of cycles until the saturation density is reached are also captured by the crack detection. It should be noted that the accuracy of the crack detection decreases when approaching saturation due to delamination and merging of cracks (see Figure 2c). From our experience, almost all cracks are detected up to approximately 80 percent of the saturation level. From there on, the merging of side-by-side cracks into one black line and delamination leads to misses and false detections. To improve the accuracy of the crack detection near saturation, image differencing techniques that allow to see only changes from one image to the next could be used (see [24]). The prerequisite to this is an extremely precise shift correction. This can be achieved with position markers on the images that allow a precise tracking of image shift and distortion. Since our images did not have these markers, a simpler version of the shift correction had to be used.

3.2. Stiffness Degradation Model

The calibration of the damage model for the material from [32] yields a correlation constant of 0.011 mm for the chosen inclusion aspect ratios of 100,1,10. Note that the correlation constant depends on the chosen aspect ratios. The results of the computed stiffness degradation are shown in Figure 7 along with experimental data for all laminates. The comparison between model and experiments for the ±45° laminates and ±60° T2 shows good agreement. Since the calibration constant is computed from the ±45° tests, good agreement of the stiffness drop is expected for ±45° specimens. Nonetheless, the curves follow the same shape as the experiments which is determined by the inclusion geometry. This indicates that the chosen inclusion geometry describes the effect of off-axis cracks for this laminate and our assumptions on the inclusion geometry are reasonable. For ±60° T1, the detected crack density is higher than for ±60° T2. Therefore, the computed stiffness degradation is also higher compared to ±60° T2. The trend of experimental data and the shape of the curves from the degradation model for ±45° and ±60° laminates is similar. Contrary to the ±45° tests, the experimentally observed stiffness degradation does not stop at the saturation of the off-axis cracks for the ±60° laminates (see Figure 7). As listed in Table 3, crack saturation is reached at around 2000 cycles for the ±60° tests. The computed stiffness of the ±75° laminates drops earlier than the experimental curves. It seems that off-axis cracks in ±75° laminates do not have the same effect at the local ply coordinate system as for ±45° laminates.

The error of the model increases from the ±45° laminates, where the calibration is carried out to the ±75° laminates. Carraro et al. [42] have shown that the macroscopic damage initiation is driven by two damage modes that depend on the level of in-plane shear stress. For plies with mostly in-plane shear stresses σ_{12} in the ply coordinate system shown in Figure 4a, the driving force for damage evolution at the micro scale is local maximum principal stress (LMPS). For plies with mostly positive in-plane transverse stress σ_{22}, local hydrostatic stress (LHS) is the driving force. The shift between LMPS and LHS in GFRP occurs at a fiber direction of around 60° [42]. Fractographic images also show different crack patterns for off-axis cracks depending on the in-plane shear stress. It has also been found that shear stress significantly reduces the number of cycles for damage initiation [7,43]. With differences in the micro-structure of the fracture plane between the two damage types, the effect of cracks on the ply stiffness can also be expected to be different for the LMPS/LHS damage types. For our model, this would require a separate correlation for the ±45° and ±75° tests, since these tests correspond to LMPS and LHS type damage, respectively. The presence of these two separate damage types would also explain the large difference in the number of cycles to damage initiation from ±45° to ±75° laminates (see Figure 6). The ±45° and ±60° tests show damage initiation at less than 500 cycles with ±45° being a bit lower than ±60°. On the other hand, the ±75° tests show damage initiation at more than 50,000 cycles, although the fatigue load level for all tests has been set to about 75% of the static strength. These findings back the theory of two distinct microscopic damage types controlled by in-plane shear stresses.

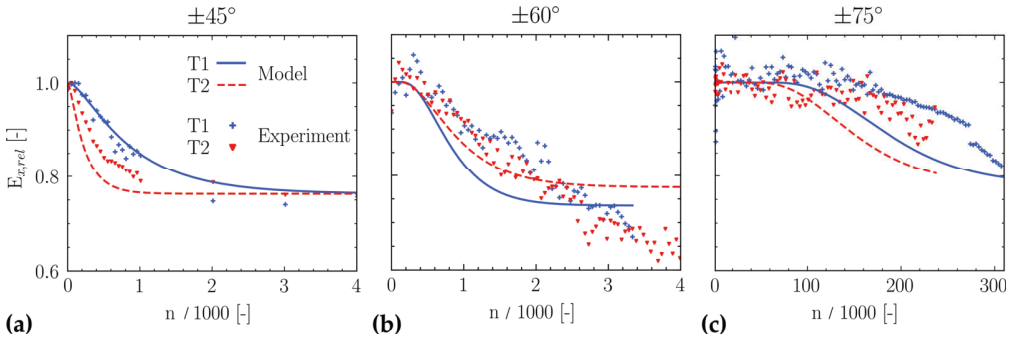

Figure 7. Stiffness degradation for the individual tests and damage model results. Comparison for (**a**) ±45° tests, (**b**) ±60° tests, and (**c**) ±75° tests.

In Figure 8, the experimental stiffness is plotted over crack density up to saturation. At the beginning, a small drop in stiffness without an increase in the crack density is visible for some specimens. After this initial drop in stiffness, all curves except ±75° T1 show a linear correlation up to saturation. Note that this does not conclude that the degradation of stiffness is linear since the crack density follows a S-shaped curve. For ±75° T1, a distinctive kink compared to the linear regression is visible. Also, the scatter of the experimental data for ±75° T1 (see Figure 7) is higher at the beginning. At around 200,000 cycles, this scatter nearly vanishes. This could be an indication of a problem in the evaluation or experimental procedure for this specimen. The linear relation between crack density and stiffness shows that the crack density is a good choice as a damage parameter.

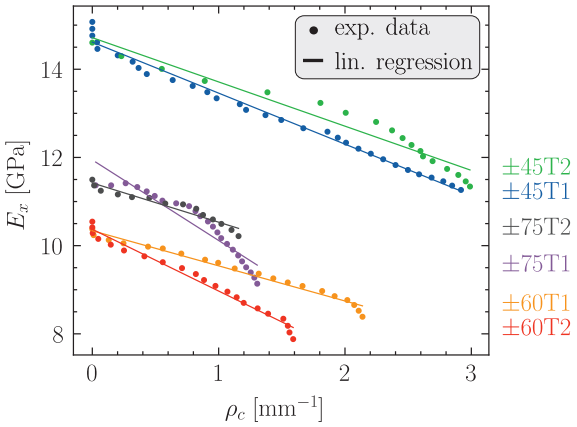

Figure 8. Relationship of the experimentally determined stiffness and crack density up to saturation. For the ±45° and ±60° specimen, the stiffness degradation correlates linearly with the crack density. Note that the fact that the stiffness for the ±75° specimen is higher compared to ±60° is a result of the given ply material properties and in accordance with classical laminate theory.

4. Conclusions

In this work, the effect of off-axis cracks in GFRP laminates is studied by using test results of the crack density and computing the effect of these cracks on the stiffness of the laminate. It is shown that crack detection can be used to efficiently evaluate images of off-axis cracks from fatigue tests and the fatigue crack density function can be modeled by a three-parametric cumulative Weibull distribution function. A mostly-automated scheme is presented for the calibration of the crack density functions from experimental data. Furthermore, the stiffness degradation model for multidirectional fiber-reinforced polymer laminates from Schuecker, which uses Mori-Tanaka homogenization on the ply-level, is tested against experimental fatigue data. The results suggest that it is necessary to distinguish the effect of off-axis cracks on the stiffness of a ply depending on the microscopic crack type. This requires a separate calibration for cracks formed under LMPS and LHS conditions, respectively. This observation agrees well with the theory by Carraro and Quaresimin which also distinguishes the evolution of off-axis fatigue cracks based on the micro-damage mechanisms driven by LMPS and LHS. A distinct jump in cycles to damage initiation is also found where the micro-damage mechanisms change. A new test campaign is under way to further test the damage model for both microscopic damage types.

Author Contributions: Conceptualization, C.S., M.P. and M.D.; methodology, M.D., C.S. and M.P.; software, M.D., validation, M.D.; formal analysis, M.D.; investigation, M.D.; data curation, M.D. and C.S.; writing—original draft preparation, M.D.; writing—review and editing, C.S. and M.P.; visualization, M.D.; supervision, C.S. and M.P.; project administration, C.S.; funding acquisition, C.S. All authors have read and agreed to the published version of the manuscript.

Funding: Part of this work has been performed within the COMET-project Experimental and numerical analysis of the damage tolerance behavior of manufactured induced defects and bonded repairs in structural aerospace composite parts (project-no.: VI-3.04) at the Polymer Competence Center Leoben GmbH (PCCL, Austria) within the framework of the COMET-program of the Federal Ministry for Transport, Innovation and Technology and the Federal Ministry for Digital and Economic Affairs with contributions by Montanuniversität Leoben (Chair of Designing Plastics and Composite Materials) and MAGNA Powertrain Engeneering Center Steyr GmbH CO KG. The PCCL is funded by the Austrian Government and the State Governments of Styria, Lower Austria and Upper Austria.

Data Availability Statement: The data presented in this study are available upon request from the corresponding author. The algorithms of the crack detection are available at GitHub (https://github.com/mattdrvo/CrackDect, accessed on 28 December 2021).

Acknowledgments: Special thanks go to René Rieser and the Chair of Materials Science and Testing of Polymers, Montanuniversitaet Leoben for providing experimental data and images for the crack detection.

Conflicts of Interest: The authors declare no conflict of interest. The funders had no role in the design of the study; in the collection, analyses, or interpretation of data; in the writing of the manuscript, or in the decision to publish the results.

Abbreviations

The following abbreviations are used in this manuscript:

GFRP	Glass fiber-reinforced polymer
TWLI	Transilluminated white light imaging
FEM	Finite element method
LMPS	Local maximum principal stress
LHS	Local hydrostatic stress

Appendix A. Quasi-Static Material Parameters

The basic characterization of the quasi-static material parameters is done with UD0° specimens for E_1 and ν_{12}, UD90° specimens for E_2 and $\pm 45°$ specimens for G_{12}. In the referenced data set [32], a miscalculation has happened in the evaluation of the in-plane shear modulus G_{12} which is corrected here according to DIN EN ISO 14129. Additional measurements of the fiber volume fraction revealed differences between the specimens. Therefore, the ply stiffness of each laminate is corrected to a fiber volume fraction of 45%. For this, the semi-empirical Chamis model is used to approximate the engineering constants as a function of the fiber volume fraction since it showed good agreement with experimental data for GRFP [44]. This modified rule of mixture (ROM) replaces the fiber volume fraction in the iso-stress model (Reuss) for E_2^c and G_{12}^c with the root of the fiber volume fraction. The iso-strain model (Voigt) for E_1^c and ν_{12}^c is not altered. For isotropic matrix and fibers, this leads to the following set of equations:

$$\begin{aligned} E_1^c &= (1 - V^f)E^m + V^f E_1^f \\ E_2^c &= \left[\frac{1 - \sqrt{V^f}}{E_m} + \frac{\sqrt{V^f}}{E_2^f}\right]^{-1} \\ \nu_{12}^c &= (1 - V^f)\nu^m + V^f \nu^f \\ G_{12}^c &= \left[\frac{1 - \sqrt{V^f}}{G_m} + \frac{\sqrt{V^f}}{G_f}\right]^{-1} \end{aligned} \tag{A1}$$

For the correction, the elastic constants of the matrix E^m and ν^m must be known. Since the elastic constants for each laminate at a certain fiber volume fraction are tested, the elastic constants of the fibers can be estimated. This estimate is then reinserted in the same equations to obtain the elastic constants of the composite as a function of the fiber volume fraction. In Table A1, the fiber volume fractions for each laminate and the tested elastic constants are listed. With this data, the elastic constants at a fiber volume fraction of 45% in Table 1 are computed. In the degradation model, the stiffness is corrected for each laminate individually.

Table A1. Fiber volume fractions of the laminates and the quasi-static elastic constants in ply-coordinates determined from tests.

Laminate	Fiber Volume Fraction [−]	Elastic Constant
0°	42.2	E_1^c: 33.6 GPa, ν_{12}^c: 0.28
90°	42.4	E_2^c: 10.3 GPa
±45°	52.8	G_{12}^c: 3.7 GPa
±60°	41.8	-
±75°	45.7	-
Matrix	-	E^m: 3.55 GPa, ν^m: 0.43 GPa

Appendix B. Fatigue Load Level

The fatigue load level of laminates is computed by Puck´s failure criterion [33]. A load level of 75% means that the laminate is loaded in the fatigue tests up to 75% of its static strength. In Figure A1, the stress space for Puck mode A with the stress vectors of the tests is shown. In the ±45° laminates used to test the in-plane shear strength according to DIN EN ISO 14129, significant transverse stresses σ_{22} are present. The shear strength R_{12} for the material is therefore corrected using Puck´s failure criterion based on the strength of the ±45° and UD90° laminates. With this corrections, the fatigue level of the tests are 75% for ±45°, 78% for ±60° and 74% for ±75° laminates. As a comparison, the stress vector for a typical carbon fiber-reinforced laminate is also shown. The higher ratio of fiber stiffness to transverse stiffness yields nearly no transverse stress so no correction is necessary for carbon fiber-reinforced composites.

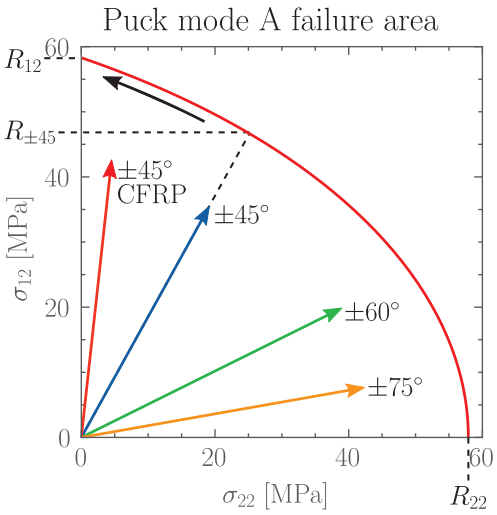

Figure A1. Puck mode A failure area (red) with stress vectors of the tests. In the ±45° laminate, significant transverse stress σ_{22} is present. Therefore, the in-plane shear strength R_{12} is corrected with Pucks failure criterion (black arrow). As a comparison, the stress vector for a typical ±45° CFRP laminate is also shown (red arrow).

References

1. Reifsnider, K.L. (Ed.) *Fatigue of Composite Materials*; Number 4 in Composite Materials Series; Elsevier: Amsterdam, The Netherlands; New York, NY, USA, 1991.
2. Tong, J.; Guild, F.J.; Ogin, S.L.; Smith, P.A. Off-axis fatigue crack growth and the associated energy release rate in composite laminates. *Appl. Compos. Mater.* **1997**, *4*, 349–359. [CrossRef]
3. Bartley-Cho, J.; Gyu Lim, S.; Hahn, H.; Shyprykevich, P. Damage accumulation in quasi-isotropic graphite/epoxy laminates under constant-amplitude fatigue and block loading. *Compos. Sci. Technol.* **1998**, *58*, 1535–1547. [CrossRef]
4. Wharmby, A.; Ellyin, F. Damage growth in constrained angle-ply laminates under cyclic loading. *Compos. Sci. Technol.* **2002**, *62*, 1239–1247. [CrossRef]

5. Wharmby, A. Observations on damage development in fibre reinforced polymer laminates under cyclic loading. *Int. J. Fatigue* **2003**, *25*, 437–446. [CrossRef]
6. Tohgo, K.; Nakagawa, S.; Kageyama, K. Fatigue behavior of CFRP cross-ply laminates under on-axis and off-axis cyclic loading. *Int. J. Fatigue* **2006**, *28*, 1254–1262. [CrossRef]
7. Quaresimin, M.; Carraro, P. Damage initiation and evolution in glass/epoxy tubes subjected to combined tension–torsion fatigue loading. *Int. J. Fatigue* **2014**, *63*, 25–35. [CrossRef]
8. Shen, H.; Yao, W.; Qi, W.; Zong, J. Experimental investigation on damage evolution in cross-ply laminates subjected to quasi-static and fatigue loading. *Compos. Part B Eng.* **2017**, *120*, 10–26. [CrossRef]
9. Carraro, P.; Quaresimin, M. A stiffness degradation model for cracked multidirectional laminates with cracks in multiple layers. *Int. J. Solids Struct.* **2015**, *58*, 34–51. [CrossRef]
10. Glud, J.; Dulieu-Barton, J.; Thomsen, O.; Overgaard, L. Fatigue damage evolution in GFRP laminates with constrained off-axis plies. *Compos. Part A Appl. Sci. Manuf.* **2017**, *95*, 359–369. [CrossRef]
11. Zhang, D.; Ye, J.; Lam, D. Ply cracking and stiffness degradation in cross-ply laminates under biaxial extension, bending and thermal loading. *Compos. Struct.* **2006**, *75*, 121–131. [CrossRef]
12. Thionnet, A.; Renard, J. Laminated composites under fatigue loading: A damage development law for transverse cracking. *Compos. Sci. Technol.* **1994**, *52*, 173–181. [CrossRef]
13. Nuismer, R.J.; Tan, S.C. Constitutive Relations of a Cracked Composite Lamina. *J. Compos. Mater.* **1988**, *22*, 306–321. [CrossRef]
14. Varna, J. Modelling mechanical performance of damaged laminates. *J. Compos. Mater.* **2013**, *47*, 2443–2474. [CrossRef]
15. Joffe, R.; Varna, J. Analytical modeling of stiffness reduction in symmetric and balanced laminates due to cracks in 90° layers. *Compos. Sci. Technol.* **1999**, *59*, 1641–1652. [CrossRef]
16. Jagannathan, N.; Gururaja, S.; Manjunatha, C. Probabilistic strength based matrix crack evolution model in multi-directional composite laminates under fatigue loading. *Int. J. Fatigue* **2018**, *117*, 135–147. [CrossRef]
17. Singh, C.V.; Talreja, R. A synergistic damage mechanics approach for composite laminates with matrix cracks in multiple orientations. *Mech. Mater.* **2009**, *41*, 954–968. [CrossRef]
18. Quaresimin, M.; Carraro, P. On the investigation of the biaxial fatigue behaviour of unidirectional composites. *Compos. Part B Eng.* **2013**, *54*, 200–208. [CrossRef]
19. Adden, S.; Horst, P. Stiffness degradation under fatigue in multiaxially loaded non-crimped-fabrics. *Int. J. Fatigue* **2010**, *32*, 108–122. [CrossRef]
20. Jespersen, K.M.; Glud, J.A.; Zangenberg, J.; Hosoi, A.; Kawada, H.; Mikkelsen, L.P. Uncovering the fatigue damage initiation and progression in uni-directional non-crimp fabric reinforced polyester composite. *Compos. Part A Appl. Sci. Manuf.* **2018**, *109*, 481–497. [CrossRef]
21. Sket, F.; Enfedaque, A.; Alton, C.; González, C.; Molina-Aldareguia, J.; Llorca, J. Automatic quantification of matrix cracking and fiber rotation by X-ray computed tomography in shear-deformed carbon fiber-reinforced laminates. *Compos. Sci. Technol.* **2014**, *90*, 129–138. [CrossRef]
22. Sørensen, B.F.; Talreja, R. Analysis of Damage in a Ceramic Matrix Composite. *Int. J. Damage Mech.* **1993**, *2*, 246–271. [CrossRef]
23. Lafarie-Frenot, M.; Hénaff-Gardin, C. Formation and growth of 90° ply fatigue cracks in carbon/epoxy laminates. *Compos. Sci. Technol.* **1991**, *40*, 307–324. [CrossRef]
24. Glud, J.; Dulieu-Barton, J.; Thomsen, O.; Overgaard, L. Automated counting of off-axis tunnelling cracks using digital image processing. *Compos. Sci. Technol.* **2016**, *125*, 80–89. [CrossRef]
25. Drvoderic, M.; Rettl, M.; Pletz, M.; Schuecker, C. CrackDect: Detecting crack densities in images of fiber-reinforced polymers. *SoftwareX* **2021**, *16*, 100832. [CrossRef]
26. Degrieck, J.; Van Paepegem, W. Fatigue damage modeling of fibre-reinforced composite materials: Review. *Appl. Mech. Rev.* **2001**, *54*, 279–300. [CrossRef]
27. Schuecker, C.; Pettermann, H. A continuum damage model for fiber reinforced laminates based on ply failure mechanisms. *Compos. Struct.* **2006**, *76*, 162–173. [CrossRef]
28. Mori, T.; Tanaka, K. Average stress in matrix and average elastic energy of materials with misfitting inclusions. *Acta Metall.* **1973**, *21*, 571–574. [CrossRef]
29. Benveniste, Y.; Dvorak, G.; Chen, T. On diagonal and elastic symmetry of the approximate effective stiffness tensor of heterogeneous media. *J. Mech. Phys. Solids* **1991**, *39*, 927–946. [CrossRef]
30. Schuecker, C.; Pettermann, H. Constitutive ply damage modeling, FEM implementation, and analyses of laminated structures. *Comput. Struct.* **2008**, *86*, 908–918. [CrossRef]
31. Carraro, P.; Maragoni, L.; Quaresimin, M. Prediction of the crack density evolution in multidirectional laminates under fatigue loadings. *Compos. Sci. Technol.* **2017**, *145*, 24–39. [CrossRef]
32. Rieser, R. Damage Mechanics of Composites under Fatigue Loads. Ph.D. Thesis, Montanuniversität Leoben, Leoben, Austria, 2016.
33. Puck, A. Failure analysis of FRP laminates by means of physically based phenomenological models. *Compos. Sci. Technol.* **2002**, *62*, 1633–1662. [CrossRef]

34. SciPy 1.0 Contributors; Virtanen, P.; Gommers, R.; Oliphant, T.E.; Haberland, M.; Reddy, T.; Cournapeau, D.; Burovski, E.; Peterson, P.; Weckesser, W.; et al. SciPy 1.0: Fundamental algorithms for scientific computing in Python. *Nat. Methods* **2020**, *17*, 261–272. [CrossRef]
35. Eshelby, J.D. The determination of the elastic field of an ellipsoidal inclusion, and related problems. *Proc. R. Soc. London Ser. Math. Phys. Sci.* **1957**, *241*, 376–396. [CrossRef]
36. Parnell, W.J. The Eshelby, Hill, Moment and Concentration Tensors for Ellipsoidal Inhomogeneities in the Newtonian Potential Problem and Linear Elastostatics. *J. Elast.* **2016**, *125*, 231–294. [CrossRef]
37. Gavazzi, A.C.; Lagoudas, D.C. On the numerical evaluation of Eshelby's tensor and its application to elastoplastic fibrous composites. *Comput. Mech.* **1990**, *7*, 13–19. [CrossRef]
38. Miskdjian, I.; Hajikazemi, M.; Van Paepegem, W. Automatic edge detection of ply cracks in glass fiber composite laminates under quasi-static and fatigue loading using multi-scale Digital Image Correlation. *Compos. Sci. Technol.* **2020**, *200*, 108401. [CrossRef]
39. Vasylevskyi, K.; Drach, B.; Tsukrov, I. On micromechanical modeling of orthotropic solids with parallel cracks. *Int. J. Solids Struct.* **2018**, *144–145*, 46–58. [CrossRef]
40. Drach, B.; Tsukrov, I.; Trofimov, A. Comparison of full field and single pore approaches to homogenization of linearly elastic materials with pores of regular and irregular shapes. *Int. J. Solids Struct.* **2016**, *96*, 48–63. [CrossRef]
41. Seabold, S.; Perktold, J. Statsmodels: Econometric and Statistical Modeling with Python. In Proceedings of the 9th Python in Science Conference, Austin, TX, USA, 28 June– 3 July 2010; pp. 92–96. [CrossRef]
42. Carraro, P.; Quaresimin, M. A damage based model for crack initiation in unidirectional composites under multiaxial cyclic loading. *Compos. Sci. Technol.* **2014**, *99*, 154–163. [CrossRef]
43. Plumtree, A. Fatigue damage evolution in off-axis unidirectional CFRP. *Int. J. Fatigue* **2002**, *24*, 155–159. [CrossRef]
44. Younes, R.; Hallal, A.; Fardoun, F.; Hajj, F. Comparative Review Study on Elastic Properties Modeling for Unidirectional Composite Materials. In *Composites and Their Properties*; Hu, N., Ed.; InTech: London, UK, 2012. [CrossRef]

Paper C

Fatigue damage model for composite laminates based on a Mori-Tanaka formulation

Authors: Drvoderic, Matthias
Pletz, Martin
Schuecker, Clara

Proceedings of the 20th European Conference on Composite Materials (ECCM20).
DOI: 10.5075/epfl-298799_978-2-970161

Composites Meet Sustainability – Proceedings of the 20th European Conference on Composite Materials,
ECCM20. 26-30 June, 2022, Lausanne, Switzerland

FATIGUE DAMAGE MODEL FOR COMPOSITE LAMINATES BASED ON A MORI-TANAKA FORMULATION

Matthias Drvoderic[a], Martin Pletz[a], Clara Schuecker[a]

a: Chair of Designing Plastics and Composite Materials, Department of Polymer Engineering and Science, Montanuniversitaet Leoben, 8700 Leoben, Austria;
matthias.drvoderic@unileoben.ac.at;

Abstract: *Unidirectional fiber reinforced composites develop matrix cracks in off-axis plies as the first form of damage in fatigue loading scenarios. Crack detection is used to quantify this form of damage and its resulting stiffness degradation is computed with a micromechanical model based on the Mori-Tanaka formulation. It is shown that the model predicts the stiffness degradation well when the calibration is based on the ratio of in-plane shear to transverse stress. Furthermore, a distinct separation into high and low dissipated energy of the fatigue cycles is found based on the in-plane to transverse stress ratio. This behavior links the dissipated energy to the two damage driving forces in Puck mode A stress space. All fatigue tests that show a high dissipated energy form a distinct cluster in SN diagrams whereas tests with low dissipated energy fall into a second cluster.*

Keywords: crack detection; fiber-reinforced polymers; fatigue damage model; composite fatigue; off-axis cracks

1. Introduction

The process of fatigue damage growth in multidirectional fiber-reinforced composite laminates comprises of distinct damage mechanisms which can be categorized into the characteristic damage states starting with matrix cracks followed by delamination and fiber failure [1]. Matrix cracks propagate along fibers and usually span the height of the whole ply as they grow in number and size during the fatigue life. The result of those cracks is a significant loss of ply-stiffness leading to a reduction of the global laminate stiffness [2–5]. For glass fiber-reinforced polymers (GFRPs), the density of matrix cracks can be directly computed from images of a specimen taken during fatigue tests. It is widely used as damage variable in progressive damage models or to calibrate numerical or phenomenological damage models [6–11]. Therefore, computing the crack density in an efficient way has become a vital part in experimental campaigns and algorithms have been developed to replace error prone and inefficient manual crack counting [12–14].

In the present work, Schuecker´s progressive damage model [9,15] which is based on Mori-Tanaka homogenization is used to compute the stiffness loss of a laminate due to off-axis cracks from fatigue loading. As shown in [16], the calibration of this model to experimental data can be done with standard fatigue tests combined with crack detection. However, the effect of off-axis cracks on the stiffness seems to depend on the microscopic crack type. Carraro et al. [17] have shown that off-axis matrix cracks are the result of two different damage driving forces. Local hydrostatic stress (LHS) or local maximum hydrostatic stress (LMPS) are identified as the critical stress depending on the biaxiality ratio of shear to transverse stress ($\lambda = \tau_{12}/\sigma_{22}$). This is also supported by fractographic images that show different crack patterns for off-axis cracks

  doi:10.5075/epfl-298799_978-2-9701614-0-0

Composites Meet Sustainability – Proceedings of the 20th European Conference on Composite Materials,
ECCM20. 26-30 June, 2022, Lausanne, Switzerland

depending on the level of in plane shear stress [18]. Therefore, the model has to be calibrated for both microscopic damage types. For this, the stiffness during fatigue tests as well as crack density is evaluated from an extended experimental campaign. The influence of the load level on the point of damage initiation is compared for different ratios of shear vs. transverse stress. The hysteresis of the fatigue cycles is also evaluated and compared against quasi-static stiffness data. Since the fracture surface is rather smooth for biaxiality rations smaller than one but shows shear cusps at biaxiality ratios higher than one, the dissipated energy should also be higher at higher biaxiality ratios since uneven fracture surface should result in more internal friction of the material.

2. Methods

2.1 Experimental Fatigue Data

Quasi-static stiffness, crack density and hysteresis cycles are evaluated from fatigue tests. The GFRP plates from which $\pm\theta_s$ specimen are cut were produced with vacuum pressing according to [19] with unidirectional (UD) glass fiber weave with an aerial weight of 220 g/m^2 (Porcher Industries Germany GmbH) and EPIKOTE™ MGS® LR160 as resin and EPIKURE™ MGS® LH160 as curing agent (Hexion Inc.). The stacking sequence of all specimens is $[+\theta_3/-\theta_3]_s$. All specimens except UD90° have a gauge length of 100 mm, a width of 20 mm and a thickness of 2 mm. For the UD90° specimen, a dogbone-like shape is used to prevent failure near the tabs with a gauge length of 200 mm [20].

To test different biaxiality ratios, $\pm$45°, $\pm$60°, $\pm$75° as well as UD90° specimen are tested at load levels from 50% to 85%. The load level is the ratio of the maximum load in the fatigue test to the static strength of the laminate computed by the Puck failure criterion [21]. For a detailed explanation of the load level, the reader is referred to [16]. The elastic stiffness from static tests as well as the transverse strength R_2 and in-plane shear strength R_{12} of the composite ply material which is needed for the computation of the load level is listed in Table 1.

The fatigue tests are performed with stress controlled sinusoidal load cycles with an R-ratio of 0.1 and a frequency of 3Hz for $\pm$45° specimen and 5Hz otherwise. The servo-hydraulic material testing system MTS 322 by MTS Systems Corporations is used for all tests. Additionally, the cycles had been periodically interrupted to perform displacement-controlled quasi-static tensile tests to track the degradation of the laminate stiffness. Images for the crack detection are made during the quasi-static tensile tests. Transilluminated white light imaging is used as imaging technique to achieve a high contrast between background and cracks.

Table 1: Elastic constants and strength of the composite ply material from static tests.

E_1 [GPa]	E_2 [GPa]	ν_{12} [-]	G_{12} [GPa]	R_2 [MPa]	R_{12} [MPa]
31.7	10.7	0.27	3.3	47.6	53.1

2.2 Crack Detection

The crack density as a function of the cycles is computed for each test according to

$$\rho_c = \frac{\sum_{i=1}^{n} L_i}{A} \tag{1}$$

  doi:10.5075/epfl-298799_978-2-9701614-0-0

with L_i as the length of the i^{th} crack and A as the evaluation area. This method also accounts for the length of cracks as it computes an average crack density weighted by the crack lengths instead of only accounting for the number of cracks. The algorithm form J.J. Bender [14] is used for the crack detection since it shows a high resilience against false detections or artefacts and showed good performance even near the point of crack saturation. The shift-distortion correction necessary for application of this algorithm as well as selecting the region of interest (evaluation region) is done with the python package *CrackDect* [13].

2.3 Damage model and calibration

The stiffness degradation part of Schuecker´s progressive damage model is used to compute the effect of the off-axis cracks based on experimentally obtained crack densities. The stiffness degradation is computed with a Mori-Tanaka homogenization where crack-like voids are used to mimic the effect of cracks in the ply-material. The Mori-Tanaka formulation for void inclusions is

$$E_{MTM,Void} = E^m \left[I + \frac{V}{1-V} (I - S)^{-1} \right]^{-1} \quad (2)$$

with E^m as the elasticity tensor for the ply material, V as the inclusion volume fraction of the crack-like voids and S as the Eshelby tensor. The aspect ratios for the crack-like inclusion are 100, 1, 10 in X, Y and Z-direction of the material coordinate system. This choice for the aspect ratios has shown to mimic the evolution of the engineering constants of the ply material as off-axis cracks grow [16].

Since the stiffness degradation of the damage model is based on a Mori-Tanaka homogenization, a calibration is necessary to map from the experimentally obtained crack density to the inclusion volume fraction of crack-like voids. For this, the crack density curves from the tests are fitted with a cumulative Weibull distribution function since the experimental curves show an S-like evolution when plotted over the logarithm of the number of cycles. The fitting approach with a correlation parameter μ from [16] is used since it has shown good results and is easy to automate. For the tests used in the calibration it is important that the crack density and the stiffness degradation correlate well and crack saturation is reached since the calibration incorporates an optimization routine which will yield wrong results otherwise. Therefore, the calibration curves are manually selected.

3. Results and Discussion

In Figure 1, the dissipated energy for the $\pm$45°, $\pm$60° and $\pm$75° laminate is shown for two load levels. There is a substantial jump in dissipated energy from the $\pm$75° and$\pm$60° to the $\pm$45° laminate. The biaxiality ratio λ for $\pm$45°, $\pm$60° and $\pm$75° is 1.7, 0.5 and 0.2, respectively. This jump could be a sign of the shift of damage driving force from LHS to LMPS. This corresponds to the findings of Quaresimin and Carraro [4], that for biaxiality ratios higher than 1, the damage driving force switches from LHS to LMPS and shear cusps start to develop resulting in an uneven and coarse fracture surface. This is expected to generate more internal friction with cyclic loading and therefore result in a higher dissipated energy. The dissipated energy also increases slightly with the applied load level, but this effect is much smaller than the gap between the $\pm$45° and $\pm$60° specimen.

Composites Meet Sustainability – Proceedings of the 20th European Conference on Composite Materials,
ECCM20. 26-30 June, 2022, Lausanne, Switzerland

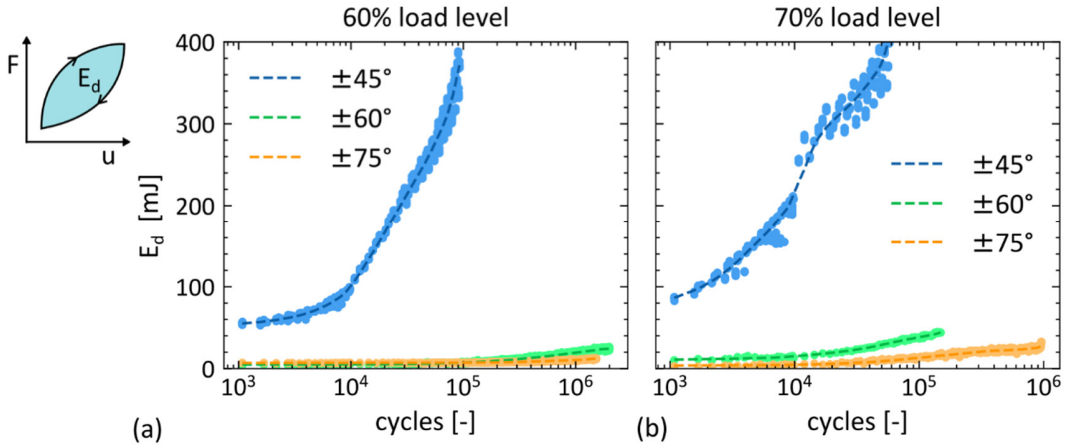

Figure 1: Dissipated energy E_d (scatter) for ±45°, ±60° and ±75° at 60% load level (a) and 70% load level (b) with overall trend for each test (dotted line). The pictogram shows the computation of the dissipated energy as integral over the hysteresis cycle.

Figure 2a shows the fitted curves for the crack detection for ±45° and ±60° tests at a load level of 55%, 60% and 70% as well as ±75° at 60% and 70% load level. Each series shows a clear trend to damage initiation at lower cycles counts for higher load levels. Also, the crack density curves show similar shape aside from ±60° at 55% and ±75° at 60% load level where the tests were stopped at 10^6 and $1.5 \cdot 10^6$ cycles, respectively. Figure 2b shows SN-data for damage initiation of the tests. The damage initiation is defined as the cycle where a crack density of 0.2 mm^{-1} is reached. It is clearly visible that the damage initiation for the ±45° tests and the other tests form two clusters in an SN-diagram. The SN-data for ±45° shows that no other tests fall into its scatter band (95% confidence interval) and all tests for ±60°, ±75° and UD90° form their own scatter band without interfering with the ±45° tests. This suggests that the dissipated energy can indeed be used as a criterion to separate the damage mechanism.

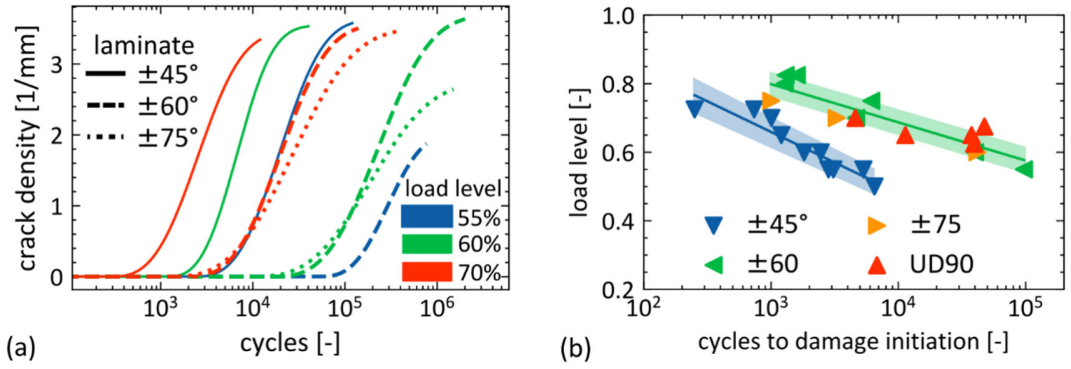

Figure 2: Fitted crack density curves (a) for ±45°, ±60° and ±75° laminates for various load levels and cycles to damage initiation (b).

To calibrate the stiffness degradation model, the method described in Section 2.3 is used. For the calibration one of the ±45° tests ($\lambda > 1$) and one of the UD90° tests ($\lambda < 1$) is selected which results in the calibration parameters $\mu_{45} = 0.012$ and $\mu_{90} = 0.004$. The correlation parameter μ_{45} computed for $\lambda > 1$ is similar to the one obtained for a different test series in [16] as $\mu_{45} = 0.011$

where the same matrix material and fibers had been used. Figure 3 shows the results of the stiffness degradation model and the experimental data for various load levels.

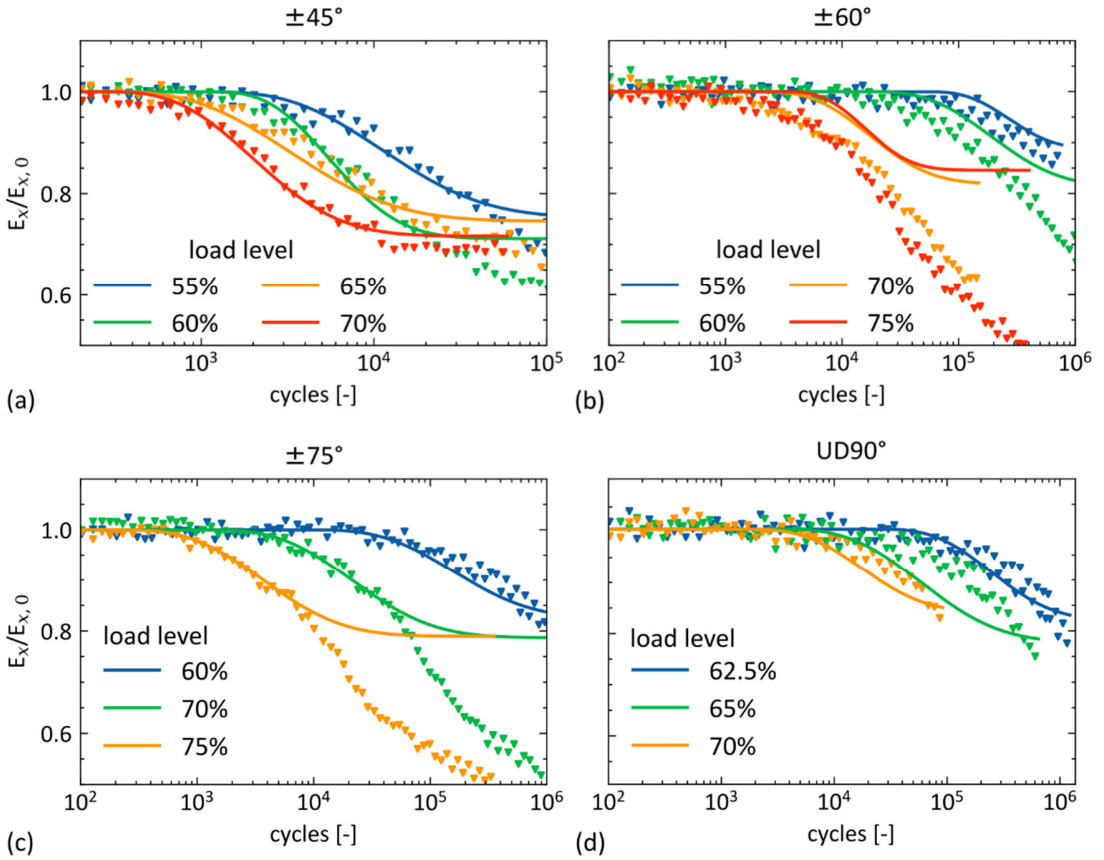

Figure 3: Experimental stiffness degradation (scatter) and computed stiffness degradation (lines) for the four tests for ±45° (a), ±60° (b), ±75° (c) and UD90° (d) at different load levels.

For the ±45° tests (Figure 3a), the computed and experimental degradation in stiffness fits well. A discrepancy between the model and experiments after crack saturation is visible. This is expected since other damage mechanisms like diffuse delamination will degrade the laminate further which is not accounted for in the model. The ±60° tests (Figure 3b) show a good model fit only for the load levels below 70%. At higher load levels, the discrepancy between model and experiments grows as the model underpredicts the stiffness degradation. In the ±75° tests (Figure 3c), the start of the computed stiffness degradation correlates well with experimental data but the experiments also show significant stiffness degradation after crack saturation. The model predicts the stiffness of the UD90° tests well. Note that the UD90° tests do not reach crack saturation due to prior failure of the specimen.

Figure 4a shows the predictions of the stiffness degradation model for the ±60° tests with μ_{90} used for load levels below 70% and and μ_{45} for higher load levels. It seems that for the ±60° tests, the separation by load level gives better predictions than the separation between the damage mechanisms based on the biaxiality ratio proposed from Quaresimin and Carraro [4].

Figure 4b shows the stress space of Puck mode A with the directions of the various laminates. As shown by the red dotted line, the separation of the damage modes intersects the ±60° tests

Composites Meet Sustainability – Proceedings of the 20th European Conference on Composite Materials,
ECCM20. 26-30 June, 2022, Lausanne, Switzerland

at a critical shear stress $\sigma_{12,c}$ whereas with a set biaxiality ratio (black dotted line), this is not possible. Using a critical shear stress $\sigma_{12,c}$ instead of the biaxiality ratio as a separation between the damage modes would mostly yield the same result. Low biaxiality ratios never reach $\sigma_{12,c}$ before the static strength is reached and the tests for high biaxiality ratios the separation is at very low load levels which is usually not tested since the fatigue life until damage initiation is extremely long or no damage starts to initiate at all. To further test this hypothesis, more experiments are necessary since it cannot explain the stiffness drop after crack saturation for the ±75° tests (see Figure 3c) and ±60° tests fall into the cluster for λ < 1 for the cycles to damage initiation (see Figure 2b) and not into both clusters.

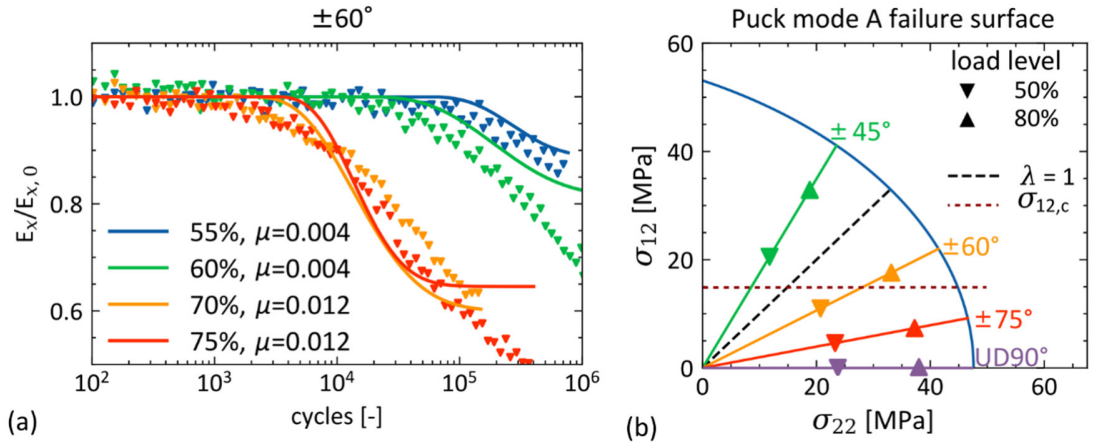

Figure 4: Experimental stiffness (scatter) vs. computed stiffness degradation (lines) for ±60° with the correlation constant for λ > 1 for load levels above 70% (a) and Puck mode A stress space (b) with the directions of the different laminates and the two criteria for the separation of the damage mode.

4. Conclusion

In this work, the effects of off-axis cracks in GRFP laminates are studied with automated crack detection of specimen in fatigue experiments. The dissipated energy is computed from hysteresis cycles and shows a substantial jump between ±60° and ±45° laminates, which correspond to a biaxiality ratio of 1.7 and 0.5, respectively, for the material used. SN-curves for damage initiation show two distinct clusters also separating the ±45° laminates from tests with a biaxiality ratio of less than 1. Quaresimin and Carraro [4] have shown that for positive transverse stresses combined with in-plane shear stress, the damage mechanism changes from in-plane shear dominated to transverse stress dominated at a biaxiality ratio of approximately 1. Our findings show that the dissipated energy is a useful tool to track the change between the damage mechanisms. A jump in dissipated energy for higher in-plane shear stresses also makes sense since fractographic images show shear cusps that result in an uneven and coarse fracture surface, which is expected to generate more internal friction in the fatigue loading cycles thus, a higher dissipated energy.

The stiffness degradation from Schuecker´s progressive damage model shows good prediction results when using different calibration parameters for λ > 1 and λ < 1. Nevertheless, it seems that the model underpredicts the stiffness degradation for the ±60° laminates at higher load

levels. The hypothesis, that the damage mechanism is only dependent on the in-plane shear stress and not the biaxiality ratio could explain this behavior but more experiments are needed to confirm it.

Acknowledgements

Special thanks go to the Chair of Materials Science and Testing of Polymers, Montanuniversitaet Leoben for providing the experimental data and images for the crack detection.

Part of this work has been performed within the COMET-project Experimental and numerical analysis of the damage tolerance behavior of manufactured induced defects and bonded repairs in structural aerospace composite parts (project-no.: VI-3.04) at the Polymer Competence Center Leoben GmbH (PCCL, Austria) within the framework of the COMET-program of the Federal Ministry for Transport, Innovation and Technology and the Federal Ministry for Digital and Economic Affairs with contributions by Montanuniversität Leoben (Chair of Designing Plastics and Composite Materials) and MAGNA Powertrain Engeneering Center Steyr GmbH CO KG. The PCCL is funded by the Austrian Government and the State Governments of Styria, Lower Austria and Upper Austria.

5. References

1. Reifsnider KL, editor. Fatigue of composite materials. Amsterdam ; New York: Elsevier; 1991. 519 p. (Composite materials series).
2. Wharmby A. Observations on damage development in fibre reinforced polymer laminates under cyclic loading. International Journal of Fatigue. 2003 May;25(5):437–46.
3. Tohgo K, Nakagawa S, Kageyama K. Fatigue behavior of CFRP cross-ply laminates under on-axis and off-axis cyclic loading. International Journal of Fatigue. 2006 Oct;28(10):1254–62.
4. Quaresimin M, Carraro PA. Damage initiation and evolution in glass/epoxy tubes subjected to combined tension–torsion fatigue loading. International Journal of Fatigue. 2014 Jun;63:25–35.
5. Tong J, Guild FJ, Ogin SL, Smith PA. On matrix crack growth in quasi-isotropic laminates—I. Experimental investigation. Composites Science and Technology. 1997 Jan;57(11):1527–35.
6. Nuismer RJ, Tan SC. Constitutive Relations of a Cracked Composite Lamina. 1987;16.
7. Zhang D, Ye J, Lam D. Ply cracking and stiffness degradation in cross-ply laminates under biaxial extension, bending and thermal loading. Composite Structures. 2006 Sep;75(1–4):121–31.
8. Adden S, Horst P. Stiffness degradation under fatigue in multiaxially loaded non-crimped-fabrics. International Journal of Fatigue. 2010 Jan;32(1):108–22.
9. Schuecker C, Pettermann HE. A continuum damage model for fiber reinforced laminates based on ply failure mechanisms. Composite Structures. 2006 Oct;76(1–2):162–73.
10. Glud JA, Dulieu-Barton JM, Thomsen OT, Overgaard LCT. Fatigue damage evolution in GFRP laminates with constrained off-axis plies. Composites Part A: Applied Science and Manufacturing. 2017 Apr;95:359–69.
11. Carraro PA, Quaresimin M. A stiffness degradation model for cracked multidirectional laminates with cracks in multiple layers. International Journal of Solids and Structures. 2015 Apr;58:34–51.

Composites Meet Sustainability – Proceedings of the 20th European Conference on Composite Materials,
ECCM20. 26-30 June, 2022, Lausanne, Switzerland

12. Glud JA, Dulieu-Barton JM, Thomsen OT, Overgaard LCT. Automated counting of off-axis tunnelling cracks using digital image processing. Composites Science and Technology. 2016 Mar;125:80–9.
13. Drvoderic M, Rettl M, Pletz M, Schuecker C. CrackDect: Detecting crack densities in images of fiber-reinforced polymers. SoftwareX. 2021 Dec;16:100832.
14. Bender JJ, Bak BLV, Jensen SM, Lindgaard E. Effect of variable amplitude block loading on intralaminar crack initiation and propagation in multidirectional GFRP laminate. Composites Part B: Engineering. 2021 Jul;217:108905.
15. Schuecker C, Pettermann HE. Constitutive ply damage modeling, FEM implementation, and analyses of laminated structures. Computers & Structures. 2008 May;86(9):908–18.
16. Drvoderic M, Pletz M, Schuecker C. Modeling Stiffness Degradation of Fiber-Reinforced Polymers Based on Crack Densities Observed in Off-Axis Plies. J Compos Sci. 2021 Dec 29;6(1):10.
17. Carraro PA, Quaresimin M. A damage based model for crack initiation in unidirectional composites under multiaxial cyclic loading. Composites Science and Technology. 2014 Jul;99:154–63.
18. Plumtree A. Fatigue damage evolution in off-axis unidirectional CFRP. International Journal of Fatigue. 2002 Apr;24(2–4):155–9.
19. Rieser R. Damage mechanics of composites under fatigue loads. [Austria]: Montanuniversität Leoben; 2016.
20. Drvoderic M. Probeneinflüsse bei der mechanischen Prüfung von Composites. [Leoben]: Montanuniversität Leoben; 2018.
21. Puck A. Festigkeitsanalyse von Faser-Matrix-Laminaten: Modelle für die Praxis. München: Hanser; 1996. 212 p.

Paper D

Comparing crack density and dissipated energy as measures for off-axis damage in composite laminates

Authors: Drvoderic, Matthias
Gfrerrer, Maria
Wiener, Johannes
Pinter, Gerald
Pletz, Martin
Schuecker, Clara

International Journal of Fatigue
DOI: 10.1016/j.ijfatigue.2022.10748

International Journal of Fatigue 169 (2023) 107486

Contents lists available at ScienceDirect

International Journal of Fatigue

journal homepage: www.elsevier.com/locate/ijfatigue

Comparing crack density and dissipated energy as measures for off-axis damage in composite laminates

Matthias Drvoderic [a], Maria Gfrerrer [b], Johannes Wiener [b], Gerald Pinter [b], Martin Pletz [a,*], Clara Schuecker [a]

[a] Chair of Designing Plastics and Composite Materials, Department of Polymer Engineering and Science, Montanuniversitaet Leoben, Austria
[b] Chair of Materials Science and Testing of Polymers, Department of Polymer Engineering and Science, Montanuniversitaet Leoben, Austria

ARTICLE INFO

Dataset link: https://github.com/mattdrvo/CrackDect

Keywords:
Composites
Multiaxial fatigue
Matrix cracks
Damage modes
Damage accumulation

ABSTRACT

To investigate off-axis cracks in composite laminates and their effect on stiffness and hysteretic energy dissipation, fatigue tests were instrumented with automated crack detection to test damage onset and progression. It was found that the onset of stiffness loss correlates well with the onset of matrix cracks, but not with the dissipated energy. To study the transition between experimentally observed damage modes occurring at the micro-scale, the experimentally obtained dissipated energy was compared with Carraro's model, which predicts this transition based on local stresses. The results show a correlation between the absolute level of dissipated energy and the micro-damage modes.

1. Introduction

The importance of testing and modelling the fatigue behaviour of fibre-reinforced composites grows with its use in components designed for long service lifes, like wind turbine blades, car frames or airplane components, just to name a few examples. Due to the microstructure of fibre-reinforced composite laminates, several distinct microscopic and macroscopic damage mechanisms interact during the fatigue life. The first characteristic damage mechanism is matrix cracking where cracks grow in number and size parallel to the fibre direction. These matrix cracks, also referred to as off-axis cracks, result in a significant reduction of stiffness, but usually do not cause ultimate failure [1–6]. Depending on the layup of a laminate and loading conditions, fibre failure and delamination in later stages of the fatigue life usually lead to ultimate failure [7].

Although many fatigue models have been developed in the past decades, there is still a lack of general and reliable progressive damage models that can predict damage accumulation and its effect on mechanical properties [8,9]. The development of these progressive damage models is driven by the ability to accurately quantify individual damage mechanisms in fatigue experiments. Therefore, Non-Destructive Test (NDT) methods with the capability of continuously monitoring damage progression are highly relevant. Common NDT methods for this purpose are acoustic emission, ultrasonic testing, digital image correlation, X-ray tomography and infrared thermography, just to name a few examples [10]. The main drawback of these methods is that they are expensive when applied to large test campaigns and require specialized equipment.

For glass-fibre reinforced polymers (GFRP), another method to directly detect off-axis cracks is crack detection from images. The transparent nature of GFRP makes it possible to shine light through a laminate so that cracks appear as distinct dark lines [1,11]. Because of the relatively simple and inexpensive test setup for crack detection from images, this method is often used in the development of damage models for off-axis cracks [2,6,12,13]. For fatigue test campaigns with multiple tests where each test results in numerous, often hundreds, of contiguous images, automated crack detection algorithms have been developed to make an evaluation of the crack density at this scale possible [14–16].

The reliable detection of off-axis cracks makes quantification of this damage mechanism on a macroscopic level possible, but does not capture the stages of micro-damage leading to those macro-cracks. It has been found that in the region of positive transverse tension σ_{22} and in-plane shear σ_{12}, the macroscopic off-axis cracks are the result of two independent micro-damage modes (see Fig. 1 for the definition of ply stresses). For plies loaded in transverse tension σ_{22}, failure initiates parallel to the fibres ether by fibre–matrix interface failure or matrix failure, depending on the material system [17,18]. On the other hand, if the in-plane shear stress σ_{12} is dominant, shear-induced micro-cracks between the fibres develop in a distinct local fracture plane.

* Corresponding author.
E-mail address: martin.pletz@unileoben.ac.at (M. Pletz).

https://doi.org/10.1016/j.ijfatigue.2022.107486
Received 21 October 2022; Received in revised form 14 December 2022; Accepted 21 December 2022
Available online 23 December 2022

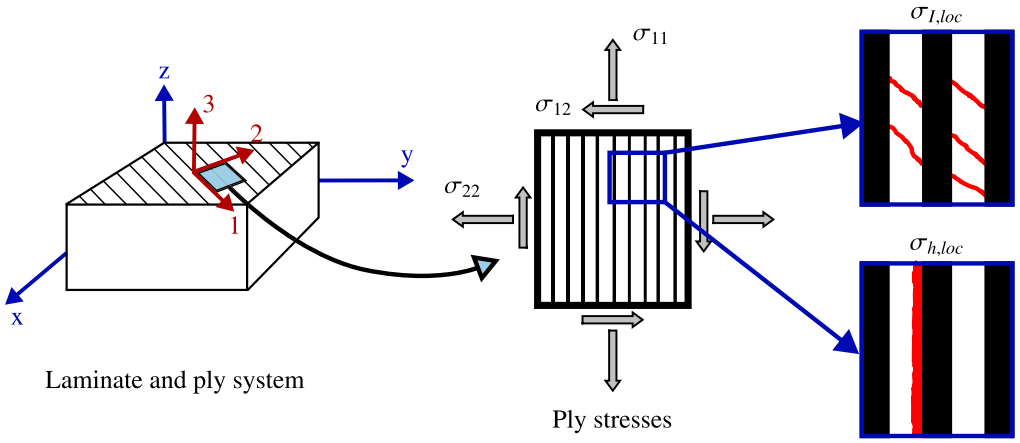

Fig. 1. Laminate coordinate system (global), ply coordinate system (material) and ply stresses. Depending on the local stress state, micro damage in the form shear-induced cracks ($\sigma_{I,loc}$) or parallel fracture ($\sigma_{h,loc}$) occurs.

This local fracture plane is not parallel to the fibres as all micro-cracks form in a specific angle of approximately 45° relative to the fibres as reported in [6,19,20]. Carraro et al. found that the local hydrostatic stress $\sigma_{h,loc}$ and local maximum principal stress $\sigma_{I,loc}$ at the micro-level can be used as the fatigue strength of the material for parallel fracture and shear induced fracture, respectively (see Fig. 1). These stresses are the maximal hydrostatic and principal stresses in the matrix between the fibres. Carraro et al. also developed a model to predict the transition between the two micro-damage modes of shear-induced and parallel fracture based on SN-diagrams of $\sigma_{h,loc}$ and $\sigma_{I,loc}$, respectively. Crack detection of the macroscopic off-axis cracks cannot differentiate if fracture was caused by $\sigma_{h,loc}$ or $\sigma_{I,loc}$. A focus of this work was to find other measures which correlate to the micro-damage modes.

Besides the crack density, which is a direct measure for off-axis damage, laminate stiffness is one of the preferred damage indicators since it is relatively easy to monitor and the correlation between laminate stiffness and damage is well documented [1–6,21]. Another approach for monitoring damage in a standard fatigue test setup is computing the dissipated energy from the hysteresis loop [22–24]. Although stiffness and dissipated energy cannot be correlated directly with a single damage mechanism, a comparison with other methods for direct damage detection, like crack detection, is possible.

Even though a lot of work on the influence of matrix cracks on the stiffness exists, the aim of this study is to further investigate the effects of matrix cracks. Up to now, the effects of the two micro-damage modes on mechanical properties has not been studied in detail. Images of fracture surfaces of the two damage modes show a relatively smooth fracture surface for parallel fracture and a rough surface with shear hackles for shear-induced micro-cracks between the fibres [6,19,20,25,26]. According to studies on toughening mechanisms in heterogeneous materials [27,28], one key characteristic of a damage mode is its dissipated energy. Therefore, we take a closer look at hysteresis cycles in this work and investigate whether they can help distinguish between the two common damage modes. Our hypothesis is that a difference in the dissipated energy between the micro-damage modes should be visible, since it can be expected that the energy needed by each damage mode to grow is different. For this purpose, we also evaluated the dissipated energy from hysteresis data and compared it to the predictions from Carraro's model.

The focus of this work is to compare stiffness, dissipated energy, dynamic- and static modulus from the hysteresis loops to the crack density obtained by image analysis. With an understanding of the relation of those parameters, additional information such as occurring damage modes can be extracted from standard fatigue tests. This can avoid using extensive test campaigns and thus save costs.

2. Experimental

2.1. Material and specimen preparation

For the test campaign, symmetric laminate plates with a fibre orientation of ±45°, ±60°, ±75° and UD90° were produced with a stacking sequence of $[+\theta_3, -\theta_3]_s$, which corresponds to a symmetric layup of 3 layers with a fibre orientation of θ on the outside and 6 layers of $-\theta$ inside the plate. From these plates, the specimens with a gauge length of 100 mm were cut with a geometry of 200 × 20 × 2.6 mm for the $\pm\theta_s$ specimens. For UD90° specimens, a special dogbone geometry according to Drvoderic [29] was selected to avoid failure near the clamping area. Tapered aluminum tabs with an angle of 14° and a thickness of 1 mm were bonded to all specimens.

All specimen were cut from GFRP laminate plates produced from UD-fabric of type UD 92145 (Porcher Industries Germany GmbH, Erbach, Germany) and epoxy matrix of type EPIKOTE™ MGS® LR160 with the curing agent EPIKURE™ MGS® LH160 (Lange + Ritter GmbH, Gerlingen, Germany) in a ratio of 4:1 (weight proportion). The UD-fabric (10% weft yarns, 220 g/m^2) was manually impregnated with the epoxy matrix and subsequently pressed in a hydraulic press at 80 °C for 1 h at 1 MPa to reach a fibre volume fraction of approximately 40%. After initial curing in the hydraulic press, the plates were post-cured at 80° for 15 h.

2.2. Testing procedure and parameters

Fatigue testing was conducted at a servo-hydraulic testing machine of the model MTS 322.31 (MTS Systems Corporations, Minnesota, USA), which was equipped with hydraulic clamping grips and a 250 kN load cell which shows an accuracy of 0.5% within the relevant measuring range of 0–5 kN. For the evaluation of the quasi-static Young's modulus, the stress-controlled sinusoidal load cycles with an R-ratio of 0.1 were periodically interrupted to perform displacement-controlled quasi-static tensile tests at a cross-head speed of 0.5 mm/min [30]. The load history is shown in Fig. 2. Additionally, the camera system CV-X420 A (Keyence Corporation, Osaka, Japan) was triggered during the periodic stops to generate pictures for the crack density evaluation. The test-frequency was set to 5 Hz for all specimen except ±45° , which were tested at 3 Hz to avoid excessive hysteretic heating. Since off-axis matrix cracks usually occur in the first stages of the fatigue life, the spacing between the quasi-static tensile tests was adapted to provide a sufficient resolution of data points. This was achieved with small blocks at the start and larger at higher cycle counts (see Table 1 in the Appendix).

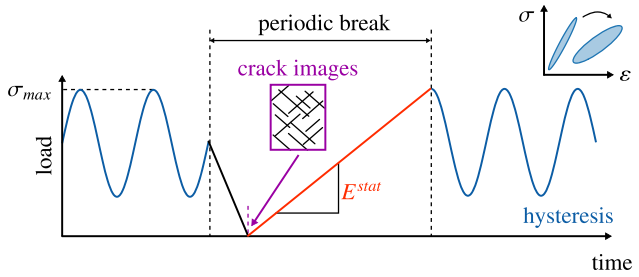

Fig. 2. The fatigue tests are periodically interrupted for the evaluation of the quasi-static Young's modulus E^{stat} and to take images for the crack detection.

The load level of the fatigue tests is defined as the ratio between the maximum ply-stress σ_{max} and the static strength σ_R of the ply (see Eq. (1)) computed by Puck's failure criterion [31].

$$load\ level = \frac{\sigma_{max}}{\sigma_R} \tag{1}$$

Ply-stresses are computed with classical laminate theory. Static stiffness and strength values for the computation of the load level are listed in Table 2 in the Appendix. Tests were conducted at load levels between 50% and 85% (see Fig. 3(a)).

The quasi-static Young's modulus E^{stat} was evaluated between 0.05% and 0.25% absolute strain during the quasi-static tensile tests. The maximum applied stress during tensile tests never exceeded the maximum stress during cyclic loading in order to minimize additional damage. Young's modulus is evaluated at 0.05% and 0.25% strain. The maximal strain is used if a test does not reach 0.25% strain. Parameters evaluated from the hysteresis loop during cyclic loading are dissipated energy e_d, dynamic and secant modulus, E^{dyn} and E^{sec} respectively (see Fig. 3(b)). The crack density ρ_c is defined as

$$\rho_c = \frac{\sum_{i=1}^{n} L_i}{A}\ , \tag{2}$$

with L_i as the length of the ith crack and A as the area of interest. For the automated evaluation of ρ_c from the images recorded during the tensile tests, the open-source software *CrackDect* is used [32].

In order to evaluate S–N curves for $\sigma_{h,loc}$ and $\sigma_{I,loc}$, Carraro's approach [33] was applied. It uses finite element analyses of a unit cell with a square fibre arrangement to compute the stress concentration matrices for the critical points. From this, $\sigma_{h,loc}$ and $\sigma_{I,loc}$ for any combination of ply loads can be computed using superposition of the stress fields, since linear elasticity is assumed in the model. From the S–N curves for $\sigma_{h,loc}$ and $\sigma_{I,loc}$, the transition of the critical damage-driving force for flat coupon specimens can be computed. For details of the unit cell see Appendix A.2.

3. Results and discussion

3.1. Off-axis cracks and stiffness degradation

The in-depth comparison of the crack density and stiffness degradation plotted over the cycle number for three ±75° specimens at distinct load levels is shown in Fig. 4 to point out the important trends. It was found that the trends of crack density and stiffness degradation for all tested laminates are qualitatively similar. Therefore, the full results for all fibre directions are shown in Fig. 12 in the Appendix.

As shown in Fig. 4, the crack density grows as the stiffness decreases during the fatigue life. The images of the detected cracks show this growth in number and size. At the later stages, a lot of diffuse delamination is already visible in the form of grey areas between the cracks. This type of delamination starts for all tested $[\pm\theta]_s$ laminates before crack saturation is reached, as shown in crack image 5 in Fig. 4. When substantial diffuse delamination sets in, the growth of crack density slows down up to crack saturation. The point when crack saturation is achieved is determined manually for all tests. A test reached crack saturation if the crack density curve has a clear S-like shape. The images of the specimen during the fatigue test in Fig. 4 also show the capability of the crack detection algorithm [32] to detect cracks even at high crack densities. The UD90° specimens fail mostly prior to crack saturation at lower crack densities. Tests exceeding 1.5 million cycles were stopped and may not show full crack saturation. All crack density curves that reach saturation show an S-like shape when plotted on a logarithmic x-axis (see Fig. 12 in the Appendix). Crack onset, which is shifted to lower cycles for higher load levels is detected accurately by the crack detection. It seems that the crack density growth for each fibre direction is relatively constant when plotted on a logarithmic axis.

For further evaluations, the crack onset is defined at the point where the crack density ρ_c reaches 0.2 mm^{-1}. This threshold was determined by manually comparing the crack density curves with crack images and is set to the cycle number where the first major cracks are visible. Smaller values showed inconsistent results for crack onset due to small artefacts, which lead to a low, but non-zero crack density. Above this value, the crack density shows a nearly linear increase in the logarithmic diagrams. For the used material system, this method has shown to be a practical way to automatically detect the crack onset.

The correlation between the crack onset and the stiffness degradation of the laminate is shown in Fig. 5.

By normalizing fatigue cycles to the crack onset n_0, it shows that hardly any stiffness degradation occurs before crack onset for all tested laminates. This indicates that the off-axis cracks are the cause for the stiffness degradation, which agrees well with already published results from a number of research groups [1–3,6,21].

3.2. Micro-damage modes

The SN-diagrams for $\sigma_{h,loc}$ and $\sigma_{I,loc}$ are shown in Fig. 6. In each diagram, several laminate angles fall into one scatter band, as already observed by Carraro. The SN-diagram for $\sigma_{h,loc}$ (see Fig. 6(a)) shows that ±60°, ±75° and UD90° specimens reach critical $\sigma_{h,loc}$ before the ±45° specimens. The SN-diagram for $\sigma_{I,loc}$ shows that for ±45° and ±60°, $\sigma_{I,loc}$ is the critical stress for micro-damage initiation. Since all tests fall into the scatter band of this two SN-curves, it shows that only two master curves are needed to characterize the fatigue strength of the material for crack onset in the Puck mode-A region.

Based on Carraro's method [33], the predicted transition angle between $\sigma_{h,loc}$ and $\sigma_{I,loc}$ for flat $\pm\theta_s$ specimens as critical damage-driving is ±62° (see Fig. 7). This agrees well with an angle of ±60° published by Carraro for a similar material system. As also discussed by Carraro, there will be no single transition point, but a transition zone. With a predicted transition at 62°, ±60° specimens are expected to fall into this transition zone which explains the overlap in the SN-diagram for $\sigma_{I,loc}$ (see Fig. 6(b)).

Fig. 8 shows microscopic images of the crack surfaces of UD90° and ±45° specimens. The UD90° crack surface reveals large smooth regions where matrix and fibres are separated. In resin-rich regions, peel fracture cusps, which are typical for mode I fatigue cracks, are visible [25]. The shear induced cracks between fibres were only found in ±45° specimens, which agrees with the predictions of Carraro's model. The fracture surface of the ±45° specimens is rather rough compared to UD90° and larger smooth areas are rare. It should be mentioned that the shear induced cracks were only found in a few spots in the ±45° images. This can be explained with the fact that images of the crack surface were taken after the fatigue tests and show the state of final separation. At this state, the saturation crack density for the ±45° specimens has already been reached (see Fig. 12), which means

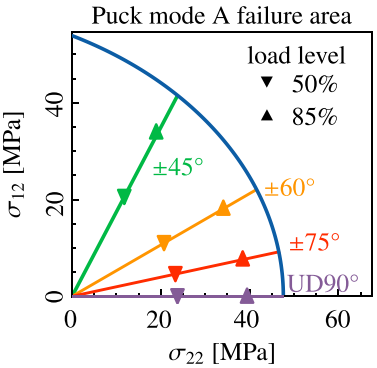

(a) Stress state for each fibre direction and load level in comparison to the strength computed with Puck´s failure criterion.

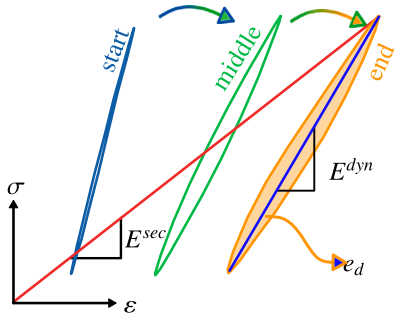

(b) Schematic representation of hysteresis cycles from the start to the end of fatigue life and their evaluation. For the evaluation of multiple tests with thousands of cycles each, the evaluation was automated using Python.

Fig. 3. Stress state for each fibre direction and load level in comparison to the strength computed with Puck's failure criterion (a) and schematic representation of hysteresis cycles from the start to the end of fatigue life and their evaluation (b). For the evaluation of multiple tests with thousands of cycles each, the evaluation was automated using Python.

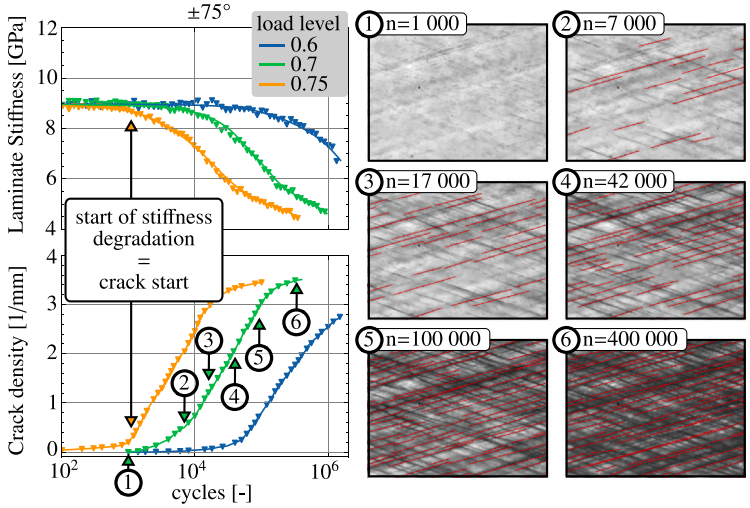

Fig. 4. Comparison of crack density and stiffness degradation for three ±75° specimens at different load levels. The trend of an earlier start of macroscopic off-axis cracks at higher load levels is evident. The right images (1–6) show the detected +75° cracks at different stages of the fatigue life.

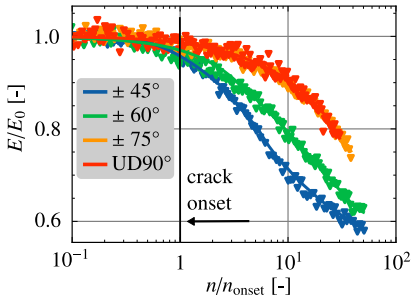

Fig. 5. Normalized stiffness reduction over normalized cycle count for all fibre directions at a load level of 0.6. The cycles are normalized to the start of off-axis cracks.

that the majority of micro-cracks had already formed a continuous macroscopic crack. Therefore, it is reasonable to expect micro-cracks only in areas with lower local stresses, thereby surviving up to specimen failure without forming a macroscopic crack.

3.3. Hysteresis results

The fatigue experiments are interrupted at periodic intervals (see Fig. 2) for the evaluation of the quasi-static Young's modulus E^{stat}. It is important to note that the first few cycles when restarting the sinusoidal load cycles cannot be used for hysteresis evaluation due to swing-in effects of the testing system. One objective was to get rid of this periodic interruptions since they complicate the test setup and use the dynamic or secant modulus, E^{dyn} and E^{sec} respectively, instead of E^{stat} as a measure for the stiffness. Brunbauer et al. [34] also compared E^{stat} and E^{dyn} with the result that the periodic interruptions are necessary for an accurate measure of the quasi-static stiffness, since E^{stat} and E^{dyn} do not correlate well. However, in their work the specimens showed significant hysteretic heating compared to the here presented tests. Fig. 9 shows two examples of E^{stat}, E^{dyn}, and E^{sec} for a ±45° and a ±75° specimens tested at 65% load level.

In general, E^{dyn} and E^{stat} show a good correlation both in absolute values and shape of the curves, whereas E^{sec} shows a similar shape but shifted to lower values. The mean difference of all tests is 5% between E^{stat} and E^{dyn} and 16% between E^{stat} and E^{sec} (see Appendix A.3

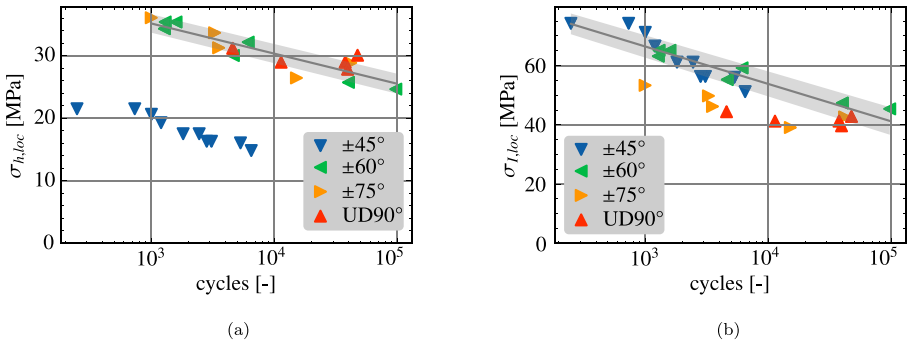

Fig. 6. SN-diagrams for crack start of local hydrostatic stress $\sigma_{h,loc}$ (a) and local maximum principal stress $\sigma_{I,loc}$ (b).

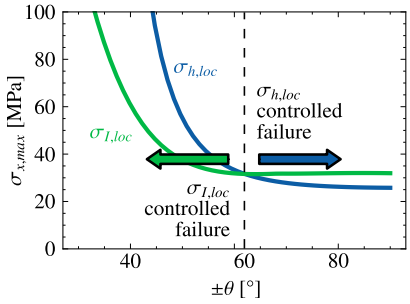

Fig. 7. Constant-life diagram for 10^4 cycles. For flat laminate specimens, the model predicts a transition from LHS-to LMPS-driven micro-damage at a fibre angle of ±62°.

for details of the error computation). This shows that E^{stat} and E^{dyn} correlate well when hysteretic heating is not significant, which was assured with the test design by lowering the frequency of the ±45° tests (see Section 2.2). This underlines the importance of controlling hysteretic heating for better comparability. If this is accomplished with the test setup, the periodic stops can be omitted when mainly the relative reduction in stiffness is of interest.

Fig. 10 shows a comparison between evaluated crack densities ρ_c and dissipated energy e_d evaluated from hysteresis cycles. The cycle number is again normalized to crack onset. A significant difference in absolute dissipated energy between ±45° and ±75° specimens with substantially higher levels of dissipated energy for ±45° is visible. The dissipated energy generally starts to increase at higher cycle numbers compared to the crack density and continues to rise even after crack saturation has been reached. A plausible explanation for this delay could be that the dissipated energy is a result if internal friction at crack faces and thereby a consequence of the increasing crack density. Also, the fact that the dissipated energy increases further after crack saturation can be explained by additional damage due to other damage mechanisms like delamination, which are not considered here. This means that dissipated energy cannot be used as a reliable measure of crack density. It is expected that higher load levels lead to a higher dissipated energy. The ±45° specimens follow this trend but the ±75° do not. It has to be noted that the absolute value of dissipated energy for the ±75° specimens is small. With a dissipated energy of under 2 mJ/cm^3 at crack start, the hysteresis cycles are extremely thin and therefore more sensitive to slight measurement errors (see Fig. 3(b)). Fig. 11 shows a comparison of the dissipated energy between all tested fibre directions at 60% and 70% load level.

A clear difference in absolute dissipated energy between ±45° and the other fibre directions is apparent. This implies that the dissipated energy also correlates with the micro-damage modes, since the predicted transition between the micro-damage modes lies around ±60° laminate angle (see Fig. 7) for the used material system. Compared to the S–N curves for $\sigma_{h,loc}$ and $\sigma_{I,loc}$ (see Figs. 6(a) and 6(b)), the ±60° specimens fall into the transition zone between the two micro-damage modes. If the dissipated energy would solely be used as the determining factor for the transition, the ±60° specimens would fall into the $\sigma_{h,loc}$ region. Its dissipated energy is similar to ±75° and UD90° laminates, which are also firmly in the $\sigma_{h,loc}$ dominated region predicted by Carraro's model. The $\sigma_{I,loc}$-driven micro-cracks result in rougher crack surfaces than $\sigma_{h,loc}$-driven failure (see Fig. 8). These rougher surfaces result in more friction which can explain the higher amount of dissipated energy.

Multiple factors like viscoelastic and plastic dissipation, friction between crack surfaces, and crack growth contribute to the dissipated energy. The various contributions cannot be separated from the global evaluation of the dissipated energy, but it is reasonable to assume that the major part is caused by damage-related phenomena, since the dissipated energy begins to rise after damage is detected. With the crack density as a function of the cycles an estimate of the contributions to the dissipated energy due to newly formed crack area compared to friction is possible. For the upper estimate of dissipated energy due to newly formed crack area, the crack area per cycle is computed based on the maximal crack growth rate and multiplied with the fracture energy. For this estimation, a fracture energy of 100 J/m^2 [35] is used and the maximal growth rate of crack surface is $8{\cdot}10^{-5}$ mm^{-1} and $2{\cdot}10^{-3}$ mm^{-1} for UD90° and ±45° specimens, which form the lower and upper limits for all tests. Based on these assumptions, the energy due to newly formed crack area is 0.01 mJ/cm^3 to 0.2 mJ/cm^3 per cycle for the UD90° and ±45° specimens, respectively. Although this is only a rough estimation, it shows that the dissipated energy due to new crack surface must be low compared to friction and other factors. Nevertheless, it is not important for the differentiation of micro-damage modes whether the dissipated energy is a result of the damage phenomenon itself or its secondary effects. Since the difference in dissipated energy already exists before delamination can be spotted, the difference in the dissipated energy before delamination must arise from the two separate micro-damage modes. Therefore, it can be concluded that the difference in dissipated energy can be used as an indicator of the underlying micro-damage mode.

4. Conclusions

Fatigue tests at several load levels were conducted on ±45°, ±60°, ±75°, and UD90° laminates with a focus on detecting off-axis cracks and comparing evaluated crack densities to the laminate stiffness and the dissipated energy. Additionally, the effects of micro-damage modes which trigger the off-axis cracks, were investigated in detail. The following points summarize the main findings.

- The evaluation of the crack density with an automated crack detection algorithm is a suitable tool for monitoring off-axis cracks in fatigue experiments. The start of visible off-axis cracks is captured well and correlates with the beginning of the degradation of laminate stiffness.

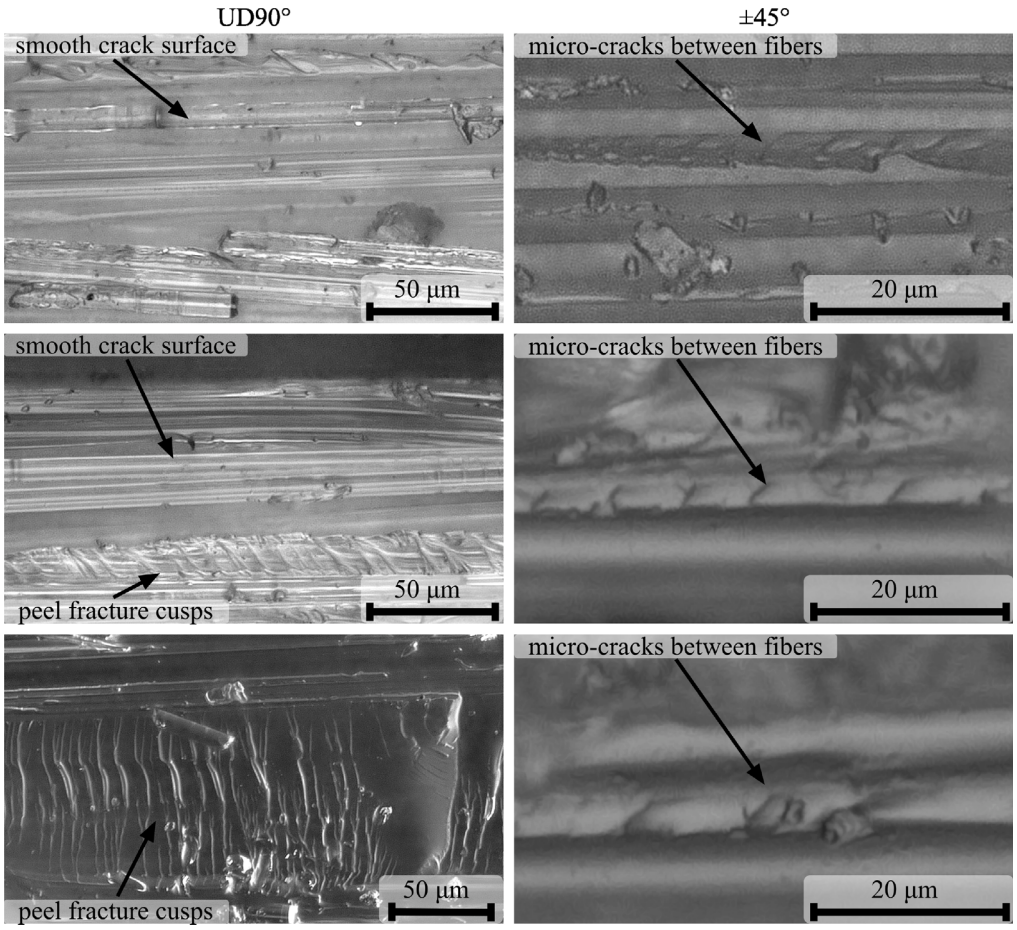

Fig. 8. Crack surface of UD90° (left) and ±45° (right) specimen. The UD90° specimens show large smooth sections where matrix and fibres separated and in resin-rich regions, peel fracture cusps are visible. Micro-cracks between fibres and matrix at a distinct nucleation plane of around 45° were only found in ±45° specimens. The images were recorded with the digital microscope VHX-7000 (Keyence Corporation, Osaka, Japan).

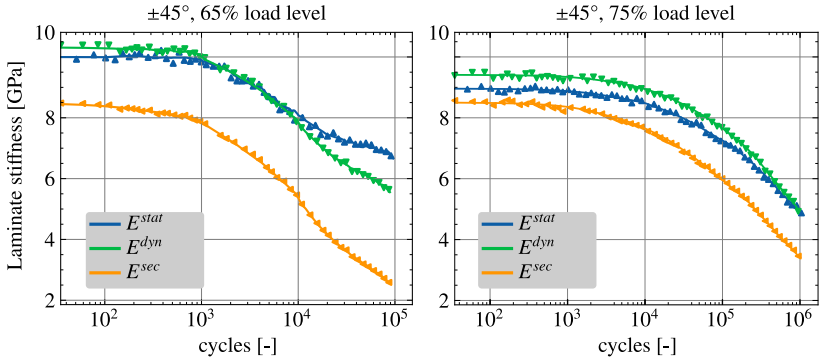

Fig. 9. Quasi-static laminate modulus, dynamic and secant modulus for a ±45° and ±75° specimen at 65% load level. Quasi-static and dynamic modulus correlate well both in absolute values and shape of the curves.

- The evolution of quasi-static Young's modulus and the dynamic modulus evaluated from hysteresis cycles correlate well, as long as the specimen temperature does not rise significantly during the test. Therefore, it is possible to omit periodic interruptions during fatigue testing for quasi-static modulus evaluation. This would reduce test complexity if the relative reduction of stiffness is of interest.
- The dissipated energy from hysteresis cycles is not a good measure for off-axis damage. Dissipated energy starts to increase at higher cycle numbers than crack onset in the fatigue life and does not stop to rise after crack saturation.
- Carraro's model for the prediction of the critical driving forces of micro-damage was used with the here presented experimental data. The results agree well with Carraro's observations for a similar material system. For multiaxially loaded plies, SN-curves of local hydrostatic stress $\sigma_{h,loc}$ and local maximum principal stress $\sigma_{I,loc}$ indeed fall into two master curves. This confirms Carraro's hypothesis that only two SN-curves are sufficient to

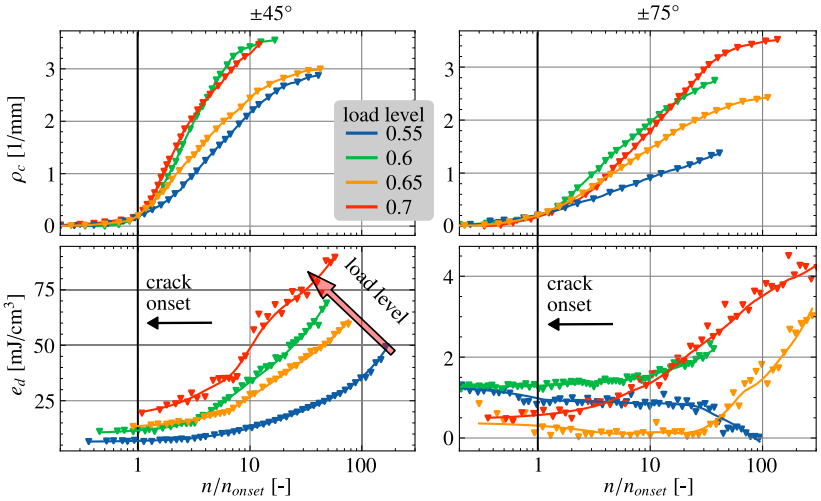

Fig. 10. Crack density ρ_c and dissipated energy e_d for ±45° and ±75° specimens at different load levels.

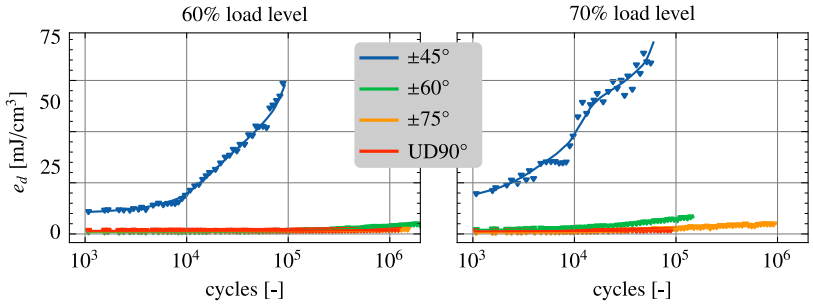

Fig. 11. Dissipated energy per volume e_d for a load level 60% and 70%. Specimens with a fibre direction of 60° or higher show little dissipated energy compared to ±45°.

characterize the crack onset for laminates with positive transverse stress and non-negative load ratios.

- Micro-cracks between fibres with a distinct fracture plane of approximately 45° with respect to the fibres can be occasionally spotted in microscopy images of specimens where $\sigma_{I,loc}$ is the damage driving force. The infrequent appearance can be attributed to the fact that only in areas with lower local stresses, these micro-cracks can survive until global failure. In all other areas, micro-cracks already formed macroscopic cracks. In specimens where $\sigma_{h,loc}$ is the dominant damage driving force, no such micro-cracks were found and the crack surface is generally smoother, with peel-fracture cusps in resin-rich regions and smooth matrix–fibre separations. This agrees well with the concept of two distinct micro-damage modes.
- The separation of the underlying micro-damage modes correlates well with the level of dissipated energy in experiments. Therefore, the dissipated energy can be used as an indicator for the micro-damage mode. All tests with $\sigma_{h,loc}$ as main damage-driving force showed dissipated energies at significantly lower levels compared to $\sigma_{I,loc}$-driven micro-damage at all tested load levels.

These findings provide a good basis for further improvements of reliable methods for fatigue prediction. On the one hand, the experimental procedure to provide the data for parameter calibration can now be performed more efficiently. On the other hand, more reliable fatigue prediction models can be achieved based on the distinction of the micro-mechanisms. Further work will be necessary to develop an appropriate interpolation for multi-axial load cases and arbitrary R-ratios in order to provide a generally-applicable fatigue model. Additionally, the role of other dissipative mechanisms (e.g. viscous effects and plasticity) needs to be investigated to gain a better understanding of the underlying physical phenomena contributing to dissipated energy and hysteretic heating.

Declaration of competing interest

The authors declare that they have no known competing financial interests or personal relationships that could have appeared to influence the work reported in this paper.

Funding

Part of this work has been performed within the COMET-project *Experimental and numerical analysis of the damage tolerance behaviour of manufactured induced defects and bonded repairs in structural aerospace composite parts* (project-no.: VI-3.04) at the Polymer Competence Center Leoben GmbH (PCCL, Austria) within the framework of the COMET-program of the Federal Ministry for Transport, Innovation and Technology and the Federal Ministry for Digital and Economic Affairs with contributions by Montanuniversität Leoben (Chair of Designing Plastics and Composite Materials) and MAGNA Powertrain Engineering Center Steyr GmbH CO KG. The PCCL is funded by the Austrian Government and the State Governments of Styria, Lower Austria and Upper Austria.

Data availability

The data presented in this study and a Python script for the FEM-simulation and evaluation of Carraro's model is available upon request from the corresponding author. The automated crack detection (open source) is available at GitHub (https://github.com/mattdrvo/CrackDect, 21.10.2022).

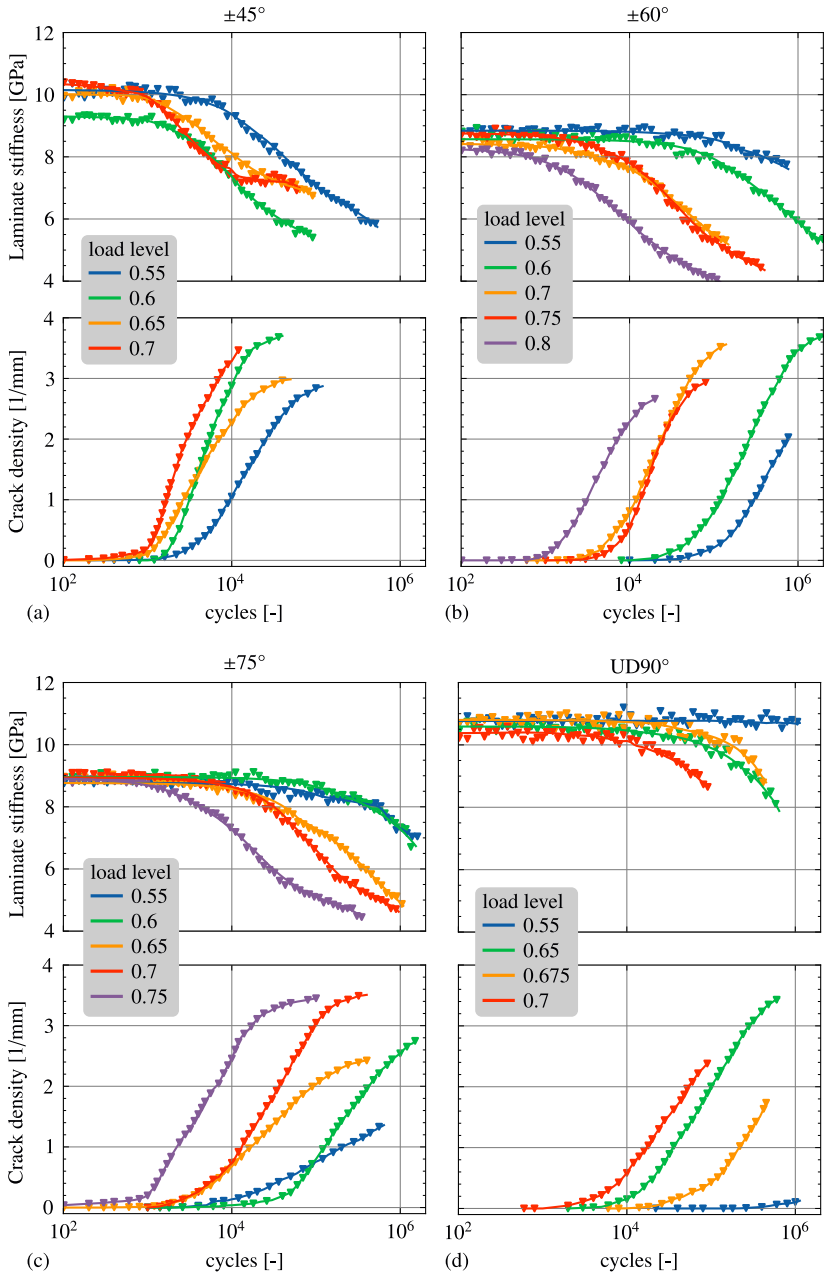

Fig. 12. Comparison of crack density and stiffness degradation for all fibre directions (a–d). The trend to an earlier start of off-axis cracks for higher load levels is observed for all fibre directions. Nearly all specimen except UD90° reached crack saturation.

Appendix

A.1. Material and testing details

Material data from static tests and block lengths used to control the periodic stops in the fatigue tests.

A.2. FEM-model details

To compute the stress concentration matrices needed to map ply-stresses to local stresses as in Carraro's model [33], a unit cell with a square fibre arrangement is loaded with the three basic load cases

Table 1
Block lengths for the periodic stops during the fatigue tests.

	Block 1	Block 2	Block 3
Cycles	0–1000	1000–10 000	10 000–End
Block length	25	100	1000

Table 2
Elastic constants and strength of the composite ply material from static tests.

E_1 [GPa]	E_2 [GPa]	ν_{12} [–]	G_{12} [GPa]	R_2 [MPa]	R_{12} [MPa]
31,7	10,7	0,27	3,3	47,6	53,2

Table 3
Material parameters for the FEM simulations.

	Young's modulus [GPa]	Poisson's ratio [–]
Fibre	70	0,22
Matrix	3,5	0,43

of stress in fibre direction σ_1, stress in transverse direction σ_2, and in-plane shear σ_{12}. For the FEM analysis, the commercial software Abaqus (Dassault Systems, 2020) was used. The full unit cell with periodic boundary conditions and 40% fibre volume fraction was generated with a mesh size of 0.01 at a height and width of the cell of 1 and a depth of 0.01. Note that for this kind of unit cell, the FEM-model is independent of the length-scale as all lengths are relative. The material parameters for fibres and matrix are listed in Table 3. For any ply load case, $\sigma_{h,loc}$ and $\sigma_{I,loc}$ can be computed from superposition of the stress fields of the basic load cases and subsequently computing the hydrostatic and principal stresses. A Python script for the creation of the unit cells in Abaqus and evaluation of the resulting stress fields is available on request from the corresponding author.

A.3. Difference of moduli curves

To compute the difference between whole curves of quasi-static Young's modulus, dynamic and secant modulus, the mean absolute percentage error of the smoothed curves is used (Eq. (3)). The relative difference is used as a measure for similarity.

$$e = \frac{100\%}{n} \sum_{i=1}^{n} \left| \frac{y_1 - y_2}{y_1} \right| \tag{3}$$

where y_1 is the quasi-static modulus and y_2 is either the dynamic or secant modulus. Smoothing of the experimental curves is performed with a locally weighted scatterplot smoothing (lowess) algorithm with a fraction of 0.1 [36]. This is necessary since the data points of the different curves must have the same cycle count to compare the curves. This is not possible from raw data, because the quasi-static modulus is evaluated during the periodic interruptions and dynamic and secant modulus are evaluated from cyclic data. Therefore, interpolation and smoothing are necessary.

References

[1] Tong J, Guild FJ, Ogin SL, Smith PA. Off-axis fatigue crack growth and the associated energy release rate in composite laminates. Appl Compos Mater 1997;4(6):349–59. http://dx.doi.org/10.1007/BF02481399, URL http://link.springer.com/10.1007/BF02481399.

[2] Wharmby A, Ellyin F. Damage growth in constrained angle-ply laminates under cyclic loading. Compos Sci Technol 2002;62(9):1239–47. http://dx.doi.org/10.1016/S0266-3538(02)00075-1, URL https://linkinghub.elsevier.com/retrieve/pii/S0266353802000751.

[3] Wharmby A. Observations on damage development in fibre reinforced polymer laminates under cyclic loading. Int J Fatigue 2003;25(5):437–46. http://dx.doi.org/10.1016/S0142-1123(02)00118-4, URL https://linkinghub.elsevier.com/retrieve/pii/S0142112302001184.

[4] Tohgo K, Nakagawa S, Kageyama K. Fatigue behavior of CFRP cross-ply laminates under on-axis and off-axis cyclic loading. Int J Fatigue 2006;28(10):1254–62. http://dx.doi.org/10.1016/j.ijfatigue.2006.02.011, URL https://linkinghub.elsevier.com/retrieve/pii/S0142112306000466.

[5] Zhang D, Ye J, Lam D. Ply cracking and stiffness degradation in cross-ply laminates under biaxial extension, bending and thermal loading. Compos Struct 2006;75(1–4):121–31. http://dx.doi.org/10.1016/j.compstruct.2006.04.048, URL https://linkinghub.elsevier.com/retrieve/pii/S0263822306001267.

[6] Quaresimin M, Carraro P. Damage initiation and evolution in glass/epoxy tubes subjected to combined tension–torsion fatigue loading. Int J Fatigue 2014;63:25–35. http://dx.doi.org/10.1016/j.ijfatigue.2014.01.002, URL https://linkinghub.elsevier.com/retrieve/pii/S0142112314000036.

[7] Reifsnider KL, editor. Fatigue of composite materials. Composite materials series, Vol. 4, Amsterdam ; New York: Elsevier; 1991.

[8] Degrieck J, Van Paepegem W. Fatigue damage modeling of fibre-reinforced composite materials: Review. Appl Mech Rev 54(4):279–300. http://dx.doi.org/10.1115/1.1381395, URL https://asmedigitalcollection.asme.org/appliedmechanicsreviews/article/54/4/279/465076/Fatigue-damage-modeling-of-fibrereinforced.

[9] Quaresimin M, Susmel L, Talreja R. Fatigue behaviour and life assessment of composite laminates under multiaxial loadings. Int J Fatigue 2010;32(1):2–16. http://dx.doi.org/10.1016/j.ijfatigue.2009.02.012, URL https://linkinghub.elsevier.com/retrieve/pii/S014211230900070X.

[10] Hassani S, Mousavi M, Gandomi AH. Structural health monitoring in composite structures: A comprehensive review. Sensors 2021;22(1):153. http://dx.doi.org/10.3390/s22010153, URL https://www.mdpi.com/1424-8220/22/1/153.

[11] Adden S, Horst P. Stiffness degradation under fatigue in multiaxially loaded non-crimped-fabrics. Int J Fatigue 2010;32(1):108–22. http://dx.doi.org/10.1016/j.ijfatigue.2009.02.002, URL https://linkinghub.elsevier.com/retrieve/pii/S0142112309000334.

[12] Lafarie-Frenot M, Hénaff-Gardin C. Formation and growth of 90° ply fatigue cracks in carbon/epoxy laminates. Compos Sci Technol 40(3):307–24. http://dx.doi.org/10.1016/0266-3538(91)90087-6, URL https://linkinghub.elsevier.com/retrieve/pii/0266353891900876.

[13] Bartley-Cho J, Gyu Lim S, Hahn H, Shyprykevich P. Damage accumulation in quasi-isotropic graphite/epoxy laminates under constant-amplitude fatigue and block loading. Compos Sci Technol 58(9):1535–47. http://dx.doi.org/10.1016/S0266-3538(97)00214-5, URL https://linkinghub.elsevier.com/retrieve/pii/S0266353897002145.

[14] Glud J, Dulieu-Barton J, Thomsen O, Overgaard L. Automated counting of off-axis tunnelling cracks using digital image processing. Compos Sci Technol 2016;125:80–9. http://dx.doi.org/10.1016/j.compscitech.2016.01.019, URL https://linkinghub.elsevier.com/retrieve/pii/S0266353816300197.

[15] Drvoderic M, Rettl M, Pletz M, Schuecker C. CrackDect: Detecting crack densities in images of fiber-reinforced polymers. SoftwareX 2021;16:100832. http://dx.doi.org/10.1016/j.softx.2021.100832, URL https://linkinghub.elsevier.com/retrieve/pii/S2352711021001205.

[16] Bender J, Bak B, Jensen S, Lindgaard E. Effect of variable amplitude block loading on intralaminar crack initiation and propagation in multidirectional GFRP laminate. Composites B 2021;217:108905. http://dx.doi.org/10.1016/j.compositesb.2021.108905, URL https://linkinghub.elsevier.com/retrieve/pii/S135983682100295X.

[17] Asp L, Berglund L, Talreja R. A criterion for crack initiation in glassy polymers subjected to a composite-like stress state. Compos Sci Technol 56(11):1291–301. http://dx.doi.org/10.1016/S0266-3538(96)00090-5, URL https://linkinghub.elsevier.com/retrieve/pii/S0266353896000905.

[18] Asp L, Berglund L, Talreja R. Prediction of matrix-initiated transverse failure in polymer composites. Compos Sci Technol 56(9):1089–97. http://dx.doi.org/10.1016/0266-3538(96)00074-7, URL https://linkinghub.elsevier.com/retrieve/pii/0266353896000747.

[19] Awerbuch J, Hahn H. Off-axis fatigue of graphite/epoxy composite. In: Lauraitis K, editor. Fatigue of fibrous composite materials. ASTM International; p. 243–73. http://dx.doi.org/10.1520/STP27624S, URL http://www.astm.org/doiLink.cgi?STP27624S.

[20] Plumtree A. Fatigue damage evolution in off-axis unidirectional CFRP. Int J Fatigue 24(2):155–9. http://dx.doi.org/10.1016/S0142-1123(01)00068-8, URL https://linkinghub.elsevier.com/retrieve/pii/S0142112301000688.

[21] Drvoderic M, Pletz M, Schuecker C. Modeling stiffness degradation of fiber-reinforced polymers based on crack densities observed in off-axis plies. J Compos Sci 6(1):10. http://dx.doi.org/10.3390/jcs6010010, URL https://www.mdpi.com/2504-477X/6/1/10.

[22] Dharan CKH, Tan TF. A hysteresis-based damage parameter for notched composite laminates subjected to cyclic loading. J Mater Sci 42(6):2204–7. http://dx.doi.org/10.1007/s10853-007-1498-9, URL http://link.springer.com/10.1007/s10853-007-1498-9.

[23] Towo AN, Ansell MP. Fatigue of sisal fibre reinforced composites: Constant-life diagrams and hysteresis loop capture. Compos Sci Technol 68(3):915–24. http://dx.doi.org/10.1016/j.compscitech.2007.08.021, URL https://linkinghub.elsevier.com/retrieve/pii/S0266353807003259.

[24] Belaadi A, Bezazi A, Maache M, Scarpa F. Fatigue in sisal fiber reinforced polyester composites: Hysteresis and energy dissipation. Procedia Eng 74:325–8. http://dx.doi.org/10.1016/j.proeng.2014.06.272, URL https://linkinghub.elsevier.com/retrieve/pii/S187770581400842X.

[25] Purslow D. Matrix fractography of fibre-reinforced epoxy composites. Composites 17(4):289–303. http://dx.doi.org/10.1016/0010-4361(86)90746-9, URL https://linkinghub.elsevier.com/retrieve/pii/0010436186907469.

[26] Quaresimin M, Carraro P, Maragoni L. Early stage damage in off-axis plies under fatigue loading. Compos Sci Technol 128:147–54. http://dx.doi.org/10.1016/j.compscitech.2016.03.015, URL https://linkinghub.elsevier.com/retrieve/pii/S0266353816301026.

[27] Ritchie RO. The conflicts between strength and toughness. Nature Mater 10(11):817–22. http://dx.doi.org/10.1038/nmat3115, URL https://www.nature.com/articles/nmat3115.

[28] Fratzl P, Kolednik O, Fischer FD, Dean MN. The mechanics of tessellations – bioinspired strategies for fracture resistance. Chem Soc Rev 45(2):252–67. http://dx.doi.org/10.1039/C5CS00598A, URL http://xlink.rsc.org/?DOI=C5CS00598A.

[29] Drvoderic M. Probeneinflüsse bei der mechanischen prüfung von composites (Diplomarbeit), Montanuniversität Leoben; 2018.

[30] Brunbauer J, Arbeiter F, Stelzer S, Pinter G. Stiffness based fatigue characterisation of CFRP. In: Advanced materials research, Vol. 891. Trans Tech Publ; 2014, p. 166–71.

[31] Puck A. Failure analysis of frp laminates by means of physically based phenomenological models. Compos Sci Technol 58(7):1045–67. http://dx.doi.org/10.1016/S0266-3538(96)00140-6, URL https://linkinghub.elsevier.com/retrieve/pii/S0266353896001406.

[32] Drvoderic M, Bender JJ, Pletz M, Schuecker C. Version 0.2 - CrackDect: Detecting crack densities in images of fiber-reinforced polymers. SoftwareX 19:101198. http://dx.doi.org/10.1016/j.softx.2022.101198, URL https://linkinghub.elsevier.com/retrieve/pii/S2352711022001182.

[33] Carraro P, Quaresimin M. A damage based model for crack initiation in unidirectional composites under multiaxial cyclic loading. Compos Sci Technol 99:154–63. http://dx.doi.org/10.1016/j.compscitech.2014.05.012, URL https://linkinghub.elsevier.com/retrieve/pii/S0266353814001596.

[34] Brunbauer J, Pinter G. On the strain measurement and stiffness calculation of carbon fibre reinforced composites under quasi-static tensile and tension-tension fatigue loads. Polym Test 40:256–64. http://dx.doi.org/10.1016/j.polymertesting.2014.09.014, URL https://linkinghub.elsevier.com/retrieve/pii/S0142941814002165.

[35] Bajpai A, Alapati A, Klingler A, Wetzel B. Tensile properties, fracture mechanics properties and toughening mechanisms of epoxy systems modified with soft block copolymers, rigid TiO2 nanoparticles and their hybrids. J Compos Sci 2(4):72. http://dx.doi.org/10.3390/jcs2040072, URL http://www.mdpi.com/2504-477X/2/4/72.

[36] Seabold S, Perktold J. Statsmodels: Econometric and Statistical Modeling with Python, 92–96. http://dx.doi.org/10.25080/Majora-92bf1922-011. URL https://conference.scipy.org/proceedings/scipy2010/seabold.html.